INVESTIGATION OF CHEMICALLY REACTING BOUNDARY LAYERS IN SOLID PROPELLANT ROCKETS: STEADY AND PERIODIC SOLUTIONS

A THESIS

Presented to

The Faculty of the Division of Graduate Studies

by

Rajeev Srivastava

In Partial Fulfillment

of the Requirements for the Degree

Doctor of Philosophy

in the School of Aerospace Engineering

Georgia Institute of Technology

February, 1977

INVESTIGATION OF CHEMICALLY REACTING

BOUNDARY LAYERS IN SOLID PROPELLANT ROCKETS:

STEADY AND PERIODIC SOLUTIONS

Approved:

Ben T. Zinn, Chairman

Warren C. Strahle

James E. Hubbart

Date approved by Chairman: 2/15/77

ACKNOWLEDGMENTS

I would like to thank Professor Ben T. Zinn, my thesis advisor, for introducing me to the thesis problem and providing constant encouragement during the entire course of this work.

The discussions with Professor E. W. Price on the "real world" difficulties encountered with solid propellant combustion were invaluable in giving a more meaningful perspective to the analysis presented in this thesis. I would like to thank Professor Price for lending me his time so generously. I would also like to take this opportunity to thank Professors Warren C. Strahle and James E. Hubbart for their careful review of the thesis and the subsequent useful suggestions.

Though last, but not least, the financial support of the Georgia Institute of Technology is gratefully acknowledged.

TABLE OF CONTENTS

LIST OF TABLES

LIST OF ILLUSTRATIONS

Figure Page

Figure Page

Figure Page

List of Symbols

A	Admittance function
a_j	Exponent of concentration in rate law
A^*	Convenient grouping defined in Eqn. (4-64)
B	Temperature independent pre-exponential factor in rate law
C_s, C_p	Specific heats of solid and gas phases
D_1	Damkohler's First Similarity Group (modified), defined in Eqn. (2-52)
E	Activation energy
f	Non-dimensional stream function
G	Constant appearing in external velocity distribution - $u_e = Gx^m$
H	Non-dimensional temperature in solid phase ($\equiv T/\bar{T}_e$)
h_i^o	Heat of formation of specie i
h_t	Total enthalpy defined in Eqn. (2-17)
I	Integral defined in Eqn. (4-62)
L	Heat release at interface (positive for endothermic)
L	Non-dimensional heat release ($\equiv \frac{L}{C_p \bar{T}_e}$)
Le	Lewis Number ($\equiv \frac{\lambda}{\rho D C_p}$)
m	Exponent in external velocity distribution
M	Mach number
n^*	Overall order of reaction
Pr	Prandtl Number ($\equiv \frac{\mu C_p}{\lambda}$)
p	Pressure
$\dot{r}$	Regression rate of the solid propellant
R	Non-dimensional unsteady regression rate ($\equiv \frac{\dot{r}}{\bar{r}}$)
R^o	Universal gas constant

R	Response function
s	A quantity defined by Eqn. (4-10)
Sc	Schmidt Number ($\equiv \frac{\mu}{\rho D}$)
T	Temperature
u	x-component of velocity
v	y-component of velocity
W_i	Molecular weight of specie i
x	Downstream distance co-ordinate
y_j	Mass fraction of specie j
Z	Modified frequency factor defined in Eqn. (2-49)

Greek Alphabets

α	Temperature exponent of pre-exponential factor in rate law
α_s	Thermal diffusivity of solid
λ	Thermal conductivity
ρ	Density
μ	Viscosity of gas
θ	Non-dimensional total energy variable defined as h_t/h_{t_e}
ω_i	Chemical production rate ($\frac{\text{mass}}{\text{vol-sec}}$) of specie i
ν_i'	Stoichiometric coefficient of reactant
ν_i''	Stoichiometric coefficient of product
τ	Non-dimensional time
τ_{flow}	Quantity related to characteristic flow time, defined in Eqn. (2-50)
τ_{chem}	Chemical time characteristic of gas phase reaction, defined in Eqn. (2-51)
ζ	Non-dimensional y-coordinate in solid phase

Ω Non-dimensional frequency ($\equiv \frac{\omega}{\bar{r}^2/\alpha_s}$)

ψ Physical stream function

ε Non-dimensional amplitude of external stream pressure oscillations

γ Ratio of specific heats ($\equiv C_p/C_v$)

Subscripts

e External stream edge conditions

i Specie number

r A reference quantity for non-dimensionalization

s Solid phase quantity

u Unburned solid quantity (i.e. at $y \to -\infty$)

o Stagnation quantity

w Solid-gas interface quantity

'1' Perturbation quantity

$( )_r$ Real part of a complex quantity

Superscripts

(-) Steady-state quantity

(') Differentiation with respect to transformed co-ordinate η

SUMMARY

In this dissertation, the problem of the unsteady combustion response of a burning solid propellant subjected to longitudinal acoustic oscillations in pressure and velocity is investigated theoretically. Initially, a steady-state theory is formulated which takes into account the erosive burning of the propellant under conditions of laminar flow. The physical model used considers the behavior of a two-dimensional, chemically reacting boundary layer over the surface of a pyrolysing homogeneous solid propellant. The system of highly coupled and non-linear conservation equations that characterise the boundary layer flow are converted to "locally similar" form and solved using the method of parametric differentiation. It is shown that this numerical technique can be used efficiently in the solution of a general class of chemically reacting boundary layer problems. Furthermore, using the method of parametric differentiation provides in a single computer run the solutions to a whole family of related, physically interesting, problems.

Having established the steady-state solutions for the profiles of all the dependent variables, the unsteady analysis is undertaken. This analysis considers the behavior of a laminar boundary layer when isentropic, standing waves of pressure and velocity are superposed on the steady flow outside the boundary layer. The behavior of the perturbations in the gas phase, which is taken to be "quasi-steady", is described by a system of linearised, two dimensional conservation equations of mass, momentum, energy and species. On the other hand, the behavior of the solid phase is determined by solving the unsteady energy conservation

equation. By coupling the solid phase solution with the gas phase solutions through appropriate interface boundary conditions, it becomes possible to obtain the "pressure-and-velocity coupled" response function which describes the modifications in the steady-state mass burning rate of the propellant due to the presence of pressure and velocity oscillations in the rocket motor. The practice in the past has been to use the response function evaluated at the burning surface as a boundary condition when analysing the stability of the acoustic waves in the combustor. It is shown here that the appropriate response function to consider in describing the contribution of the burning propellant towards the growth or the decay of the acoustic waves in the combustor, is the one evaluated at the edge of the boundary layer. Based on a comparison of the response functions at the boundary layer edge and at the burning surface, it is concluded that using the latter can lead to erroneous predictions of the combustor's stability. The effect of several parameters describing the behavior of the gas and solid phases upon the predicted response functions is then analysed. The results indicate that for typical solid propellant burning conditions, the influence of some parameters, that were not analysed to date, can be significant. Finally, a study of the variation of the response function with position along the length of a charge is made. This reveals that velocity oscillations parallel to the burning surface have a strong influence on the response function and, from the viewpoint of combustion stability, can be more detrimental than the associated pressure oscillations.

CHAPTER I

INTRODUCTION

Background

In solid propellant rocket motors, the interaction of flow disturbances with the burning process can lead to instability and possible motor failure. Therefore, it is important to understand the physical processes governing this interaction. Usually, the purpose of such studies is to investigate the conditions under which the burning propellant will amplify the flow disturbances, leading possibly to unstable operation. In a real engine these flow disturbances often occur as small amplitude acoustic waves. In many instances, as a result of the interaction between these small amplitude waves and the burning propellant, a finite amplitude wave motion develops and this is detrimental to motor operation.

The above mentioned interaction between flow disturbances and the combustion process is of a feedback type. Consider, for instance, the presence of a pressure wave in the flow field of the combustion chamber. Since the chemical reaction rate is directly related to the pressure, a combustion disturbance is generated. This, in turn, changes the steady volumetric flow of gas into the flow field, causing the local pressure to change and setting up a propagating pressure disturbance. In view of the complex nature of this feedback process, it is customary to study just the effect of an externally imposed flow disturbance on the combustion process, without regard to how this might further modify the flow disturbance itself. Even with this simplification, the strong

coupling between the fluid-mechanics and the combustion process, that governs the unsteady burning poses an extremely difficult analytical problem.

Instabilities in tubular rocket motors having large length-to-diameter ratios are characterised by the dominance of longitudinal acoustic waves in the flow field of the combustion chamber. It has been observed that the frequencies associated with these waves usually vary from low to moderate values; that is, 100 to 1000 cycles per second. Hence, such instabilities have been referred to as being of the "axial-mode, intermediate frequency" type [1]. In order to understand the nature of this instability it is essential to determine how the various combustion and fluid-mechanical processes near a burning propellant's surface interact with the longitudinal waves present within the chamber. However, this interaction, because of its complexity, is only partially understood. Consider, for instance, a longitudinal flow disturbance, involving changes in both pressure and velocity, above the surface of a burning propellant charge and parallel to it. Such a disturbance would be expected to affect the propellant's burning rate through different physical mechanisms that may prevail simultaneously. For example, a pressure disturbance may manifest itself by modifying the gas phase chemical kinetics and the propellant's regression rate, while a velocity disturbance (parallel to the surface) would be expected to influence the burning rate by changing the "erosion" of the propellant's surface, already being caused by the steady flow of hot combustion gases above it. Therefore, the presence of pressure and velocity oscillations in the

combustor may be expected to yield an oscillatory burning rate, which describes the response of the propellant. Physically, this unsteady response results in an unsteady "pumping" action at the burning surface which performs displacement work on the acoustic waves in the combustion chamber - leading possibly to an increase of acoustic energy of the waves and their subsequent amplification. Of course, the final stability of the chamber would depend on the net effect of the various amplifying and attenuating mechanisms present in the combustor. In this thesis, however, attention will be focused only on the contribution of the burning propellant towards the overall stability of the combustion chamber.

There has been a considerable amount of work done on combustion instability with the view of studying the combustion response of a solid propellant. However, owing to the complexity of the problem, most investigations have restricted attention to certain limiting cases. The majority of the work done deals with models that describe the effect of only pressure oscillations, normal to the burning surface, on the propellant's response. An excellent review of these analyses is available in Reference 2. Most of these so-called "pressure coupled" theories have several features in common. For instance, most of them use a model in which the gas phase is assumed to respond instantaneously to the imposed pressure oscillations (i.e., the "quasi-steady" assumption), while the solid phase response time is considered large enough to warrant an unsteady analysis. As such a treatment is applicable to a wide class of solid propellant burning situations[2], it will be retained in the analysis presented in this thesis. Also, these pressure-coupled analyses invari-

ably use one-dimensional models in which all physical quantities are allowed to vary only in a direction normal to the burning surface. Finally, assuming the amplitude of the pressure oscillations to be small, the combustion response of the propellant is described in terms of a "response function" - defined as the ratio of the burning rate perturbation to the pressure perturbation, evaluated at the burning surface. A formula for this response function is ultimately derived in terms of the various gas and solid phase parameters involved in the analysis. This response function can then be used as the boundary condition at the propellant surface, when analysing the stability of the waves in the combustor.

Contrary to the above mentioned case where only pressure oscillations are present above the propellant surface, the opposite limiting case with only velocity oscillations parallel to the propellant surface present, has also been considered. In fact, it has been established that velocity oscillations alone could have a significant effect on the combustion response of a solid propellant[3,4,5]. When longitudinal velocity oscillations, parallel to the burning surface, are present in the chamber one can expect an unsteady erosive effect to control the propellant's response. This phenomenon has been referred to in the literature as "acoustic erosion" or "velocity coupling". Since velocity coupling may, in general, involve non-acoustic, finite amplitude oscillations the response of the combustion to velocity oscillations poses an immensely complicated analytical problem. For this reason, the formulation of a meaningful velocity-coupled response function still

remains to be accomplished. However, some conclusions have been reached about its nature based on heuristic arguments[3,4,5]. These conclusions relate to the possible linear and non-linear effects of velocity coupling on motor stability.

To date, little effort has been made to analytically investigate the more general problem considering the effects of both the pressure and velocity oscillations upon the combustion response of a burning propellant. This situation occurs commonly in practice. It was only recently that the first analysis of the "pressure-and-velocity coupled" response of a solid propellant was published[6]. In this study, Lengellé considers a model in which acoustic oscillations of pressure and velocity are superposed on a turbulent stream of hot combustion gases flowing over the pyrolysing surface of a composite solid propellant. Through a simplified analysis of a turbulent, incompressible boundary layer over a flat plate, with blowing occurring at its surface, Lengellé is able to find expressions for the turbulent transport coefficients in terms of the flow variables of the propellant combustion problem. Then, using these in a one-dimensional model, with the granular diffusion flame concept[7], Lengellé couples the quasi-steady gas phase solutions with the unsteady solid phase solutions. Thus he obtains an expression for the response function of the propellant at its surface. However, due to the nature of the considered gas phase flame model, and the fact that the turbulent boundary layer is only used as a device to yield relations for the turbulent transport coefficients, Lengellé's analysis is at best a heuristic one.

In view of the past work done towards understanding the unsteady combustion response of a solid propellant to both pressure and velocity oscillations, it is apparent that a need for a more unified analysis exists. The one-dimensional models of earlier analyses might be applicable to instabilities in "cigarette type", end-burning solid rockets (which are not commonly used), but it is doubtful whether they can properly describe the unsteady propellant response in a rocket with a tubular grain. In the latter case a velocity field containing steady and unsteady velocity components, parallel and normal to the propellant surface, is present just above the burning surface. Therefore, at least a two-dimensional description of the gas phase is required in the region that lies between the burning surface and the location above it where all velocities are nearly parallel to the surface. This region also contains the complex interaction between the combustion and fluid-mechanical processes referred to earlier.

Moreover, existing models do not consider the variation of the response function along a direction normal to the burning surface, across the interaction zone. In these analyses, the response function evaluated at the burning surface is used as the boundary condition in the combustor stability analysis. In reality, the presence of such processes as gas phase reactions and viscous dissipation inside the interaction region may cause a variation in the characteristics of the response function, depending upon the location above the solid propellant. This possible variation of the response function also needs to be investigated as it may be of fundamental importance from the stability standpoint. For example, in the case of a boundary layer flow over the

propellant surface (where the boundary layer acts as the interaction zone) the edge of the boundary layer separates the isentropic oscillations in the main combustor flow from the "non-isentropic" processes within the boundary layer. Therefore, the response function to be used as the boundary condition for the combustion instability problem should be the one evaluated at the boundary layer edge rather than the one at the burning surface. The difference between the two needs to be established, as it may be too large to be ignored.

In this thesis a theoretical study of the combustion response of a solid propellant in the presence of both pressure and velocity oscillations is undertaken, keeping in mind the above mentioned requirements. Such an analysis must necessarily consider the unsteady behavior of both the gas and solid phases, which in turn are dependent on the properties of the steady reactive flow near the propellant surface. Therefore, initially a steady state theory is formulated to determine the properties of the steady reactive flow. This steady analysis also considers the "erosive" effect associated with the steady flow above the burning propellant surface. This effect has been referred to in the literature as "erosive burning"[8]. More specifically, erosive burning refers to the phenomenon where the regression rate of the solid propellant increases with an increase in the velocity of the hot combustion gases flowing parallel to its surface. In side-burning rockets the velocity of the mean flow increases from the head-end to the nozzle-end in a complicated manner depending upon the internal geometry of the grain. Since many commonly used grains are of the side-burning type, erosive burning may

be especially important in the early stages of combustion, when the port cross-sectional area is the smallest. In general, erosive burning is detrimental to the rocket motor since it results in the propellant grain burning in non-parallel layers and sometimes even thermal failure of the outer casing. For this reason, several experimental and semi-empirical studies have been conducted to study the mechanisms responsible for this phenomenon. An excellent review of these studies is available in Reference 9. Analytically, the problem is made difficult by the complex nature of the coupling between the flow and combustion processes that governs the regression rate under typical combustion chamber conditions. Moreover, the additional complications of turbulence and heterogeneities in propellant composition, that are little understood, render the problem even less amenable to a theoretical analysis at the present time.

To date, the most comprehensive theoretical analysis of the erosive burning problem has been the one by Tsuji[10]. He considered a model with a laminar chemically reacting boundary layer over an ablating solid propellant surface. The temperature of this surface was assumed to be constant and the external stream velocity was taken to increase linearly with downstream distance from the leading edge. Through various approximations, Tsuji was able to develop "similarity" solutions that necessitated the numerical solution of only one ordinary differential equation (for the temperature), which contained the burning rate as an eigenvalue. His results showed that the burning rate increased with increasing velocity gradient of the external stream. Although this work was a first attempt at the construction of an aerothermochemical model, it neglected

certain important features of the erosive burning problem. For instance, the assumption of a constant wall temperature (necessary to achieve "similarity" solutions) makes the analysis questionable since the burning rate of the propellant is expected to vary with downstream distance during erosive burning, and in an Arrhenius fashion with surface temperature. Furthermore, Tsuji's analysis considered only a linear variation of external stream velocity with distance (i.e., $u_e = Gx$). It turns out that this special case of a general power law merely predicts one aspect of the erosive burning trend.

The present analysis of erosive burning, given in Chapter II of this thesis, is similar to Tsuji's in that it is also based on a boundary layer model. However, there is little else in common. By treating the gas phase in terms of a different set of dependent variables it has been possible to reduce the non-linearity of the system of equations. Furthermore, the temperature is related to the regression rate through an Arrhenius pyrolysis law and all properties are permitted to vary in the streamwise direction consistent with the idea of "local similarity"[11,12]. The resulting system of steady-state equations forms a highly coupled and non-linear boundary value problem. In order to achieve a solution, a novel numerical technique, the method of parametric differentiation, is introduced and used successfully. This will be discussed in Chapter III of the thesis.

Objectives of the Present Investigation

In summary, the objectives of this thesis are:

a) Formulation of an improved model to study erosive burning trends (Chapter II).

b) Development of the Method of Parametric Differentiation for the solution of the "locally similar", chemically reacting boundary layer equations encountered in the formulation of the erosive burning problem. This numerical technique and some typical results are discussed in Chapter III of the thesis.

c) By superposing standing, small amplitude, longitudinal, harmonic oscillations on the mean flow outside the boundary layer, the unsteady response of the propellant is studied. A "pressure-and-velocity" coupled response function is formulated and its variation across the boundary layer is investigated. This unsteady problem is formulated in Chapter IV of the thesis.

d) The developed theory and computer programs are used to investigate the characteristics of this response function and the computed results are used to determine the response function dependence upon location within the boundary layer and a variety of parameters characteristic of both the gas and solid phases. These results and their discussion is presented in Chapter V of the thesis.

CHAPTER II

THE STEADY STATE THEORY

The Model and Main Assumptions

In this chapter a theory of laminar erosive burning is formulated based on a simplified model that retains much of what are believed to be essential physics of the real solid propellant burning situation, so as to illuminate certain aspects of this complicated phenomenon. In most solid rocket combustion chambers with a tubular geometry a boundary layer can be expected to form a few diameters downstream from the head-end, after the gases issuing out of the ignited solid propellant surface have acquired a sufficiently high velocity in the direction along the surface. Although the flow may remain laminar in a region immediately following the leading edge of the boundary layer, the high surface blowing rates that characterise typical solid rocket burning conditions cause turbulent flow conditions to prevail over a significant portion of the combustor's length. Owing to the complexity of the true flow situation within a practical rocket motor having a complicated internal geometry and in view of the ultimate purpose of the steady-state theory in the present thesis, it has been necessary in this analysis to regard the combustion chamber as having a chemically reacting, laminar boundary layer immediately adjacent to the walls while the "core flow" consists of a one-dimensional flow of hot combustion gases - mainly products of combustion - with properties that can, in general, vary in an arbitrary manner along the length of the chamber. Thus, if the properties of the "core flow" are specified, either from experimental data

or from analytical considerations, the present theory could be used to study the behavior of the burning solid propellant under steady flow conditions. Although the simplification of the real combustor aerodynamics may appear drastic, it is hoped that the model treated will yield correct qualitative trends and provide insight into the complex interaction between the processes of combustion and fluid mechanics that characterise the "erosive burning" of a solid propellant.

Specifically, the model treated consists of a flow of hot combustion gases over the pyrolysing surface of a homogeneous solid propellant. A distributed chemical reaction zone, where the premixed reactants transform into products, is confined to within the laminar boundary layer that forms over the surface. The situation is illustrated in Fig. 1. The velocity of the external stream is assumed to increase with downstream distance according to a general power law of the form, $u_e = Gx^m$. As the gas phase reaction proceeds, the heat released is partially used to pyrolyse more of the propellant into reactant gases that are needed to sustain the flame in the boundary layer.

In order to keep this model analytically manageable, the following assumptions are made:

a) The Lewis number is unity.

b) The total enthalpy of the external stream is much greater than its kinetic energy.

c) The product of density and viscosity (in the gas phase) is a constant or a function of x only; that is, $\rho\mu = f(x)$ at most.

d) The composition of the external stream is constant, since all chemical reactions take place within the boundary layer.

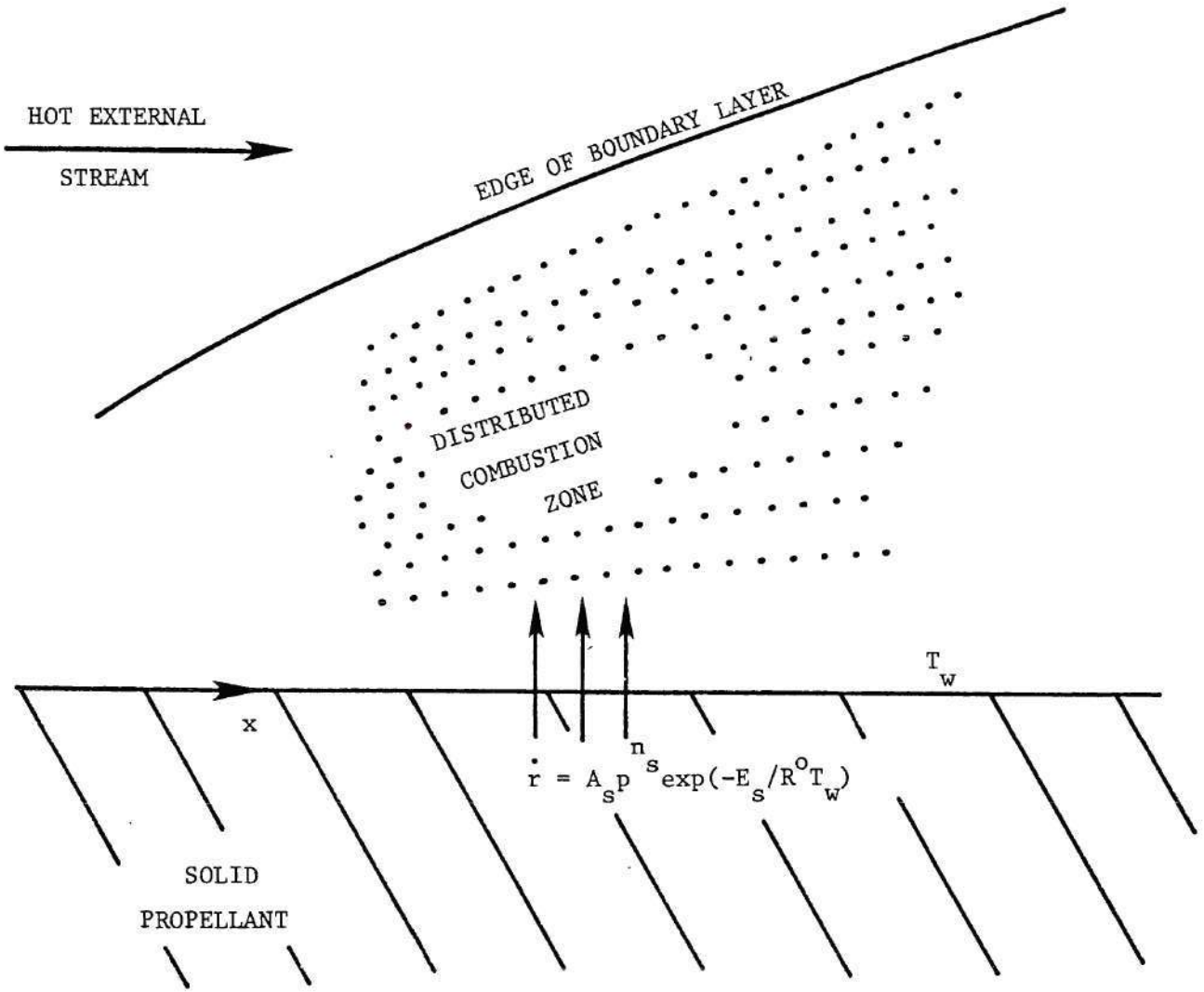

Figure 1. Schematic of a reacting boundary layer flow over a solid propellant.

e) Radiative heat transfer, barodiffusion and thermal diffusion are negligible.

f) The chemistry of the gas phase is described by a global, one-step, unopposed reaction of the type $R \rightarrow P$.

g) Lees[13] "heavy surface layer" approximation applies. This permits the momentum equation to be decoupled from other conservation equations. This approximation is valid herein as the pyrolysis products at the propellant surface are considerably cooler than the combustion products at the boundary layer edge. When this condition prevails, the pressure gradient term of the momentum equation becomes small and its effect on the boundary layer profiles is also expected to be small.

h) The gas phase is thermally and calorically perfect.

i) A steady state prevails in the gas and solid phases.

j) The density, specific heat and thermal conductivity of the solid phase are constant.

k) The solid phase is homogeneous and isotropic.

l) All pyrolysis and other reactions taking place within the solid phase are confined at the solid-gas interface, where they are described by the following Arrhenius type of law:

$$\dot{r} = A_s \, p^{n_s} \exp\left[\frac{-E_s}{R^o T_w}\right] \qquad (2\text{-}1)$$

m) Axial heat conduction within the solid phase is negligible.

Conservation Equations

Mathematically, the problem is to establish the basic conservation equations in the solid and gas phases and then couple them using

appropriate conservation laws at the interface. These two phases are characterised by the following distinct regions that are to be analytically described:

i) The external stream of hot gases, mainly products of combustion, whose properties are specified. The fluid flow here is considered isentropic.

ii) The boundary layer over the propellant surface wherein the processes of convection, diffusion and chemical reaction interact with one another. The diffusion of momentum, heat and species are accounted for separately within the boundary layer. In this region the gas properties undergo significant changes as required by the boundary layer conservation equations of continuity, momentum, energy and species.

iii) A thin thermal layer just below the gas-solid interface, where the effect of the heat transfer from the gas is predominant. Across this layer the temperature of the solid changes continuously from the hot surface value (T_w) to that of the cold solid (T_u), according to the energy conservation equation.

iv) The rest of the solid, below the thermal layer, which constitutes a region of constant temperature - the cold, unburned solid with a specified temperature T_u.

The solid phase analysis is greatly simplified under Assumptions (i) through (m) of the last section. The problem reduces to the solution of only an energy equation, the equations of continuity and momentum being automatically satisfied[1]. Choosing a co-ordinate system that is fixed to the burning surface (see Figure 1) one can use the following equation

to describe the energy balance within the solid phase:

$$\dot{r}\,\frac{dT}{dy} = \alpha_s \frac{d^2T}{dy^2}^{**} \quad , \quad -\infty < y < 0 \tag{2-2}$$

subject to the following boundary conditions:

a) $T = T_u$, as $y \to -\infty$ (2-2a)

b) $$\lambda \left.\frac{\partial T}{\partial y}\right|_{y=0^+} = \lambda_s \left.\frac{\partial T}{\partial y}\right|_{y=0^-} + \rho_s \dot{r} L \tag{2-2b}$$

The first of these (i.e., Eqn. (2-2a)) merely describes the temperature deep within the cold solid propellant. Equation (2-2b) describes the energy balance at the gas-solid interface, requiring the heat flux from the gas phase (at $y = 0^+$) to account for both the heat conducted into the solid phase (at $y = 0^-$) and the heat necessary to pyrolyse the solid.

The solution to the above differential equation (i.e., Eqn. (2-2)) subject to the prescribed boundary conditions is easily obtained analytically to yield the following result for the temperature profile in the solid phase:

$$T(y) = \hat{G}\,\frac{\alpha_s}{\dot{r}} \exp\left[\frac{\dot{r}y}{\alpha_s}\right] + T_u \tag{2-3}$$

where $$\hat{G} \equiv \left\{\lambda \left.\frac{\partial T}{\partial y}\right|_{y=0^+} - \rho_s \dot{r} L\right\} \Big/ \lambda_s \tag{2-3a}$$

** The x-derivative term, accounting for axial heat conduction, has been neglected because the thickness of the thermal layer within the solid is very small (being $O(\alpha_s/\dot{r})$). Thus, the gradients of temperatures across this layer can be expected to be much greater than those along it.

and $$\alpha_s \equiv \frac{\lambda_s}{\rho_s C_s} \tag{2-3b}$$

This equation couples the solid phase to the gas phase through the term $\lambda \frac{\partial T}{\partial y}\Big|_{y=0^+}$, the heat flux from the gas to the solid at their interface.

The corresponding gas phase problem is described by the well-known, steady, compressible, two-dimensional, laminar boundary layer equations for the conservation of overall mass, momentum, total energy and species[13,14]; that is

Overall mass

$$\frac{\partial}{\partial x}(\rho u) + \frac{\partial}{\partial y}(\rho v) = 0 \tag{2-4}$$

For conciseness, defining a "convective" operator, L_1, and a "diffusion" operator, L_2, by the expressions

$$L_1[\ \ ] \equiv \rho u \frac{\partial}{\partial x} + \rho v \frac{\partial}{\partial y} \tag{2-5}$$

$$L_2[;Q] \equiv \frac{\partial}{\partial y}\ \left(Q \frac{\partial}{\partial y}\right) \tag{2-6}$$

one can write the remaining conservation equations as

Momentum

$$L_1[u] = \rho_e u_e \frac{du_e}{dx} + L_2[u;Q \equiv \mu] \tag{2-7}$$

Total Enthalpy (energy)

$$L_1[h_t] = L_2[h_t;Q \equiv \frac{\mu}{Pr}] + L_2[\frac{u^2}{2};Q \equiv \mu(1 - \frac{1}{Pr})]$$
$$+ L_2[y_i;Q \equiv \frac{\mu}{Pr}(\frac{1}{Le} - 1) \sum_i h_i] \tag{2-8}$$

Species

$$L_1[y_i] = L_2[y_i; Q \equiv \frac{\mu}{Sc}] + \omega_i, \quad i = 1,2...N-1 \tag{2-9}$$

where the following parameters have been defined:

$$Pr \equiv \frac{\mu C_p}{\lambda}, \quad \text{Prandtl number} \tag{2-10}$$

$$Sc \equiv \frac{\mu}{\rho D}, \quad \text{Schmidt number} \tag{2-11}$$

$$Le \equiv \frac{\lambda}{\rho D C_p} = \frac{Sc}{Pr}, \quad \text{Lewis number} \tag{2-12}$$

In dealing with the energy equation (i.e., Eqn. (2-8)) the following additional relations were used:

$$h_t \equiv h + \frac{u^2}{2} \tag{2-13}$$

$$h = \sum_i y_i h_i \tag{2-14}$$

$$h_i = h_i^o + \int_{T_u}^{T} C_{p_i} \, dT \tag{2-15}$$

$$C_p = \sum_i y_i C_{p_i} \tag{2-16}$$

Using Equations (2-14),(2-15) and (2-16), together with the assumption of a calorically perfect gas mixture, Eqn. (2-13) for the total enthalpy yields:

$$h_t = C_p(T-T_u) + \sum_i y_i h_i^o + \frac{u^2}{2} \tag{2-17}$$

It should be noted that the present formulation uses the total enthalpy, rather than the commonly used temperature or sensible static enthalpy as the dependent variable in the energy equation. This choice eliminates the need to consider the highly nonlinear "Arrhenius" rate term explicitly in the energy equation. Other forms of this equation contain

the rate term explicitly to account for the heat release due to the gas phase reaction.

The above gas phase conservation equations are supplemented by specifying a global reaction rate law of the form:

$$\frac{\omega_i}{W_i} = (\nu_i''-\nu_i')BT^{\alpha} \exp\left[\frac{-E}{R^oT}\right] \prod_{j=1}^{M}\left(\frac{\rho y_j}{W_j}\right)^{a_j} \tag{2-18}$$

which is applicable in general to a reaction scheme of the type:

$$\sum_{i=1}^{N} \nu_i' M_i \rightarrow \sum_{i=1}^{N} \nu_i'' M_i$$

The above system of equations is completed by the inclusion of the thermal equation of state (valid under Assumption (h)):

$$p = \rho R^oT \sum_{i=1}^{N} y_i/W_i \tag{2-19}$$

Finally, to complete the formulation of the problem, the boundary conditions for the above mentioned differential equations are required.

At the gas-solid interface (i.e., y = 0) the following physical constraints need to be imposed:

i) $\rho_s \dot{r} = (\rho v)_w$ (2-20)

ii) $u = 0$ (2-21)

iii) $T_w\Big|_{y=0^+} = T_w\Big|_{y=0^-}$ (2-22)

iv) $\rho D \frac{\partial y_i}{\partial y}\Big|_{y=0^+} = (\rho v)_w [y_{i_w} - (y_{i_w})_-]$ (2-23)

Condition (i) is a statement of the continuity of overall mass across the interface with $\dot{r}$ being expressed by the pyrolysis law of Equation (2-1). Condition (ii) states that the x-component of the gas flow velocity at

the surface of the solid propellant is zero because of "no slip". Condition (iii) expresses continuity of temperature at the interface. Finally, condition (iv) requires that the net mass flux of specie i convected away from the interface must balance the mass flux of specie i due to diffusion from the gas to the interface.

At the edge of the boundary layer the following conditions are specified:

$$u = u_e = Gx^m \tag{2-24}$$

$$h_t = h_{t_e} = C_p(T_e - T_u) + \sum_i y_{i_e} h_i^o + \frac{u_e^2}{2} = \text{(constant)} \tag{2-25}$$

$$y_i = y_{i_e} \quad \text{(a specified constant)} \tag{2-26}$$

Owing to the parabolic nature of the partial differential equations (i.e., Eqns. (2-7) to (2-9)) encountered in the above formulation, it would normally have been necessary to also specify initial conditions with respect to the streamwise co-ordinate x. However, in the present analysis this system of equations will be transformed to a system of ordinary differential equations (as shown in the next section), that form a two-point boundary value problem.

The Transformed Problem

The solution to the system of highly coupled and non-linear governing equations of the last section poses an extremely difficult problem. In the past, the concept of "similarity" has been extensively employed in related boundary layer problems to convert the original problem to a system of ordinary differential equations, which are considerably easier to solve. Although the system of partial differential equations en-

countered here could perhaps be solved using finite-difference methods, the idea of "similarity" will be utilized in this analysis for the sake of simplicity in the final unsteady combustion response analysis. Basically, "similarity" consists of defining a transformation to a new system of co-ordinates. These transformations are so chosen that at least one of the new co-ordinates is a function of all the co-ordinates in the original problem. Then, if the transformed problem can be described in terms of just one independent variable, "true similarity" is said to exist. When applied to boundary layers, truly similar solutions imply that the profiles of all dependent variables retain a geometrically "similar" shape along the boundary layer; that is, all properties can be described in terms of one length scale. Few practical situations conform with the requirements of true similarity. Usually, some restrictions have to be imposed on the analysis to force truly similar solutions. Very often, in treatments of chemically reacting boundary layers these restrictions turn out to be too rigid and impair the usefulness of the analysis. As an alternative, a less restrictive approach is often applicable. This is the approximation of "local similarity". According to this, the transformed problem is described in terms of more than one length scale but all derivatives must appear with respect to just one of the new co-ordinates or length scales. For instance, a "locally similar" solution of the reacting boundary layer problem, being considered in this analysis, would necessarily impose the restriction that all properties be at most "slowly varying" functions of the streamwise co-ordinate. Physically, this implies that "similar"

solutions exist at every x-location, although they vary in a completely non-similar manner throughout the flow field. This idea has been used here to convert the partial differential equations encountered into ordinary differential equations.

As is customary[13,14,17], to begin with, the system of compressible boundary layer equations (i.e., Eqns. (2-4) to (2-9)) is first rendered "incompressible" using the Lees-Dorodnitsyn[18] transformations in the following form:

$$\xi = \int_o^x \rho_e \mu_e u_e \, dx' \tag{2-27a}$$

$$\eta = \frac{u_e}{(2\xi)^{1/2}} \int_o^y \rho \, dy' \tag{2-27b}$$

Next, introducing the stream function ψ such that

$$\rho u = \frac{\partial \psi}{\partial y} \tag{2-28a}$$

$$\rho v = - \frac{\partial \psi}{\partial x} \tag{2-28b}$$

eliminates the need to further consider the overall continuity equation (i.e., Eqn. (2-4)). The transformed "convective" and "diffusion" operators of Eqns. (2-5) and (2-6) then become

$$L_1[\ \ ] = \frac{\rho u_e^2 \rho_e \mu_e}{(2\xi)^{1/2}} \left(\frac{\partial \psi}{\partial \eta} \frac{\partial}{\partial \xi} - \frac{\partial \psi}{\partial \xi} \frac{\partial}{\partial \eta} \right) \tag{2-29}$$

$$L_2[\ \ ] = \frac{\rho u_e^2}{2\xi} \frac{\partial}{\partial \eta} \left(\rho Q \frac{\partial}{\partial \eta} \right) \tag{2-30}$$

Finally, using Equations (2-27) through (2-30) and introducing the non-dimensional variables f, θ and g_i in the following manner

$$\psi = (2\xi)^{1/2} f(\eta) \tag{2-31}$$

$$u = u_e(\xi) f'(\eta) \tag{2-32}$$

$$h_t = h_{t_e}\, \theta(\eta) \tag{2-33}$$

$$y_i = y_{i_e}\, g_i(\eta), \text{ or simply, } y_i = y_i(\eta) \tag{2-34}$$

the following system of "locally similar" ordinary differential equations describing the boundary layer flow is obtained:

Momentum

$$\left[\left(\frac{\rho\mu}{\rho_e\mu_e}\right) f''\right]' + ff'' = \frac{-2\xi}{u_e}\frac{du_e}{d\xi}\left[\frac{\rho_e}{\rho} - (f')^2\right] \tag{2-35}$$

Energy

$$\left[\frac{1}{Pr}\left(\frac{\rho\mu}{\rho_e\mu_e}\right)\theta'\right]' + f\theta' = \frac{2\xi f'\theta}{h_{t_e}}\frac{dh_{t_e}}{d\xi} + \left[\frac{1}{Sc}\left(\frac{\rho\mu}{\rho_e\mu_e}\right)\left(\frac{1}{Le} - 1\right) \quad \ldots\ldots \right.$$

$$\left. \ldots\ldots \sum_i h_i y_i'\right]' + \left\{\frac{u_e^2}{h_{t_e}}\right\}\left[\left(\frac{1}{Pr} - 1\right)\left(\frac{\rho\mu}{\rho_e\mu_e}\right) f'f''\right]' \tag{2-36}$$

Species

$$\left[\frac{1}{Sc}\left(\frac{\rho\mu}{\rho_e\mu_e}\right) y_i'\right]' + fy_i' = \frac{2\xi f' y_i}{y_{i_e}}\frac{dy_{i_e}}{d\xi} - \frac{2\xi\left(\frac{\omega_i}{\rho}\right)}{u_e^2\rho_e\mu_e} \tag{2-37}$$

In the above equations, the primes denote differentiation with respect to η.

Under the assumptions of the present model (given earlier in this chapter), Equations (2-35) to (2-37) above may be further simplified since:

$$\frac{\rho\mu}{\rho_e\mu_e} = 1 \qquad \text{(Assumption (c))} \qquad (2\text{-}38)$$

$$\left[\frac{\rho_e}{\rho} - (f')^2\right] \cong 0 \qquad \text{(Assumption (g))} \qquad (2\text{-}39)$$

$$\frac{dh_{t_e}}{d\xi} = 0, \text{ or } h_{t_e} = \text{constant} \qquad \text{(Eqn. (2-25), for an isentropic external stream)} \qquad (2\text{-}40)$$

$$Le = 1 \qquad \text{(Assumption (a))} \qquad (2\text{-}41)$$

$$\frac{u_e^2}{h_{t_e}} \cong 0 \qquad \text{(Assumption (b))} \qquad (2\text{-}42)$$

$$\frac{dy_{i_e}}{d\xi} = 0, \text{ or } y_{i_e} = \text{constant} \qquad \text{(Assumption (d))} \qquad (2\text{-}43)$$

Incorporating these simplifications, the "locally similar" boundary layer equations finally take the following form:

Momentum

$$f''' + ff'' = 0, \quad 0 < \eta < \infty \qquad (2\text{-}44)$$

Energy

$$\frac{1}{Pr}\theta'' + f\theta' = 0, \quad 0 < \eta < \infty \qquad (2\text{-}45)$$

Species

$$\frac{1}{Sc}y_i'' + fy_i' = -\frac{2\xi\left(\frac{\omega_i}{\rho}\right)}{u_e^2\rho_e\mu_e}, \quad 0 < \eta < \infty \qquad (2\text{-}46a)$$

$$i = 1,2,\ldots N\text{-}1$$

Using the rate law given by Eqn. (2-18) and the thermal equation of state, Eqn. (2-19), the right hand side of Eqn. (2-46a) may be expressed in terms of the pertinent dependent variables of the present analysis to yield the following species equation that will be needed later:

Species

$$\frac{1}{Sc} y_i'' + f y_i' = D_1 B_i \left(\frac{F}{C_p T_e} \right)^{1-n^*+\alpha} \left\{ \frac{\Sigma y_i / W_i}{\Sigma y_{i_e} / W_i} \right\}^{1-n^*} \exp\left[- \frac{E C_p}{R^o F} \right] \cdots$$

$$\cdots \prod_{j=1}^{M} y_j^{a_j} \qquad (2\text{-}46b)$$

The following definitions were used in deriving Eqn. (2-46b):

$$\hat{W} \equiv \sum_{i=1}^{N} \nu_i' W_i = \sum_{i=1}^{N} \nu_i'' W_i \qquad (2\text{-}47)$$

$$n^* \equiv \sum_{j=1}^{M} a_j \quad \text{(overall order of the reaction)} \qquad (2\text{-}48)$$

$$Z \equiv \frac{B \hat{W}}{\prod_{j=1}^{M} W_j^{a_j}} \quad \text{(a modified frequency factor)} \qquad (2\text{-}49)$$

$$\tau_f \equiv \frac{2x}{(m+1) u_e} \quad \text{(a characteristic flow time)} \qquad (2\text{-}50)$$

$$\tau_c \equiv \left(Z \rho_e^{n^*-1} T_e^{\alpha} \right)^{-1} \quad \text{(a characteristic chemical reaction time)} \qquad (2\text{-}51)$$

$$D_1 \equiv \frac{\tau_f}{\tau_c} \cong \frac{2x^{1-m}}{(m+1) G} Z \rho_e^{n^*-1} T_o^{\alpha} \quad \text{(Damkohler number)} \qquad (2\text{-}52)^{**}$$

** In Eqn. (2-52), use has been made of the assumption that the kinetic energy is small compared to the thermal energy, in the external stream of the boundary layer. Thus the approximation

$$T_e \cong T_o$$

could be used.

$$F \equiv \theta h_{t_e} - \sum_i y_i h_i^o - \frac{u_e^2 (f')^2}{2 g_c J_c} + C_p T_u \tag{2-53}$$

$$B_i \equiv (\nu_i' - \nu_i'') W_i / \hat{W} \tag{2-54}$$

In order to complete the formulation of the "transformed problem", the above ordinary differential equations describing the "locally similar" boundary layer must be subjected to boundary conditions at the gas-solid interface ($\eta = 0$) and the boundary layer edge ($\eta = \infty$). These boundary conditions are obtained by transforming Eqns. (2-20) through (2-26) using Equations (2-27), (2-28) and (2-31) through (2-34), to yield:

Momentum boundary conditions

(i) $f'(0) = 0$ (no slip) (2-55)

(ii) $f'(\infty) = 1$ ($u = u_e$ at boundary layer edge) (2-56)

(iii) $f(0) = \frac{-\rho_s A_s}{\sqrt{\rho_e \mu_e}} p^{n_s} \sqrt{\tau_f} \exp\left[\frac{-E_s C_p}{R^o F_w}\right]$ (pyrolysis law) (2-57)

Energy boundary conditions

(iv) $h_{t_e} \theta'(0) - \sum_i y_i'(0) h_i^o = -Pr\, f(0) \left[L + \frac{C_s}{C_p} (\theta(0) h_{t_e} - \sum_i y_i(0) h_i^o)\right]$

(energy balance at interface) (2-58)

(v) $\theta(\infty) = 1$ ($h_t = h_{t_e}$ at boundary layer edge) (2-59)

Species boundary conditions

(vi) $y_i'(0) = -Sc\, f(0) \left[y_i(0) - (y_{i_w})\right]$ (species balance at interface) (2-60)

(vii) $y_i(\infty) = y_{i_e}$ (a specified constant) (2-61)

It is to be noted that in the above system of equations, describing the "transformed problem", all derivatives are with respect to η, while ξ (or x) appears in the equations only as a parameter. This consequence of the "locally similar" approximation is also used to advantage in defining the characteristic flow time, τ_f, with respect to the parameter x. Since the Damkohler number, D_1, is defined herein as the ratio of this flow time to a characteristic chemical reaction time (see Eqn. (2-52)), it also becomes a function of the streamwise co-ordinate. The usefulness of this will become clearer in the next chapter. For the present, it is sufficient to recognise that the state of non-equilibrium that usually prevails in a chemically reacting flow is characterised by finite values of the Damkohler number. Very small values of this number (i.e., $D_1 \to 0$) represent a frozen flow situation. Physically this implies that no chemical reaction occurs in the boundary layer and all profiles are established purely by processes of convection and diffusion. On the other hand, in the limit of very large Damkohler numbers (i.e., $D_1 \to \infty$) the chemical reaction occurs infinitely fast corresponding to an equilibrium flow situation.

CHAPTER III

DEVELOPMENT OF A NUMERICAL SOLUTION TECHNIQUE - THE METHOD OF PARAMETRIC DIFFERENTIATION

Introduction

The system of conservation equations governing the reacting boundary layer, as formulated in Chapter II, is strongly coupled and non-linear.

In general, the numerical solution of such systems poses serious mathematical difficulties as well as requires a considerable amount of computation time. In the past, a variety of numerical solution techniques have been applied. Notable amongst these are the methods of gradients[19] (or steepest ascent[20]), invariant imbedding[21], finite differences[22], integral matrix[23], and quasilinearisation[24].

Among these methods, the method of quasilinearisation has been most frequently applied in recent years in the solution of the class of reacting boundary layer problems discussed in this thesis (e.g., see References 25 and 26). Although this method produces the desired solutions, its iterative nature requires considerable computer time, whose length depends on the "closeness" of the initial guess to the final solution. In this chapter, a novel numerical technique, the method of parametric differentiation (abbreviated here as MPD), will be developed for the efficient solution of the "locally similar" system of differential equations (i.e., Eqns. (2-44) to (2-46)) subject to the general boundary conditions given by Eqns. (2-55) to (2-61).

The MPD

The MPD was first proposed by Kiriya[27] and Davidenko[28] in the early fifties for solving systems of non-linear algebraic equations. Later,

Rubbert and Landahl[29] developed a variant of the method suitable for certain classes of fluid - mechanical problems, including the Falkner-Skan incompressible boundary layer problem[30]. More recently, Narayana and Ramamoorthy[31] used the MPD to analyse the behaviour of a compressible laminar boundary layer.

As the name suggests, the MPD consists of differentiating the original non-linear equations and boundary conditions with respect to a parameter that may be present in the differential equations, or boundary conditions, or both. This procedure reduces the solution of the original non-linear boundary value problem to the solution of a linear boundary value problem and a non-linear initial value problem. These resulting problems are considerably easier to handle numerically.

For instance, consider solving the following two-point, non-linear boundary value problem using the MPD:

$$\frac{d^2y}{dx^2} = \alpha\, xy^2, \quad x_1 < x < x_2 \tag{3-1}$$

subject to the boundary conditions:

$$y(x_1) = C_1 = \text{constant}$$

$$y(x_2) = C_2 = \text{constant}$$

where α is a parameter in the differential equation.

Differentiating the above system with respect to α yields the following linear boundary value problem (LBVP) for $p = \partial y/\partial\alpha$:

$$\frac{d^2p}{dx^2} = xy^2 + 2\alpha xyp, \quad x_1 < x < x_2 \tag{3-2}$$

subject to the boundary conditions

$$p(x_1) = 0$$

$$p(x_2) = 0$$

together with the following non-linear initial value problem (NLIVP) for y:

$$\frac{\partial y}{\partial \alpha} = p(x, y, \alpha), \quad \alpha > \alpha_i \tag{3-3}$$

subject to some initial condition; say

$$y(\alpha_i) = y_o$$

The LBVP may be easily integrated numerically provided the variable coefficients in Eqn. (3-2) are known. In the present example, the solution of Eqn. (3-1) in the limit when $\alpha = 0$ can be shown by inspection to be

$$y = \left(\frac{C_1 - C_2}{x_1 - x_2} \right)(x - x_1) + C_1 \tag{3-4}$$

Thus, the solution procedure would be conveniently started by solving the LBVP (Eqn. (3-2)) for the case $\alpha = 0$. In this case, the above solution for y will be used to determine the variable coefficients in the Eqn. (3-2). Then knowing $p(x,y,0)$, one may proceed with the solution of the NLIVP (Eqn. (3-3)) to obtain $y(x, \Delta\alpha)$, where $\Delta\alpha$ is a small increment in the parameter α. Repeating this procedure, the method marches explicitly in α producing a family of solutions for different values of the parameter α until reaching the value of the parameter characteristic of the particular problem under consideration. In the next section this general procedure is first applied to the solution of some simple problems, with a view of finding the most suitable parameter for differentiation in the present analysis.

Application of the MPD to Some Simple Boundary Layer Problems

As a first step in the development of the MPD, the compressible boundary layer problem previously solved in Reference 31 was considered. In this study the MPD had been successfully applied to the solution of a coupled system of momentum and energy equations in "similar" form. These equations were differentiated with respect to the Falkner-Skan parameter (β). In the present study, as an initial attempt in the application of the MPD, the solution of the "similar" momentum and energy equations with zero pressure gradient was considered. However, in the present analysis the Prandlt number was used as the parameter for differentiation. Solutions were obtained by marching in Prandlt number (Pr) from Pr = 0 to Pr = 1 and good agreement with the results of Reference 31 was obtained.

It turns out, however, that the Prandlt number is a poor parameter for use in the MPD. This is because of the sensitivity of the thermal boundary layer thickness to the magnitude of the Prandlt number. For small values of the Pr number the integration of the LBVP has to be carried out across an unduly thick boundary layer. This not only increases the computation time considerably but also results in the possibility of greater accumulation of numerical errors. Furthermore, in the limit of Pr = 0 it should be pointed out that an apparent ambiguity exists. Physically, this limit corresponds to an inviscid flow situation with no viscous boundary layer at all. However, it is seen from the momentum and energy equations that govern the flow that the $f(\eta)$ related profiles are not directly influenced by the Prandlt number. Thus, the mathematically correct starting solutions to use in

the MPD correspond to the usual $f(\eta)$ related profiles and a temperature profile that consists of a linear variation of the temperature between the wall and the boundary layer edge. It should also be noted that although the thermal boundary layer is expected to be infinitely thick when Pr = 0, in practice only a certain critical finite thickness for the boundary layer was found to be important. For this case, the critical thickness corresponded to a value of $\eta = 15$. If a thinner boundary layer was considered during the solution of the LBVP, the expected asymptotic solutions were not obtained. For thickness greater than $\eta = 15$, the solutions for the boundary layer profiles remained virtually unchanged to within the increased numerical error that would be expected to accumulate for larger intervals of integration.

The next step in the development involved the search for an alternative, more efficient, parameter for the solution of the reacting boundary layer equations formulated earlier (i.e., Eqns. (2-44) through (2-46)). However, the boundary conditions were simplified by assuming a constant wall temperature distribution T_w and a constant value for the wall blowing rate f(0). The resulting system of "similar" equations was then solved using the MPD. First, the Schmidt number (= Pr in this analysis) was again used as the parameter for differentiation and solutions were obtained by marching in Sc from zero to one. Next, the Damkohler number, which appears explicitly in the chemical rate term of the species equation (i.e., Eqn. (2-46b)), was used as the parameter for differentiation in the same problem. Solutions were obtained by marching in D_1 from zero to about 400. The solutions could be carried beyond this value if desired. These solutions agreed well with those obtained

earlier, using the Sc number as the parameter for differentiation. It was found, however, that when D_1 was used as the parameter there was no need to integrate over unduly large boundary layer thicknesses. Also, the final solutions were expected to be more accurate numerically because of less accumulated error. Furthermore, D_1 proved to be a convenient parameter since solutions were readily available in the limit of $D_1 = 0$, which corresponds to frozen flow conditions. In this limit the momentum, energy and species profiles are determined purely by diffusion and convection processes and may be expressed by the well-known Crocco relations applicable for the case Pr = Sc = 1. This is further discussed in the next section together with the extension to the more realistic cases where Pr and Sc numbers are not unity.

The success in obtaining a solution using Schmidt number as the parameter for the "similar" reacting boundary layer problem with a constant wall temperature and blowing rate might lead one to explore the possibility of using the Sc number also as the parameter for the erosive burning problem formulated in this thesis. It turns out, however, that there is a difficulty that arises in this case which may be instructive to follow through. In the limiting case of Sc = 0 (which implies $\mu_e \to 0$) it becomes troublesome to obtain the starting solutions for the MPD because the wall blowing rate becomes infinite (see boundary condition, Eqn. (2-57)). Some iterative procedure is therefore needed to establish solutions at some value of Sc number close to zero, so that these could be used instead as the starting solutions for the MPD. Although this is a theoretically feasible way of circumventing the above-mentioned difficulty, it would reduce the attractiveness of the MPD by decreasing

the overall efficiency of the solution procedure.

Solutions to the Present Problem of Erosive Burning Using the MPD

Having established the advantages of using the Damkohler number as the parameter for differentiation in applying the MPD to the solution of the "similar" reacting boundary layer equations, the problem of laminar erosive burning as formulated earlier, in Chapter II, was solved. In this case the wall blowing rate, temperature and mass fractions may all be x-dependent as they are governed by general interface boundary conditions - the pyrolysis law, the energy balance and the species balance at the gas-solid interface. As pointed out before, the "locally similar" system of equations (i.e., Eqn. (2-44) through (2-46) and the boundary conditions given by Eqns. (2-55) through (2-61)) contain x as a parameter only. Thus, the solutions are "similar" about any one x-location, although they may vary in a completely non-similar manner in the flow field. The gas phase flow is also characterised by arbitrary values of Pr and Sc numbers.

A. Starting Solutions

The solution procedure starts by establishing solutions to the problem for Damkohler number equal to zero. As mentioned earlier, in this limiting case the flow within the boundary layer is chemically frozen and all boundary layer profiles are established purely by convection and diffusion. This fact becomes evident when one inspects the system of conservation equations (i.e., Eqns. (2-44) through (2-46)) in the limit $D_1 = 0$. In the special case when $Pr = Sc = 1$, the momentum, energy and species equations are identical in form and the enthalpy and mass fraction

profiles are linearly related to the velocity profile within the boundary layer. Thus, the solutions to the energy and species equations in this limiting case may be written as follows:

$$\theta(\eta) = C_1 f'(\eta) + C_2 \tag{3-5}$$

$$y_i(\eta) = C_3 f'(\eta) + C_4 \tag{3-6}$$

where C_1, C_2, C_3 and C_4 are arbitrary constants that may be easily determined from the boundary conditions. These are the well-known Crocco integrals.

However, in order to solve the problem for a general Pr number, the Crocco relations (i.e., Eqns. (3-5) and (3-6)) have to be replaced by the following equations:

$$\theta(\eta) = C_1 \int_0^{\eta} (f'')^{Pr}\, d\eta + C_2 \tag{3-7}$$

$$y_i(\eta) = C_3 \theta(\eta) + C_4 \tag{3-8}$$

Again, C_1, C_2, C_3 and C_4 may be easily determined from the boundary conditions. Equations (3-7) is the analytical solution of the total energy equation (i.e., Eqn. (2-45)) and is valid for arbitrary values of Pr and Sc numbers. Equation (3-8) follows from the identical forms of the energy and species equations (Eqns. (2-45) and (2-46b)) in the limit of $D_1 = 0$. Combining Equations (3-7) and (3-8) with the interface conditions (i.e., Eqns. (2-57), (2-58) and (2-60)) leads to the following non-linear algebraic equation for the wall blowing rate, f(o), valid for general Pr (or Sc) numbers:

$$h_{t_e}\,\Gamma(o) - y_{1_e}\,\Gamma(o)(h_1^o - h_2^o) + Pr\ L = Pr\ C_s\ T_u + \left\{\frac{Pr\ E_s\ C_s}{R^o \ell n\left[\frac{-f(o)}{K\sqrt{\tau_f}}\right]}\right\} + \Gamma(o)\left[h_2^o - C_p\ T_u - \left\{\frac{E_s\ C_p}{R^o \ell n\ \frac{-f(o)}{K\sqrt{\tau_f}}}\right\}\right] \qquad (3\text{-}9)$$

where

$$K \equiv \rho_s\ A_s\ p^{n_s}/(\sqrt{\rho_e \mu_e}) \qquad (3\text{-}10)$$

$$\Gamma(o) \equiv \frac{(f''(o))^{Pr}}{f(o)\int_o^\infty (f'')^{Pr}\,d\eta} \qquad (3\text{-}11)$$

Equation (3-9) may be solved numerically using a "bisection technique" (see Reference 32), applicable in general to non-linear algebraic equations. The method consists of first guessing a value for f(o), obtaining the corresponding solution to the momentum equation

$$f''' + ff'' = 0 \qquad (3\text{-}12)$$

subject to the boundary conditions

$$f'(o) = 0$$

$$f(o) = f_w$$

$$f'(\infty) = 1$$

to yield f"(o), and then evaluating the definite integral $\int_o^\infty (f'')^{Pr}\,d\eta$, using Simpson's rule[33]. The procedure was repeated according to the "bisection technique" for several other values of f(o) until the root was located. In this study the solution to the momentum equation above was

obtained using a "shooting technique" which consisted of guessing a value for f"(o), f(o) and f'(o) being known, and integrating the Blasius equation using Runge Kutta (fourth order) and Hamming's modified predictor-corrector[34] techniques. This integration was performed treating the problem as an initial value problem up to the edge of the boundary layer (i.e., $\eta \cong 8$). Then a new guess was made for f"(o), based on the following empirically derived convergence criterion:

$$f''_{j+1}(o) = \frac{f''_j(o)}{f'_j(\infty)} \tag{3-13}$$

where j is the iteration index. The process was repeated until the solutions converged to their respective values at the edge of the boundary layer. Convergence was found to occur usually in less than five iterations and the computational time involved was very short.

Having found the blowing rate f(o) (as described above) and the corresponding solutions to the momentum equation, in the limit of $D_1 = 0$, the "energy" and "species" solutions could all be obtained by using Eqns. (3-7) and (3-8). Thus the complete solution to the problem could be easily established for the limiting case of $D_1 = 0$.

B. The Parametrically Differentiated Problem

The LBVP and the NLIVP (referred to in the Introduction to this chapter) resulting from the differentiation of the present non-linear boundary value problem (i.e., Eqns. (2-44) through (2-61)) with respect to the parameter D_1, will now be obtained. Defining the parametrically differentiated dependent variables as

$$q \equiv \frac{\partial f}{\partial D_1} \tag{3-14a}$$

$$r \equiv \frac{\partial \theta}{\partial D_1} \tag{3-14b}$$

$$p_i \equiv \frac{\partial y_i}{\partial D_1} \quad , \; i = 1 \tag{3-14c}$$

and differentiating both sides of the differential equations with respect to D_1, one gets the "parametrically differentiated" momentum, energy and species equations. For convenience in numerical integration, these differential equations in q, r and p_i are then expressed as a system of seven first order differential equations, as follows:

$$\begin{bmatrix} y_1' \\ y_2' \\ y_3' \\ y_4' \\ y_5' \\ y_6' \\ y_7' \end{bmatrix} = \begin{bmatrix} 0 & 0 & 0 & 0 & 1 & 0 & 0 \\ 1 & 0 & 0 & 0 & 0 & 0 & 0 \\ 0 & 0 & 0 & 1 & 0 & 0 & 0 \\ 0 & -Pr\theta' & 0 & -Prf & 0 & 0 & 0 \\ 0 & -f'' & 0 & 0 & -f & 0 & 0 \\ 0 & 0 & 0 & 0 & 0 & 0 & 1 \\ E_1 & -Scy_1' & E_2 & 0 & 0 & E_3 & -Scf \end{bmatrix} \begin{bmatrix} y_1 \\ y_2 \\ y_3 \\ y_4 \\ y_5 \\ y_6 \\ y_7 \end{bmatrix} + \begin{bmatrix} 0 \\ 0 \\ 0 \\ 0 \\ 0 \\ 0 \\ ScC_1 \end{bmatrix} \tag{3-15}$$

For the sake of brevity in expressing the above system of equations, the following definitions are enployed:

$$y_1 \equiv q' \tag{3-16a}$$

$$y_2 \equiv q \tag{3-16b}$$

$$y_3 \equiv r \tag{3-16c}$$

$$y_4 \equiv r' \tag{3-16d}$$

$$y_5 \equiv q'' \tag{3-16e}$$

$$y_6 \equiv p_1 \tag{3-16f}$$

$$y_7 \equiv p_1' \tag{3-16g}$$

$$C_1 \equiv B_1\left(\frac{F}{C_p T_e}\right)^{\alpha} \exp\left[\frac{-EC_p}{R^o F}\right] y_1^{a_1} \tag{3-17a}$$

$$C_2 \equiv D_1 B_1 \exp\left[\frac{-EC_p}{R^o F}\right] y_1^{a_1} \tag{3-17b}$$

$$C_3 \equiv D_1 B_1\left(\frac{F}{C_p T_e}\right)^{\alpha} \exp\left[\frac{-EC_p}{R^o F}\right] a_1 y_1^{a_1-1} \tag{3-17c}$$

$$C_4 \equiv C_2\left(\frac{F}{C_p T_e}\right)^{\alpha}\left\{\frac{\alpha}{F} + \frac{EC_p}{R^o F^2}\right\} \tag{3-17d}$$

$$E_1 \equiv -Sc\ C_4 \frac{u_e^2 f'}{g_c J_c} \tag{3-18a}$$

$$E_2 \equiv Sc\ C_4\ h_{t_e} \tag{3-18b}$$

$$E_3 \equiv Sc\left\{C_3 - C_4(h_1^o - h_2^o)\right\} \tag{3-18c}$$

The y_k ($k = 1,2....7$) represent the dependent variables that characterise the LBVP. To complete the formulation of this problem seven linear boundary conditions are needed. These are obtained by differentiating Equations (2-55) through (2-61) with respect to D_1, to yield:

$$\text{i)}\quad y_1(o) = 0 \tag{3-19a}$$

$$\text{ii)}\quad y_1(\infty) = 0 \tag{3-19b}$$

$$\text{iii)}\quad y_2(o) + G_1\, y_3(o) + G_2\, y_6(o) = 0 \tag{3-19c}$$

where

$$G_1 \equiv K\sqrt{\tau_f} \exp\left[\frac{-E_s C_p}{R^o F_w}\right]\left\{\frac{E_s C_p}{R^o F_w^2}\right\} h_{t_e}$$

$$G_2 \equiv - \frac{G_1}{h_{t_e}} (h_1^o - h_2^o)$$

$$F_w \equiv \theta(o)\, h_{t_e} + y_1(o)(h_2^o - h_1^o) - h_2^o + C_p T_u$$

iv) $$G_3 y_2(o) + G_4 y_3(o) + h_{t_e} y_4(o) + G_5 y_6(o) + (h_2^o - h_1^o) y_7(o) = 0 \qquad (3\text{-}19d)$$

where

$$G_3 \equiv Pr \left\{ L + \frac{C_s}{C_p} (\theta(o) h_{t_e} + y_1(o)(h_2^o - h_1^o) - h_2^o) \right\}$$

$$G_4 \equiv Pr \frac{C_s}{C_p} f(o)\, h_{t_e}$$

$$G_5 \equiv - \frac{G_4}{h_{t_e}} (h_1^o - h_2^o)$$

v) $$y_3(\infty) = 0 \qquad (3\text{-}19e)$$

vi) $$G_6 y_2(o) + G_7 y_6(o) + y_7(o) = 0 \qquad (3\text{-}19f)$$

where

$$G_6 \equiv Sc \left[y_1(o) - (y_{1w})_- \right]$$

$$G_7 \equiv Sc\, f(o)$$

vii) $$y_6(\infty) = 0 \qquad (3\text{-}19g)$$

In addition to the above LBVP, the following NLIVP, which is directly related to the definitions given in Equations (3-14) and (3-16), is also obtained:

$$\frac{\partial f}{\partial D_1} = q\ (\eta, D_1) \tag{3-20a}$$

$$\frac{\partial f'}{\partial D_1} = q'\ (\eta, D_1) \tag{3-20b}$$

$$\frac{\partial f''}{\partial D_1} = q''\ (\eta, D_1) \tag{3-20c}$$

$$\frac{\partial \theta}{\partial D_1} = r\ (\eta, D_1) \tag{3-20d}$$

$$\frac{\partial \theta'}{\partial D_1} = r'\ (\eta, D_1) \tag{3-20e}$$

$$\frac{\partial y_1}{\partial D_1} = p_1\ (\eta, D_1) \tag{3-20f}$$

$$\frac{\partial y_1'}{\partial D_1} = p_1'\ (\eta, D_1) \tag{3-20g}$$

The solutions to the momentum, energy and species equations for $D_1 = 0$ (found earlier) serve as the initial conditions for the above equations.

C. Numerical Solution of the LBVP and the NLIVP

The LBVP in the present instance is of seventh order with seven corresponding boundary conditions. It is to be noted that three of these conditions are in the form of linear algebraic equations (i.e., Eqns. (3-19c), (3-19d) and (3-19f)), involving several of the dependent variables evaluated at $\eta = 0$. The remaining boundary conditions specify the values of the other dependent variables at the gas-solid interface ($\eta = 0$) or the boundary layer edge ($\eta \to \infty$). A non-iterative numerical scheme was used to obtain a solution to this LBVP. The method consisted of treating the $\eta = 0$ location as the initial point and the corresponding

boundary conditions as initial conditions. The LBVP was split into the solution of two initial value problems consisting of a homogeneous differential equation with Kronecker delta initial conditions and an inhomogeneous differential equation with the known initial conditions (i.e., the specified boundary conditions at $\eta = 0$) and null initial conditions for the remaining dependent variables. Then by solving a system of linear algebraic equations at the terminal point (i.e., the end point in the interval of integration), the missing boundary conditions were determined and the complete solution was constructed as the sum of the homogeneous and particular solutions. The details of this procedure are given in Appendix A. All integrations were performed using a Hamming's[34] modified predictor-corrector method. A local truncation error bound of 10^{-6} was maintained in the computations throughout the integration with respect to η, using single-precision accuracy.

The numerical solution of the NLIVP (see Eqn. (3-20)) was achieved using an Adams-Moulton predictor-corrector[33] scheme. The integration of this problem was done with respect to D_1 as the independent variable. A local truncation error bound of 10^{-4} was maintained during this integration, in single precision accuracy. It must be pointed out that the non-linearity of the original problem is contained in this NLIVP. Because of this, it is important to use numerically stable schemes of integration like the fourth-order Adams-Moulton method. Furthermore, the integration with respect to D_1 is an "explicit" one, and this also suggests the need for a stable integration scheme. Finally, it is to be emphasized that the use of the above predictor-corrector, instead of the often used fourth-order Runge-Kutta method, greatly increases the

overall efficiency of the solution procedure. This is generally true because the fourth-order Runge Kutta method requires the evaluation of the "derivative function" four times at every step of the integration, whereas an Adam's-Moulton scheme, once started, evaluates this only twice at every step. This becomes especially important in the present situation because the derivative function (which is the right hand side of each one of the Eqns. (3-20a) through (3-20g)) is available only after the complete LBVP has been solved. However, since the Adam's-Moulton method is not "self-starting"[33], the solutions at three Damkohler number stations, following $D_1 = 0$, are obtained using a fourth-order Runge Kutta method.

Using the solutions for $D_1 = 0$ for the variable coefficients in Eqn. (3-15), the LBVP is solved. Knowing these solutions and using the solutions for $D_1 = 0$ as initial conditions for the NLIVP, the complete solutions to the original problem are established at $D_1 = \Delta D_1$. That is, all boundary layer profiles for momentum, energy and species are obtained at the above value of D_1. Henceforth, the procedure "marches" in sufficiently small D_1 steps producing solutions to the problem at different values of D_1, until reaching the value of D_1 characteristic of the problem under consideration. This final value of D_1 depends, of course, upon the particular choice of values for the physico-chemical parameters governing the solid propellant burning situation, and on the external stream variables which are specified in this analysis.

Results and Discussion

Before presenting some typical results of the computations performed, it would be of interest to reconsider the definition of D_1 as

given by Equation (2-52)

$$D_1 \cong \frac{2x^{1-m}}{(m+1)G} Z \rho_e^{n^*-1} T_o^{\alpha}$$

Specializing the above expression to the present analysis where the gas phase chemistry is controlled by a first order reaction (i.e., $n^* = 1$) gives

$$D_1 = \frac{2x^{1-m}}{(m+1)G} Z T_o^{\alpha} \tag{3-21}$$

Since the modified frequency factor, Z, may be assumed to be a characteristic constant of the gas phase, the Damkohler number becomes an x-dependent quantity (i.e., $D_1 \sim x^{1-m}$). Therefore, as the solution procedure produces solutions for different Damkohler numbers, these solutions also describe the flow behaviour at different values of x.

It is to be expected physically that as the Damkohler number increases, the rate of chemical reaction increases and this leads to an increased heat transfer rate from the gas phase to the propellant surface. The result is a higher wall temperature and hence a faster regression rate for the solid propellant, as required by the pyrolysis law (see Eqn. (2-1)). Indeed, this was found to be the trend in Figure 2, which shows the variation of the wall blowing rate with Damkohler number. These solutions were obtained using the values of constants given in Appendix B under Case 1.

It is common in the boundary layer literature to find results valid for Pr = 1, as this assumption leads to greater mathematical simplicity. Figure 2 also shows the possibly significant effect of using more realistic values for the Pr and Sc numbers (e.g., Pr = Sc = 0.7). For Prandlt

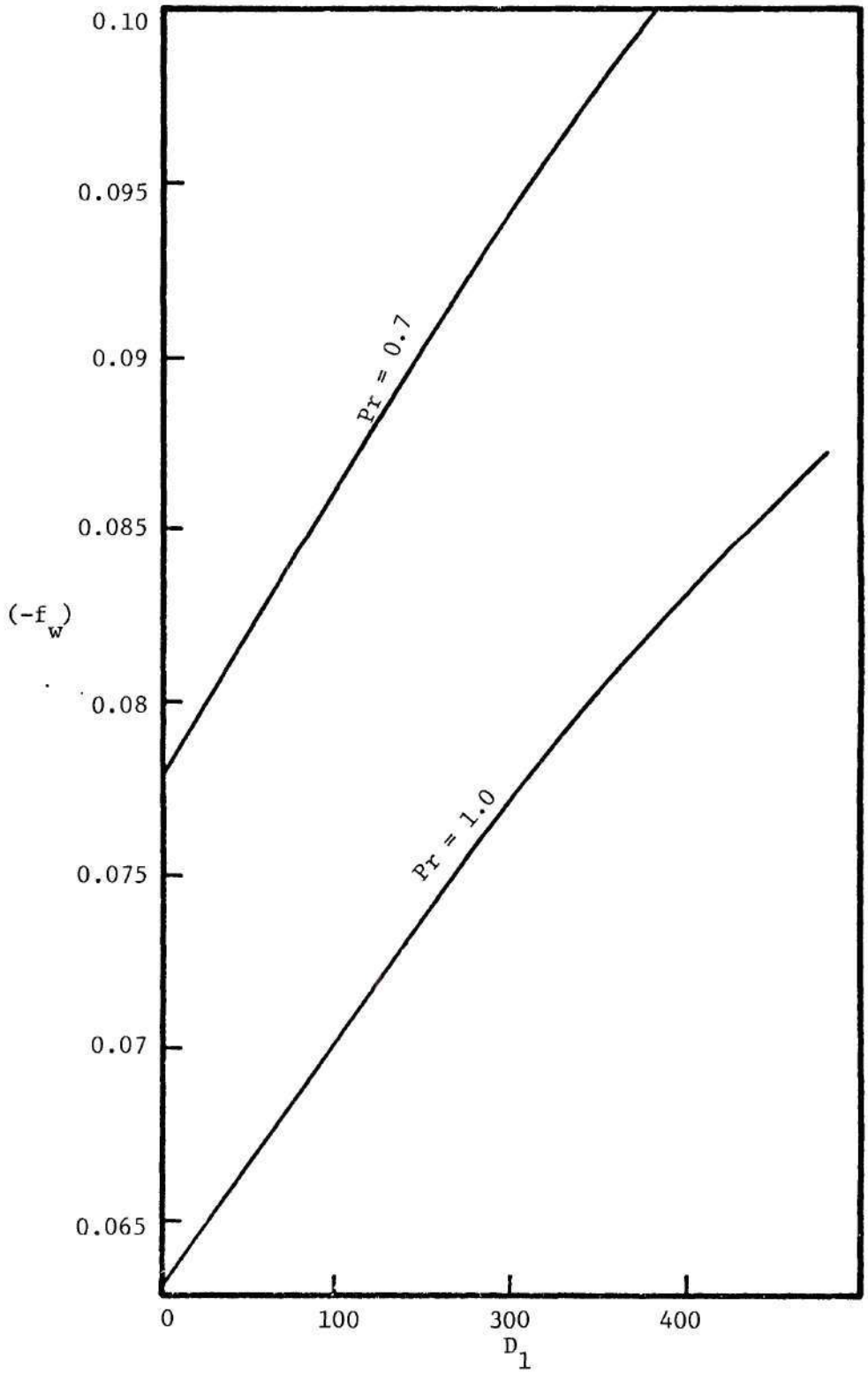

Figure 2. Variation of wall blowing rate ($-f_w$) with Damkohler number (D_1) for different Prandtl numbers (Pr).

numbers less than unity, the heat transfer from the gas to the interface would be increased, as expected from the definition of Prandlt number (see Eqn. (2-10)), and hence the regression rate would be faster; that is, f(o) increases in absolute magnitude.

Figures 3 and 4 show the corresponding temperature and reactant mass fraction profiles across the boundary layer for the same burning situation as before. The case of no combustion, represented by the frozen flow limit with $D_1 = 0$, is compared to a situation with a significant rate of combustion (i.e., $D_1 = 350$). Again, as pointed out earlier, the increased rate of chemical reaction occuring at $D_1 = 350$ produces a higher wall temperature because of the increased heat transfer rate to the propellant surface (see Figure 3). On the other hand, the effect on the reactant mass fraction is quite the opposite. The increased chemical reaction rate leads to a greater consumption of reactants which results in a lower reactant mass fraction at the propellant surface (see Figure 4). Furthermore, because of the faster rates of chemical reaction at $D_1 = 350$, the thickness of the distributed combustion zone would be smaller so that the "thermal" and "species" boundary layers would be reduced in thickness. This is also evident from Figures 3 and 4 as the temperature and species profiles converge to the specified external stream values at lower values of η when $D_1 = 350$ than in the case of $D_1 = 0$.

Figure 5 shows that within the boundary layer, the combustion rate has a negligible effect upon $f'(\eta)$, the x-component of velocity. The velocity profiles for $D_1 = 0$ and 350 remain virtually unchanged. Hence, the effect of the combustion manifests itself mainly through the energy

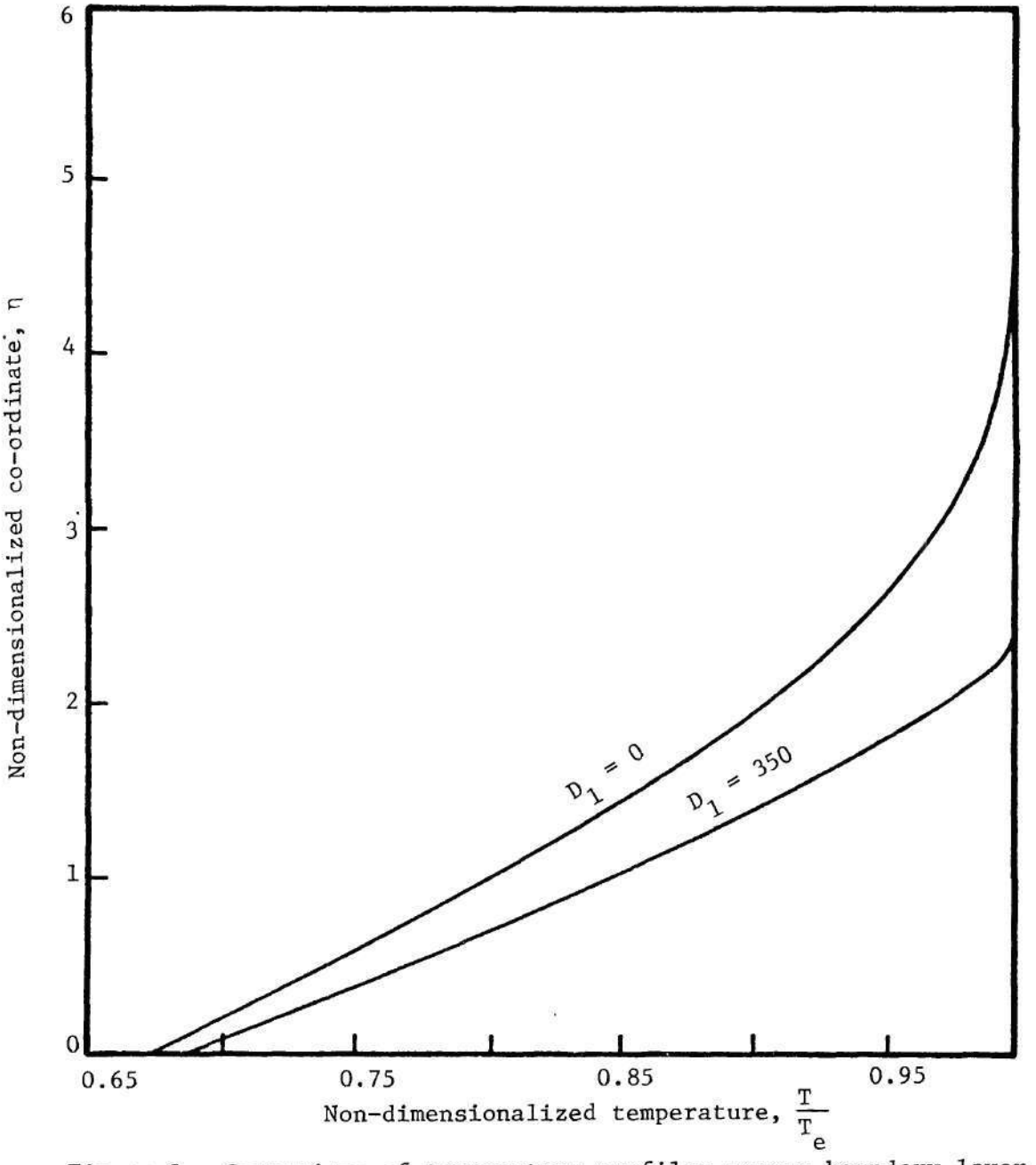

Figure 3. Comparison of temperature profiles across boundary layer with and without combustion for a general Pr = 0.7 (Sc = Pr).

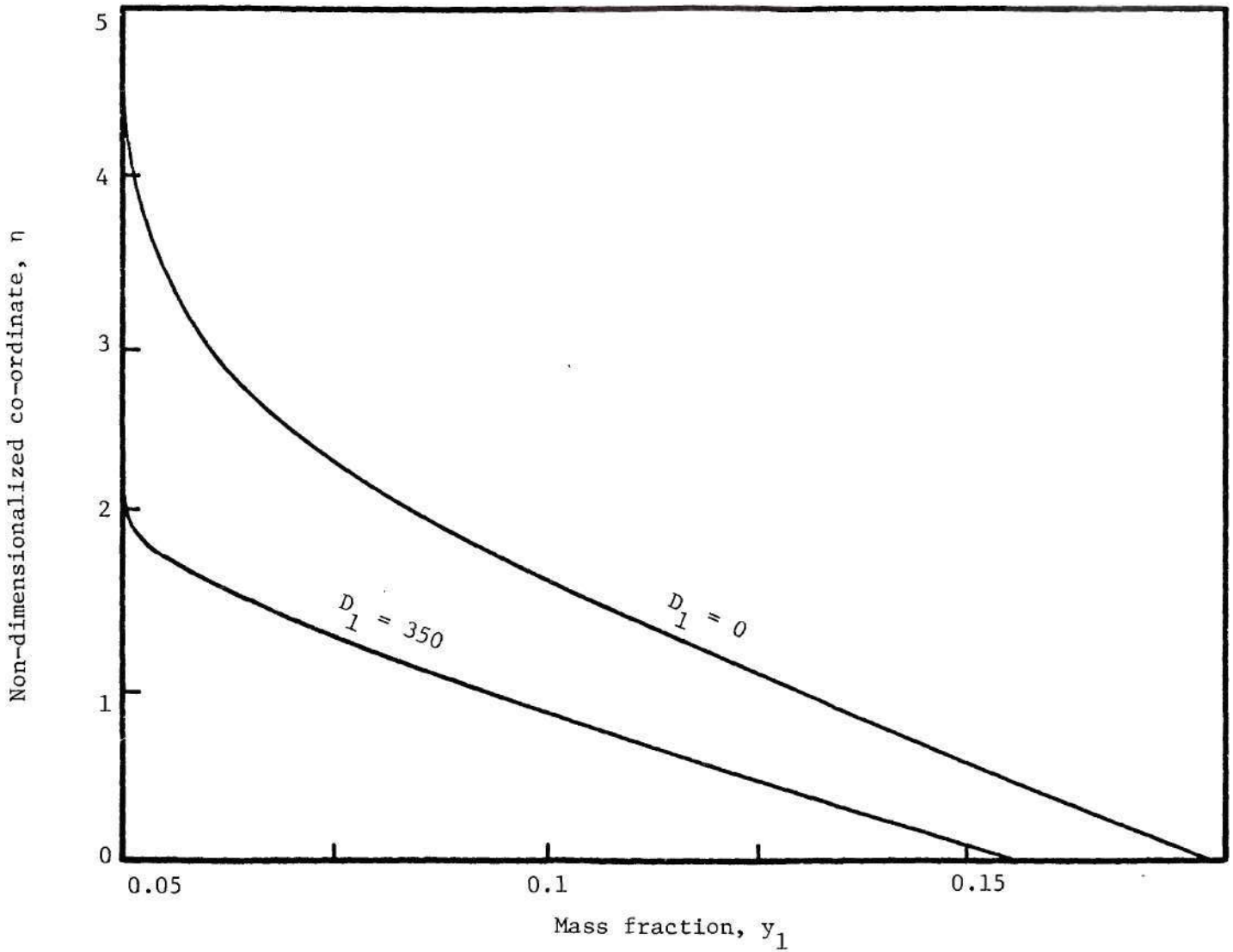

Figure 4. Comparison of reactant mass fraction profiles across boundary layer with and without combustion (Pr = Sc = 0.7).

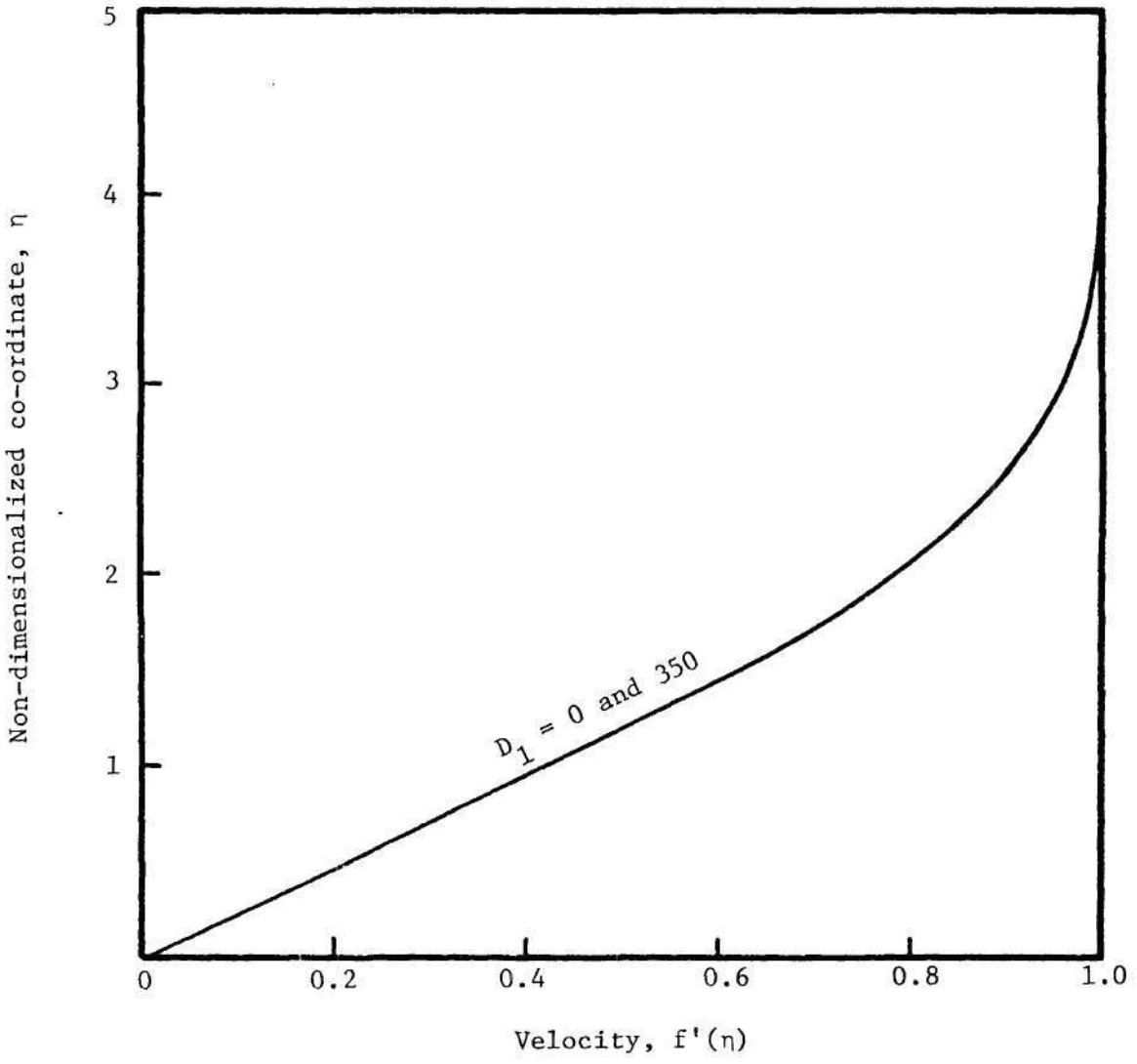

Figure 5. Comparison of velocity profile across boundary layer with and without combustion (Pr = Sc = 0.7).

and species variables (like temperature and mass fraction). This is to be expected since the energy and species differential equations as well as boundary conditions are strongly coupled (see Eqns. (2-45), (2-46b), (2-58) and (2-60)) and are directly affected by the combustion process through the chemical rate term. In contrast, the momentum equation which determines the velocity profile is decoupled from the remaining equations. This is due directly to the fact that the pressure gradient term of the momentum equation was expected to be negligible (see Assumption (g), Chapter II). Neglecting this term, which couples the velocity components within the boundary layer to the processes of combustion, is responsible for the behaviour exhibited in Fig. 5. It is also to be noted that a coupling is nevertheless present at the gas-solid interface through the pyrolysis law - which relates f(o) to the wall temperature (see Eqn. (2-57)). The effect of this coupling influences only the y-component of velocity at the interface (represented by f(o)). In fact, this latter effect is found to be significant, as shown earlier in Fig. 2, but not strong enough to alter $f'(\eta)$ over the D_1 range considered.

It must be pointed out that these results are only intended to represent the trends predicted by the steady state theory. The somewhat low range of values of the blowing rate parameter that occur are due to the particular choice of constants (see Case 1, Appendix B) used for this computer run. In the physically more realistic cases studied later for the unsteady analysis the typical magnitude of the blowing rate parameter, -f(o), was about 0.4. The general trends shown, however, remained the same.

For the cases discussed above solutions for the reacting flow field

were obtained by "marching" in D_1 from $D_1 = 0$ to $D_1 = 520$, with an average step size of $\Delta D_1 = 10$. The solution could be carried beyond the value $D_1 = 520$, if desired, until reaching the equilibrium limit, which corresponds to $D_1 \to \infty$. Physically, however, the meaningful final value of D_1 would be the one corresponding to the particular values of m, G, T_o and Z that characterize a given burning situation.

The computation time required to obtain the above solutions was about 17 seconds (CPU time on UNIVAC 1108) per step; that is the time required to determine all the boundary layer profiles of velocity, temperature and concentration for a given value of D_1, starting with known solutions at the previous step where the parameter equalled $D_1 - \Delta D_1$.

Although the results discussed so far were obtained for the case of $m = 1$ (see Case 1 in Appendix B), the results for the other two possible cases when $m \lesssim 1$ show similar qualitative trends. It is noteworthy in this regard that when m is unity, the Damkohler number has a certain characteristic constant value throughout the gas phase (see Eqn. (3-21)), corresponding to the particular reaction situation being considered. This implies that the solutions produced by the MPD for different Damkohler numbers represent "imaginary" solutions to the problem for burning situations with different chemical relaxation times. However, when $m \lesssim 1$, D_1 is a function of x. Therefore, in these latter cases the solutions obtained using the MPD apply at different x-locations. This attribute enhances the attractiveness of the MPD for the present problem even further and goes to show that the MPD can be used to yield in a single computer run, the solutions of a whole family of related,

physically interesting, problems. Table 1 shows the results of a computation performed for the case when m = 0.5, the other constants being described by the values given under Case 2 of Appendix B. The table shows the variation of the wall blowing rate, total enthalpy and reactant mass fraction with axial distance. Notice the "slow variation" of wall properties with x (or ξ), as required by the "local similarity" approximation that was used in the analysis.

Finally, the validity of the Lee's approximation was investigated. This approximation (see Assumption (g), Chapter II) permits the pressure gradient term of the momentum equation, that is,

$$\beta\left[\frac{\rho_e}{\rho} - (f')^2\right]$$

where $\beta \equiv -\frac{2\xi}{u_e}\frac{du_e}{d\xi}$ is the pressure gradient parameter, to be dropped in typical solid propellant burning situations since

$$\left[\frac{\rho_e}{\rho} - (f')^2\right] \to 0 \qquad (3\text{-}22)$$

Figure 6 shows the variation of the quantity in the above brackets across the momentum boundary layer. It is seen that this approximation is worse near the wall; it is better satisfied in the upper half of the boundary layer. However, it is expected that the integrated effect of this approximation across the entire boundary layer thickness is still small enough and therefore the approximation is reasonably good for the computation of the velocity profile. The error introduced through the approximation in the computation of the temperature and concentration profiles is expected to be even smaller. Thus, Lee's approximation

Table 1. Variation of wall properties with position downstream of the leading edge.

x	$-f(o) \times 10$	$\theta(o) \times 10$	$y_1(o) \times 10$
0.00001	5.5492	2.4716	7.6462
0.00453	5.5493	2.4715	7.6463
0.01727	5.5495	2.4714	7.6463
0.0674	5.5496	2.4713	7.6464
0.1048	5.5498	2.4711	7.6465
0.1504	5.5499	2.4710	7.6466
0.2042	5.5500	2.4709	7.6466
0.2663	5.5502	2.4708	7.6467
0.3365	5.5503	2.4707	7.6468
0.5017	5.5506	2.4704	7.6469
0.6998	5.5509	2.4702	7.6471
0.9307	5.5512	2.4699	7.6472
1.1945	5.5514	2.4697	7.6474
1.4912	5.5517	2.4695	7.6475
1.8208	5.5520	2.4692	7.6477
2.5785	5.5526	2.4687	7.6480
3.4677	5.5531	2.4683	7.6483
4.4884	5.5537	2.4678	7.6486
5.6406	5.5542	2.4673	7.6488
6.9243	5.5548	2.4668	7.6491
8.3395	5.5553	2.4664	7.6494
11.5644	5.5564	2.4654	7.6500
15.3152	5.5575	2.4645	7.6506

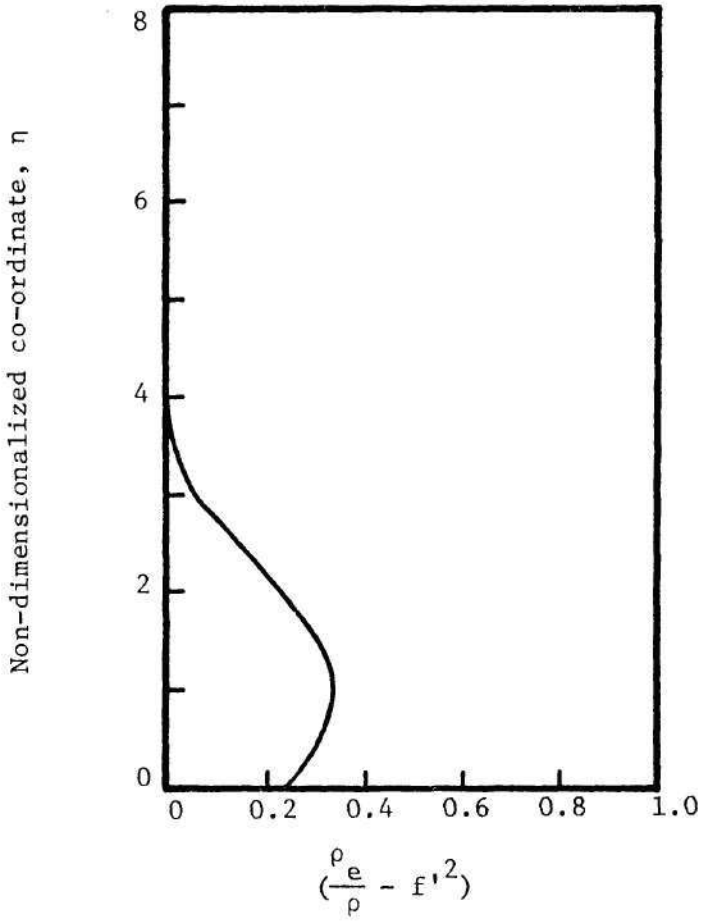

Figure 6. Verification of Lee's Approximation.

should be valid in the present study.

CHAPTER IV

UNSTEADY COMBUSTION RESPONSE ANALYSIS

The Model and its Assumptions

In this chapter an unsteady analysis is presented to determine the "pressure-and-velocity" coupled response of a burning solid propellant. The physical model for this analysis remains essentially the same as the one used in Chapter II for the steady-state analysis, earlier. However, in this case a longitudinal acoustic oscillation, parallel to the burning surface, is superimposed upon the steady-state flow in the external stream above the boundary layer. To keep the problem as simple as possible, yet physically meaningful, the following assumptions are made:

i) The longitudinal oscillations in the external stream are taken to be simple harmonic standing waves with a definite frequency corresponding to the fundamental mode of the combustor. Although the true acoustic wave pattern inside a rocket motor is usually complicated - consisting of several superimposed standing waves with frequencies corresponding to the various normal modes of the chamber - the higher frequencies tend to get damped out and one occasionally encounters just the fundamental mode.[9]

ii) The external stream oscillations are considered isentropic and chemically frozen. This assumption is compatible with the notion of a boundary layer within which effects like diffusion and chemical reaction are predominant while the external flow is regarded as being isentropic in comparison.

iii) Only small amplitude, acoustic type oscillations are considered.

iv) Since it is true for a wide class of propellants that the gas phase

responds to oscillations much faster than the solid phase[1,2], the present model treats the solid as being completely unsteady while the gas phase is considered "quasi-steady".

v) It is assumed that a constant amplitude, periodic behavior prevails throughout the gas and solid phases; that is, after all transients have settled and "steady periodic"behavior is established.

vi) The "local similarity" approximation is used to describe the boundary layer flow.

vii) The assumptions of the steady-state theory, presented in Chapter II, apply here also.

Solid Phase Analysis

Under the assumptions pertaining to the solid phase (that is, Assumptions (j) through (m) of Chapter II and Assumption (iv) above), the equation describing the solid phase behavior is the energy conservation equation - the continuity and momentum conservation being satisfied. Hence, the behavior of the solid phase is described by

$$\frac{\partial T}{\partial t} + \dot{r}\,\frac{\partial T}{\partial y} = \alpha_s\,\frac{\partial^2 T}{\partial y^2} \quad , \quad -\infty < y < 0 \tag{4-1a}$$

subject to the boundary conditions:

(interface energy balance)

a) $$\lambda\,\frac{\partial T}{\partial y}\bigg|_{y=0^+} = \lambda_s\,\frac{\partial T}{\partial y}\bigg|_{y=0^-} + \rho_s\,\dot{r}\,L \tag{4-1b}$$

(temperature equals that of the cold solid)

b) $$T = T_u, \text{ as } y \to -\infty \tag{4-1c}$$

It is to be noted that no initial conditions need be imposed since only "steady periodic" solutions are sought. Also, the co-ordinate system is

still considered fixed to the solid-gas interface, even though this interface now oscillates with a small amplitude about a mean position. It has been shown [1,35,36] that the additional terms that are introduced into the analysis through an inertial frame of reference are of negligible importance here. This is the case in the present linear analysis because these terms are an order of magnitude smaller than the terms being retained.

The system described by Eqn. (4-1) is non-dimensionalised using the following steady-state quantities as reference

$$T_r \equiv \bar{T}_e \tag{4-2a}$$

$$y_r \equiv \frac{\alpha_s}{\dot{\bar{r}}} \tag{4-2b}$$

$$t_r \equiv \frac{\alpha_s}{\dot{\bar{r}}^2} \tag{4-2c}$$

to obtain the following non-dimensional energy equation

$$\frac{\partial H}{\partial \tau} + R \frac{\partial H}{\partial \zeta} = \frac{\partial^2 H}{\partial \zeta^2} \quad , \; -\infty < \zeta < 0 \tag{4-3a}$$

subject to the boundary conditions

a) $$\left.\frac{\partial H}{\partial \zeta}\right|_{\zeta = 0^+} = \frac{\lambda s}{\lambda} \left[\left.\frac{\partial H}{\partial \zeta}\right|_{\zeta = 0^-} + \frac{C_P}{C_s} RL \right] \tag{4-3b}$$

b) $$H \;\; (\zeta \to -\infty) = H_u \tag{4-3c}$$

where

$$R \equiv \frac{\dot{\bar{r}}}{\dot{r}} \tag{4-4}$$

$$H \equiv \frac{T}{\bar{T}_e} \tag{4-5}$$

$$\zeta \equiv \frac{y\dot{\bar{r}}}{\alpha_s} \tag{4-6}$$

Now, since the oscillations are of small amplitude (Assumption (iii)), all unsteady quantities may be considered to consist in general of a space and time dependent perturbation superposed on the space dependent steady-state solution. Consider the following expansions expressed in terms of non-dimensional quantities:

$$R(\tau) = 1 + R_1(\tau) \tag{4-7}$$

$$H(\zeta,\tau) = \bar{H}(\zeta) + H_1(\zeta,\tau) \tag{4-8}$$

where the small perturbations in the regression rate and the temperature are required to satisfy the conditions $|R_1| << 1$ and $|\frac{H_1}{\bar{H}}| << 1$, respectively.

By substituting Equations (4-7) and (4-8) into Eqn. (4-3), and separating the various orders of magnitude, the following systems are obtained:

Zeroth order problem, $O(\bar{H}$ or $\bar{R})$

$$\frac{d\bar{H}}{d\zeta} = \frac{d^2\bar{H}}{d\zeta^2}$$

subject to the boundary conditions

$$\bar{H}(0) = H_w$$

$$\bar{H}(\zeta \to -\infty) = H_u$$

The solution to this is simply the steady-state solution (see Chapter II) given by

$$\bar{H} = (\bar{H}_w - H_u)e^{\zeta} + H_u \equiv s\exp(\zeta) + H_u \tag{4-9}$$

where $$s \equiv \bar{H}_w - H_u = \frac{\bar{T}_w - T_u}{\bar{T}_e} \tag{4-10}$$

First order problem, $\mathcal{O}(H_1$ or $R_1)$

$$\frac{\partial H_1}{\partial \tau} + \frac{\partial H_1}{\partial \zeta} + R_1 \, se^{\zeta} = \frac{\partial^2 H_1}{\partial \zeta^2} \tag{4-11a}$$

subject to the boundary conditions

a) $$\left.\frac{\partial H_1}{\partial \zeta}\right|_{\zeta = 0^-} = \frac{\lambda}{\lambda_s} \left.\frac{\partial H_1}{\partial \zeta}\right|_{\zeta = 0^+} - \frac{C_p}{C_s} LR_1 \tag{4-11b}$$

b) $$H_1(\zeta \to -\infty) = 0 \quad \text{(since all disturbances die outside a finite thermal layer)} \tag{4-11c}$$

Equations (4-11) describe the behavior of the temperature perturbations within the solid phase. To solve this system, simple harmonic solutions (i.e., see Assumption (i)) having the following form are assumed.

$$H_1(\zeta,\tau) = \Phi(\zeta) \exp(i\Omega\tau) \tag{4-12}$$

$$R_1(\tau) = R_o \exp(i\Omega\tau) \tag{4-13}$$

where the non-dimensional frequency is defined by

$$\Omega \equiv \frac{\omega}{(\bar{r}^2/\alpha_s)} \tag{4-14}$$

Substituting Equations (4-12) and (4-13) into Eqns. (4-11), the following time independent problem for $\Phi(\zeta)$ is obtained:

$$\frac{d^2\Phi}{d\zeta^2} - \frac{d\Phi}{d\zeta} - i\Omega\Phi = R_o \, se^{\zeta} \tag{4-15a}$$

subject to the boundary conditions:

a) $$\left.\frac{d\Phi}{d\zeta}\right|_{\zeta = 0^-} = \frac{\lambda}{\lambda_s} \left.\frac{d\Phi}{d\zeta}\right|_{\zeta = 0^+} - \frac{C_p}{C_s} LR_o \tag{4-15b}$$

b) $$\Phi(\zeta \to -\infty) = 0 \tag{4-15c}$$

Equation (4-15a) is a linear, second order, inhomogeneous ordinary differential equation whose general solution can be constructed as the sum of a homogeneous solution and a particular solution. Obtaining these solutions using standard analytical methods one gets the following expression for Φ

$$\Phi(\zeta) = \left[\frac{\frac{\lambda}{\lambda_s} \frac{d\Phi}{d\zeta} \Big|_{\zeta = 0^+} - \frac{C_p}{C_s} LR_o - \frac{isR_o}{\Omega}}{\Lambda} \right] \exp(\Lambda\zeta) + \frac{isR_o}{\Omega} \exp(\zeta) \qquad (4\text{-}16)$$

Multiplying Equation (4-16) by $\exp(i\Omega\tau)$ provides an expression that describes the space and time dependence of the temperature perturbation in the solid phase; that is, $H_1(\zeta,\tau)$.

Evaluating $H_1(\zeta,\tau)$ at the solid-gas interface (i.e. $\zeta = 0$) gives the following expression for the surface temperature perturbation

$$H_1(0,\tau) = \frac{Je^{i\Omega\tau}}{\Lambda} + \frac{iR_1 s}{\Omega} \qquad (4\text{-}17)$$

where

$$\Lambda \equiv \frac{1}{2} + \frac{1}{2}\sqrt{1 + i4\Omega} \qquad (4\text{-}18)$$

$$J \equiv \frac{\lambda}{\lambda_s} \frac{d\Phi}{d\zeta} \Big|_{\zeta = 0^+} - \frac{C_p}{C_s} LR_o - \frac{isR_o}{\Omega} \qquad (4\text{-}19)$$

It is to be noted that Eqn. (4-17) contains the as yet unknown heat flux perturbation from the gas side, as characterised by the term $\frac{\lambda}{\lambda_s} \frac{d\Phi}{d\zeta} \Big|_{\zeta = 0^+}$. Equation (4-17) will be used in the next section to couple the solid phase with the gas phase, at their interface.

Gas Phase Analysis

Since the gas phase has been assumed to be "quasi-steady" (i.e., Assumption (iv)), one can start the gas phase analysis with the steady, compressible, 2-D form of the boundary layer conservation equations for

chemically reacting flows. These equations are presented in Chapter II (i.e., Eqns. (2-4) through (2-9) and Eqn. (2-19)). However, in the present analysis the dependent variables of momentum, total energy and species are also time-dependent quantities, although quasi steady-state prevails from instant to instant. Also, the Lees-Dorodnitsyn transformations, which depend on the density (i.e., see Eqn. (2-27)), are now time-dependent.

In this analysis it is expedient to transform the above mentioned system of basic conservation equations into an "incompressible" form using the following redefined co-ordinates:

$$\bar{\xi} \equiv \int_o^x \bar{\rho}_e \bar{\mu}_e \bar{u}_e dx' \tag{4-20a}$$

$$\eta \equiv \frac{\bar{u}_e}{(2\bar{\xi})^{1/2}} \int_o^y \rho(x,y',t)dy' \tag{4-20b}$$

where the superposed bars denote steady-state quantities. For convenience, the bar on ξ will be dropped henceforth. In terms of these co-ordinates, the following expansions are used to express the unsteady dependent variables in terms of a steady-state part and a small perturbation about the steady state:

$$\psi(\xi,\eta) = (2\xi)^{1/2}[\bar{f}(\eta) + f_1(\eta)] \tag{4-21}$$

$$u(\xi,\eta) = \bar{u}_e(\xi)[\bar{f}'(\eta) + f_1'(\eta)] \tag{4-22}$$

$$h_t(\xi,\eta) = \bar{h}_{t_e}(\xi)[\bar{\theta}(\eta) + \theta_1(\eta)] \tag{4-23}$$

$$y_i(\xi,\eta) = y_{i_e}(\xi)[\bar{g}_i(\eta) + g_{i_1}(\eta)], \text{ or simply,}$$

$$y_i(\eta) = \bar{y}_i(\eta) + y_{i_1}(\eta) \tag{4-24}$$

With the help of Eqns. (4-20) through (4-24), the system of differential equations (i.e., Eqns. (2-4) through (2-9)) describing the conservation of overall mass, momentum, total energy and species is transformed to yield a system of equations in terms of the above non-dimensional variables (i.e., $\bar{f}, f_1$ etc.) and the redefined co-ordinates ξ and η. Then, separating terms of different orders of magnitude, and keeping in mind the assumptions of the steady-state analysis of Chapter II, two systems of equations are obtained. To zeroth order (i.e., $O(\bar{f}, \bar{\theta}$ or $\bar{y}_i)$) the equations are identical to the steady-state system (i.e., Eqns. (2-44) through (2-46)). However, to first order, the following system of equations describing the behavior of the perturbations in the gas phase is obtained (see Appendix C for derivation):

Momentum

$$f_1''' + \bar{f} f_1'' + \bar{f}'' f_1 = \frac{2\xi}{\bar{u}_e} \frac{d\bar{u}_e}{d\xi} \left[2\bar{f}' f_1' - \left\{ \frac{\bar{\rho}_e}{\bar{\rho}} \right\} \left\{ \frac{\rho_{e_1}}{\bar{\rho}_e} + \frac{2u_{e_1}}{\bar{u}_e} - \frac{\rho_1}{\bar{\rho}} + \ldots \right. \right.$$

$$\left. \left. \ldots + \bar{u}_e \frac{\frac{\partial}{\partial \xi} \left\{ \frac{u_{e_1}}{\bar{u}_e} \right\}}{\frac{d\bar{u}_e}{d\xi}} \right\} \right] - \bar{f}''' \left\{ \frac{p_1}{\bar{p}} \right\} \quad (4\text{-}25)$$

Energy

$$\frac{1}{Pr} \theta_1'' + \bar{f} \theta_1' + \bar{\theta}' f_1 = - \frac{1}{Pr} \bar{\theta}'' \left\{ \frac{p_1}{\bar{p}} \right\} \quad (4\text{-}26)$$

Species

$$\frac{1}{Sc} y_{i_1}'' + \bar{f} y_{i_1}' + \bar{y}_i' f_1 = - \frac{2\xi \left\{ \frac{\omega_i}{\rho} \right\}}{\bar{u}_e^{\,2} \bar{\rho}_e \bar{\mu}_e} 1 - \frac{1}{Sc} \bar{y}_i'' \left\{ \frac{p_1}{\bar{p}} \right\} \quad (4\text{-}27)$$

$$i = 1, 2 \ldots N-1$$

Now the term $\left(\frac{\omega_i}{\rho}\right)_1$ appearing on the right hand side of the species equation can be expressed in terms of the pertinent dependent variables of this analysis. To do this a reaction rate law in the same form as formulated earlier for the steady-state analysis is used; that is,

$$\frac{\omega_i}{\rho} = - ZB_i T^{\alpha} \rho^{n^*-1} \exp\left[- \frac{E}{R^o T} \right] \prod_j y_j^{a_j} \tag{4-28}$$

where all the symbols retain their original meanings. Then, using the state equation (i.e., Eqn. (2-19)) and the following expression for temperature (which is obtained from Eqn. (2-17))

$$T = \frac{1}{C_p}\left[\theta \bar{h}_{t_e} - \Sigma y_i h_i^o - \frac{\bar{u}_e^2 \bar{f}'^2}{2 g_c J_c} + C_p T_u \right] \equiv \frac{F}{C_p} \tag{4-29}$$

Eqn. (4-28) can be linearised to yield the following first order expression for $\left(\frac{\omega_i}{\rho}\right)_1$ (see Appendix C for details)

$$\left(\frac{\omega_i}{\rho}\right)_1 = \left(\overline{\frac{\omega_i}{\rho}}\right)\left\{ \frac{F_1}{\bar{F}} \left(\alpha + \frac{EC_p}{R^o \bar{F}} \right) + \frac{y_{1_1}}{\bar{y}_1} \right\} \tag{4-30}$$

where

$$F_1 \equiv \theta_1 \bar{h}_{t_e} - \Sigma_i y_{i_1} h_i^o - \frac{\bar{u}_e^2 \bar{f}' f_1'}{g_c J_c} \tag{4-31}$$

$$\bar{F} \equiv \bar{\theta} \bar{h}_{t_e} - \Sigma_i \bar{y}_i h_i^o - \frac{\bar{u}_e^2 \bar{f}'^2}{2 g_c J_c} + C_p T_u \tag{4-32}$$

Again, as expected, to zeroth order the steady-state rate law of Eqn. (2-18) is recovered.

Finally, to complete the system of first-order gas phase equations the thermal equation of state (as given by Eqn. (2-19)) is linearised to yield

State

$$\frac{\rho_1}{\bar{\rho}} = \frac{p_1}{\bar{p}} - \frac{F_1}{\bar{F}} - \frac{\sum_i y_{i_1}/W_i}{\sum_i \bar{y}_i/W_i} \tag{4-33}$$

Next, the boundary conditions for the first order gas phase conservation equations (i.e., Eqns. (4-25) through (4-27)) are considered. At the gas-solid interface these conditions have the same form as those used for the steady-state analysis (i.e., Eqns. (2-1) and Eqns. (2-20) through (2-23)). At the edge of the boundary layer, which is the other boundary, because of the presence of the longitudinal acoustic waves superposed on the steady external flow, the following conditions hold:

$$u = u_e = \bar{u}_e + u_{e_1} \tag{4-34}$$

$$h_t = h_{t_e} = \bar{h}_{t_e} + h_{t_{e_1}} \tag{4-35}$$

$$y_i = y_{i_e} = \bar{y}_{i_e} + y_{i_{e_1}} = \bar{y}_{i_e} \quad \text{(using Assumption (ii))} \tag{4-36}$$

When these boundary conditions are transformed using Equations (4-20) through (4-24) and terms of different orders of magnitude separated, it is found that to zeroth order the boundary conditions are identical to those of the steady-state analysis (i.e., Eqns. (2-55) to (2-61)) and to first order one obtains (see Appendix C):

Momentum boundary conditions

i) $$f_1'(0) = 0 \tag{4-37}$$

ii) $$f_1'(\infty) = \left(\frac{u_{e_1}}{\bar{u}_e}\right) \tag{4-38}$$

$$\text{iii)}\quad \frac{f_1(0)}{\bar{f}(0)} = n_s\left(\frac{p_1}{\bar{p}}\right)+\left\{\frac{E_s C_p}{R^o \bar{F}_w}\right\}\left(\frac{F_{1w}}{\bar{F}_w}\right) \tag{4-39}$$

where $$F_{1w} = \theta_1(0)\bar{h}_{t_e} - \Sigma\, y_{i_1}(0)h_i^o$$

$$\bar{F}_w = \bar{\theta}(0)\bar{h}_{t_e} - \Sigma\, \bar{y}_i(0)h_i^o + C_p T_u$$

Energy boundary conditions

$$\text{iv)}\quad A[\theta_1'(0)\bar{h}_{t_e} - \Sigma_i\, y_{i_1}'(0)h_i^o] = \left[\frac{C_p}{C_s}L + \frac{is}{\Omega} - \frac{is\Lambda}{\Omega}\right] f_1(0) + \frac{\Lambda \bar{f}(0)}{C_p \bar{T}_e}[\theta_1(0)\bar{h}_{t_e} - \Sigma_i\, y_{i_1}(0)h_i^o] \tag{4-40}$$

where $A \equiv -\frac{1}{Pr}\frac{1}{C_s \bar{T}_e}$

This is the energy balance boundary condition at the gas-solid interface, obtained by combining Eqn. (4-17) obtained in the solid phase analysis with Eqn. (4-31) for the gas phase temperature perturbation, using the following condition expressing the continuity of the wall temperature perturbation at the interface

$$\left(T_{1_w}\right)_{0^-} = \left(T_{1_w}\right)_{0^+}$$

$$\text{v)}\quad \theta_1(\infty) = \frac{C_p \bar{T}_e\left(\frac{T_{e_1}}{\bar{T}_e}\right) + \frac{\bar{u}_e^2}{g_c J_c}\left(\frac{u_{e_1}}{\bar{u}_e}\right)}{\bar{h}_{t_e}} \tag{4-41}$$

Species boundary conditions

$$\text{vi)}\quad y_{i_1}'(0) = -Sc[\bar{f}(0)y_{i_1}(0) + f_1(0)\{\bar{y}_i(0) - \left(y_{i_w}\right)_-\}] - \bar{y}_i'(0)\frac{p_1}{\bar{p}} \tag{4-42}$$

$$\text{vii)}\quad y_{i_1}(\infty) = 0 \tag{4-43}$$

The system of "first order" differential equations as well as the first order boundary conditions above indicate the influence of the imposed acoustic oscillations, in the external stream of the boundary layer, on the behavior of perturbations within the boundary layer itself. This external "driving" manifests itself through the terms $\left(\frac{p_1}{\bar{p}}\right)$, $\left(\frac{u_{e_1}}{\bar{u}_e}\right)$, $\left(\frac{T_{e_1}}{\bar{T}_e}\right)$, $\left(\frac{\rho_{e_1}}{\bar{\rho}_e}\right)$ that appear in the differential equations and the boundary conditions. Expressions that characterise these terms, for the particular type of oscillations considered in this analysis (i.e., Assumption (i)), are derived in the next section. Once these waveforms are specified, the above gas phase formulation would be complete.

Selection of Waveforms

The combustion chamber is treated like a one-dimensional cavity of length ℓ, having closed ends, in deriving the "external waveforms". Since typical rocket combustion chambers are characterised by low Mach number mean flows the effect of the mean flow is neglected in this analysis. Under these assumptions one can write:

$$\frac{\partial^2 p_1}{\partial x^2} - \frac{1}{\bar{a}_e^2} \frac{\partial^2 p_1}{\partial t^2} = 0 \qquad (4\text{-}44)$$

subject to the boundary conditions

$$\left.\frac{\partial p_1}{\partial x}\right|_{x = 0} = \left.\frac{\partial p_1}{\partial x}\right|_{x = \ell} = 0$$

The above "wave equation" and boundary conditions describe the behavior of a longitudinal isentropic pressure oscillation, p_1, in the chamber. The steady-state speed of sound, $\bar{a}_e$, is given by

$$\bar{a}_e^2 = \frac{\gamma \bar{p}}{\bar{\rho}_e} \tag{4-45}$$

In complex notation, the simple harmonic pressure wave being considered here can be described by

$$p_1 = p_o(x) e^{i\omega t} \tag{4-46}$$

Introducing Eqn. (4-46) into Eqn. (4-44) and the corresponding boundary conditions one obtains an ordinary differential equation in $p_o(x)$, whose solution for the fundamental mode is

$$p_o(x) = P \cos kx \tag{4-47}$$

where

$$k \equiv \frac{\omega}{\bar{a}_e} = \frac{\pi}{\ell} \text{ (wave number)} \tag{4-48}$$

and P is the dimensional amplitude of the pressure wave at x = 0. Substituting Eqn. (4-47) into Eqn. (4-46) yields the following waveform for the standing, longitudinal pressure oscillation

$$p_1 = P \cos kx \; e^{i\omega t} \tag{4-49}$$

To obtain the corresponding velocity wave, Eqn. (4-49) is used in the acoustic momentum equation

$$\bar{\rho}_e \frac{\partial u_1}{\partial t} = - \frac{\partial p_1}{\partial x}$$

to give

$$u_{e_1} = - \frac{iP}{\bar{\rho}_e \bar{a}_e} \sin kx \; e^{i\,t} \tag{4-50}$$

The corresponding density and temperature waveforms are finally obtained from the substitution of Equation (4-49) into the isentropic relation[1]

$\rho_{e_1} = \frac{p_1}{\bar{a}_e^2}$, and the perturbed state equation $\frac{T_{e_1}}{\bar{T}_e} = \frac{p_1}{\bar{p}} - \frac{\rho_{e_1}}{\bar{\rho}_e}$,

to yield:

$$\rho_{e_1} = \frac{P}{\bar{a}_e^2} \cos kx \, e^{i\omega t} \tag{4-51}$$

$$T_{e_1} = \frac{P}{\bar{p}} \bar{T}_e \left(\frac{\gamma-1}{\gamma}\right) \cos kx \, e^{i\omega t} \tag{4-52}$$

Then, by defining a non-dimensional amplitude for the pressure waveform as

$$\varepsilon \equiv \frac{P}{\bar{p}} \tag{4-53}$$

it becomes possible to express the pressure, velocity, density and temperature waveforms in the following non-dimensional manner:

$$\frac{p_1}{\bar{p}} = \varepsilon \cos kx \, e^{i\Omega\tau} \tag{4-54}$$

$$\frac{u_{e_1}}{\bar{u}_e} = -i \frac{\varepsilon}{\gamma \bar{M}_e} \sin kx \, e^{i\Omega\tau} \tag{4-55}$$

$$\frac{\rho_{e_1}}{\bar{\rho}_e} = \frac{\varepsilon}{\gamma} \cos kx \, e^{i\Omega\tau} \tag{4-56}$$

$$\frac{T_{e_1}}{\bar{T}_e} = \varepsilon\left(\frac{\gamma-1}{\gamma}\right) \cos kx \, e^{i\Omega\tau} \tag{4-57}$$

Formulation of the Response Function

The response function is defined as a complex ratio of the mass flux perturbation to the pressure perturbation, usually evaluated at a boundary. In the present model, the appropriate boundary is the edge of the boundary

layer since it separates the isentropic acoustic field from the "non-isentropic" region within the boundary layer. However, as pointed out in Chapter I, the practice in the past has often been to evaluate the response function at the surface of the burning propellant. This will also be done later in this section, for the sake of comparison.

Define the response function at the boundary layer edge as

$$R_e \equiv (m_{e_1}/\bar{m}_e)/(p_1/\bar{p}) \tag{4-58}$$

where $m_e = (\rho v)_e$ is the mass flux at the boundary layer edge in a direction normal to the burning surface (i.e., the y-direction). This $(\rho v)_e$ product may be expressed in terms of the streamfunction ψ as

$$(\rho v)_e = - \left.\frac{\partial \psi}{\partial x}\right|_e \tag{4-59}$$

Expressing this in the (ξ,η) co-ordinate system using Equation (4-20) and introducing Equation (4-21) for $\psi(\xi,\eta)$, the following relation is obtained

$$(\rho v)_e = - \frac{\bar{\rho}_e \bar{\mu}_e \bar{u}_e}{(2\xi)^{1/2}} \left[\bar{f}(\infty) + f_1(\infty) + 2\xi \left(\frac{\partial \eta}{\partial \xi}\right)_{\eta\to\infty} (\bar{f}'(\infty) + f_1'(\infty)) \right] \tag{4-60}$$

Now, from the definition of η(see Eqn. (4-20b)) it can be shown, by differentiation, that

$$\left(\frac{\partial \eta}{\partial \xi}\right)_{\eta\to\infty} = \frac{\bar{u}_e}{(2\xi)^{1/2}} \left[\frac{\partial I}{\partial \xi} + I \left(\frac{1}{\bar{u}_e} \frac{d\bar{u}_e}{d\xi} - \frac{1}{2\xi} \right) \right]_{\eta\to\infty} \tag{4-61}$$

where

$$I = \int_o^y \rho(x,y',t)dy' \tag{4-62}$$

Combining Equations (4-60) and (4-62) and using the fact that $\bar{f}'(\infty) = 1$,

$f_1'(\infty) = \dfrac{u_{e_1}}{\bar{u}_e}$ (the zeroth and first order boundary conditions on velocity at the boundary layer edge) the following relation is finally obtained for the normal unsteady mass flux at the boundary layer edge:

$$m_e = (\rho v)_e = -\frac{\bar{\rho}_e \bar{\mu}_e \bar{u}_e}{(2\xi)^{1/2}} \left[\bar{f}(\infty) + f_1(\infty) + (2\xi)^{1/2} \bar{u}_e \left\{ \bar{I}_\xi + A^*(\bar{I}+I_1) + I_{\xi_1} + \left(\frac{u_{e_1}}{\bar{u}_e}\right) \left(\bar{I}_\xi + A^*\bar{I}\right) \right\} \right] \tag{4-63}$$

where

$$A^* \equiv \frac{1}{\bar{u}_e} \frac{d\bar{u}_e}{d\xi} - \frac{1}{2\xi} \tag{4-64}$$

$$\bar{I}_\xi \equiv \frac{1}{\bar{\rho}_e \bar{\mu}_e \bar{u}_e} \int_o^\infty \frac{\partial \bar{\rho}}{\partial x} dy' \tag{4-65}$$

$$\bar{I} \equiv \int_o^\infty \bar{\rho}\, dy' \tag{4-66}$$

$$I_{\xi_1} \equiv \frac{1}{\bar{\rho}_e \bar{\mu}_e \bar{u}_e} \int_o^\infty \frac{\partial \rho_1}{\partial x} dy' \tag{4-67}$$

$$I_1 \equiv \int_o^\infty \rho_1\, dy' \tag{4-68}$$

Recalling that this unsteady mass flux is described by

$$m_e = \bar{m}_e + m_{e_1} \tag{4-69}$$

and separating terms of different orders of magnitude one obtains

$$\bar{m}_e = -\frac{\bar{\rho}_e \bar{\mu}_e \bar{u}_e}{(2\xi)^{1/2}} \left[\bar{f}(\infty) + \bar{u}_e (2\xi)^{1/2} \left\{ \bar{I}_\xi + A^*\bar{I} \right\} \right] \tag{4-70}$$

and

$$m_{e_1} = -\frac{\bar{\rho}_e \bar{\mu}_e \bar{u}_e}{(2\xi)^{1/2}} \left[f_1(\infty) + \bar{u}_e (2\xi)^{1/2} \left\{ A^* I_1 + I_{\xi_1} + \frac{u_{e_1}}{\bar{u}_e} \left(\bar{I}_\xi + A^*\bar{I} \right) \right\} \right] \tag{4-71}$$

Substituting Equations (4-70) and (4-71) into Equation (4-58), the response function at the boundary layer edge is given by

$$R_e = \frac{1}{(p_1/\bar{p})}\left[\frac{f_1(\infty) + \bar{u}_e(2\xi)^{1/2}\left\{ I_{\xi_1} + A^*\left(I_1 + \frac{u_{e_1}}{\bar{u}_e}\,\bar{I}\right) + \frac{u_{e_1}}{\bar{u}_e}\,\bar{I}_\xi\right\}}{\bar{f}(\infty) + \bar{u}_e(2\xi)^{1/2}\left\{\bar{I}_\xi + A^*\bar{I}\right\}}\right] \quad (4\text{-}72)$$

The following features regarding this response function are noteworthy:

a) The "non-isentropic" effects of the boundary layer processes are contained in $f_1(\infty)$ and the integrals I_1, I_{ξ_1}, $\bar{I}_\xi$ and $\bar{I}$. These integrals also reflect the effects of compressibility as contained in the unsteady version of the Lees-Dorodnitsyn transformations (see Eqn. (4-20b)).

b) The effect of the steady-state pressure gradient in the external flow enters explicitly through A*.

c) The dependence on the mean flow, $\bar{u}_e$, and the axial co-ordinate ξ is also explicitly present.

d) The complicated expression for R_e in Equation (4-72) shows the explicit dependence of this response function on both the pressure and velocity oscillations in the external stream of the boundary layer. Of course, the indirect effect of these oscillations on the boundary layer is expressed through the boundary layer related variables - f_1 and the integrals of Equations (4-65) through (4-68).

For the sake of comparison, the response function at the gas-solid interface will now be considered. Defining this response function as

$$R_w \equiv \left(\frac{m_{w_1}}{\bar{m}_w}\right) \Big/ \left(\frac{p_1}{\bar{p}}\right)$$

where $m_w = (\rho v)_w$, and proceeding as before by transforming the ρv product one obtains

$$(\rho v)_w = - \frac{\bar{\rho}_e \bar{\mu}_e \bar{u}_e}{(2\xi)^{1/2}} \left[\bar{f}(0) + f_1(0) + 2\xi \left(\frac{\partial \eta}{\partial \xi} \right)_{\eta = 0} \left(\bar{f}'(0) + f_1'(0) \right) \right] \quad (4\text{-}73)$$

Since the "no slip" condition requires $\bar{f}'(0) = 0 = f_1'(0)$, the above expression for the unsteady normal mass flux at the wall yields

$$m_w = (\rho v)_w = - \frac{\bar{\rho}_e \bar{\mu}_e \bar{u}_e}{(2\xi)^{1/2}} \left[\bar{f}(0) + f_1(0) \right] \quad (4\text{-}74)$$

Recalling again that

$$m_w = \bar{m}_w + m_{w_1}$$

and separating orders of magnitudes, it is possible to construct the ratio

$$\frac{m_{w_1}}{\bar{m}_w} = \frac{f_1(0)}{\bar{f}(0)}$$

Since the continuity of overall mass at the interface requires $\rho_s \dot{r} = m_w$ (see Eqn. (2-20)) it can be shown that the above ratio is exactly equal to the ratio of the regression rate perturbation ($\dot{r}_1$) to the steady regression rate ($\bar{\dot{r}}$); that is,

$$\frac{f_1(0)}{\bar{f}(0)} = \frac{\dot{r}_1}{\bar{\dot{r}}} \quad (4\text{-}75)$$

Hence the response function at the burning surface is

$$R_w = \frac{\left(f_1(0)/\bar{f}(0) \right)}{\left(p_1/\bar{p} \right)} \quad (4\text{-}76)$$

Comparing the expressions for R_e and R_w (i.e., Eqns. (4-72) and (4-76)) one finds that the latter is much simpler. The reason for this

should be obvious from the derivations presented above. The unsteady mass flux perturbation at the wall is due to nothing more than the perturbation of the propellant's burning rate. The effects of the boundary layer and the external stream are implicitly present, to the extent that they govern this regression rate. In contrast, the unsteady normal mass flux perturbation at the edge of the boundary layer (see Eqn. (4-71)), and hence the response function, depends explicitly upon the effects of the external isentropic velocity oscillations $\left\{ \frac{u_{e_1}}{\bar{u}_e} \right\}$, the steady-state pressure gradient as well as the "non-isentropic" and compressibility effects present within the boundary layer.

The above mentioned differences are expected to cause the response function to vary across the thickness of the boundary layer. In the next chapter, results are presented that provide insight into the characteristics of these response functions. The numerical evaluation of these response functions is outlined in Appendix D.

CHAPTER V

RESULTS AND DISCUSSION

In this chapter results of the various numerical computations performed are presented. To begin with the typical behaviour of the response data, computed at the boundary layer edge and the gas-solid interface, is discussed. After this the results of a parametric study to determine the individual effects of several key parameters that enter the analysis are discussed. The values of constants used in the computation of the results are given in Appendix E, corresponding to the different computer runs.

The set of gas phase equations presented in the last chapter (i.e., Eqns. (4-25) to (4-27) and Eqns. (4-37) through (4-43)) that describe the behaviour of the perturbations, form a complex system of seven first order ordinary differential equations. The solution of this system of equations is carried out by splitting each equation into its real and imaginary counterparts. The resulting problem consists of a coupled system of fourteen first order, real ordinary differential equations with the corresponding boundary conditions. This forms a linear boundary value problem whose solution is obtained numerically using the non-iterative technique used earlier in this study in the solution of similar problems that were encountered during the application of the Method of Parametric Differentiation in Chapter III. However, a separate computer program has been developed for the unsteady combustion response study. All profiles and other relevant solutions found using the computer program for the steady state analysis are stored and used later as inputs for the "unsteady program". That is, steady state

solutions describing the behaviour of the variables are first obtained for different x-locations along the boundary layer. Then, using the steady-state solutions at a given x-location, the solutions of the unsteady equations are computed. Since the behaviour of the steady-state solutions has already been established in Chapter III, they will not be considered here. The numerical results presented in this chapter were obtained solving the unsteady equations derived in Chapter IV.

From the viewpoint of analysing the stability of the acoustic waves in the combustion chamber of a solid rocket, it has been shown[8,9] that it is the real part of the complex response function (or the related "admittance function"**) that contributes to the growth or decay of the waves. Physically, this real part can be related to the amount of displacement work performed on the waves by the boundary whose behaviour is characterised by the response function under consideration. More specifically, the "gain" in wave energy, E, may be expressed by the proportionality[9]

**The "admittance function" is defined as a complex ratio of the velocity perturbation normal to a boundary to the pressure perturbation. That is, the admittance function can be expressed as

$$A_e = \left(\frac{v_1}{p_1}\right)_e = \left\{\frac{\bar{v}_e}{\bar{p}}\right\}\left[R_e - \frac{\left(\frac{\rho_{e_1}}{\bar{\rho}_e}\right)}{\left(\frac{p_1}{\bar{p}}\right)}\right],$$

evaluated at the boundary 'e'.

$$E \sim |p_1|^2 \text{ Real}\{A \text{ or } R\}$$

Since $|p_1|^2$ will have a certain prescribed value corresponding to a given location and frequency (e.g., $\varepsilon_p^{2-2} \cos^2 kx$, in the present case, as seen from Eqn. (4-54)), it is to be expected that the greater the positive real part of the response function, the greater will be the tendency of the boundary to sustain the waves. In fact, it can also be deduced[1,9] that for acoustic waves in a cavity whose boundary performs only a "$p_1 v_1$" type displacement work, a necessary condition (but not sufficient) for wave amplification is that the real part of the response function be greater than $\frac{1}{\gamma}$ (for isentropic waves) or unity (for isothermal waves).

In view of the importance of the real part of the response function, as pointed out above, many of the results to be presented will be concerned with the behavior of this quantity. Figure 7 shows a typical dependence of the real parts of R_e and R_w on the non-dimensional frequency Ω. As the curves in Fig. 7 are indicative of the general trends exhibited by the computed response factors data, their significance will be examined now. The following features are noteworthy:

i) The general shape of both curves is the same, consisting of a positive branch followed by a negative one and with the real part of the response function becoming infinitely large at some intermediate frequency. The reason for this type of behavior will be explained later. Physically, this indicates that for frequencies corresponding to the positive branch (i.e., the lower frequencies) the burning propellant tends to amplify the waves while for the "higher" frequencies, corresponding to the negative branch, a stable tendency prevails. It is also noticeable that in the

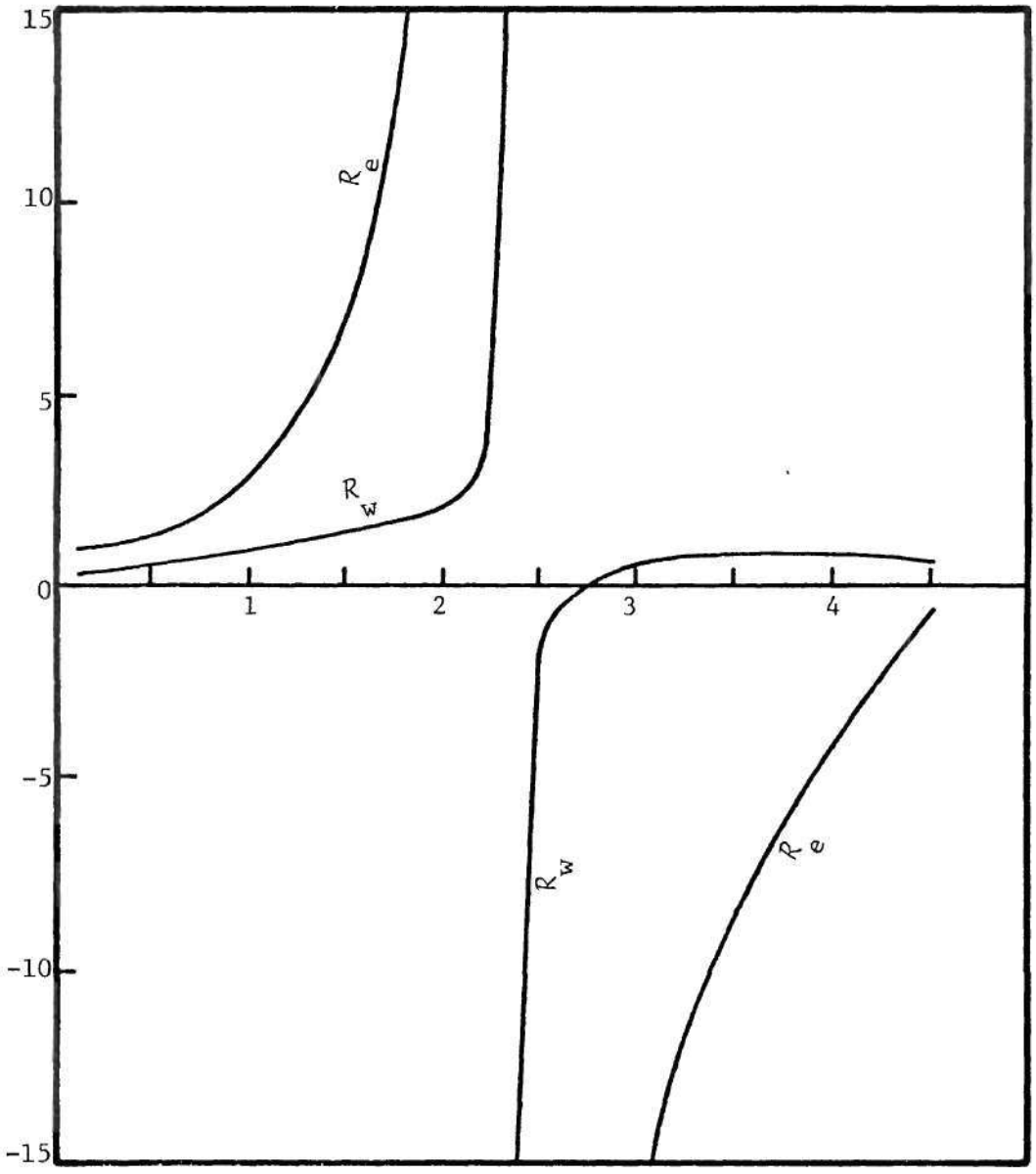

Figure 7. Variation of the combustion response function with frequency at the boundary layer edge (e) and the gas-solid interface (w).

close vicinity of that critical frequency, where the response function would actually become infinite, the values of $(R_e)_r$ and $(R_w)_r$ change drastically for small changes in frequency. In this sensitive frequency range, which here corresponds to $2.3 < \Omega < 2.4$, the response function values become numerically large, apparently indicating an extremely strong destabilizing influence being exerted by the burning propellant on the imposed acoustic waves. However, in the present model this cannot be taken to imply that the "growth constant" of the waves is infinitely large. In fact, since the energy input to the waves is proportional to the product of the square of the pressure perturbation (i.e., $\epsilon^2 \cos^2 kx$) and $(R_e)_r$, the actual "gain" would be small in the vicinity of the critical frequency because the pressure perturbation (i.e., $\epsilon \cos kx$) itself tends to zero there. Indeed, as will be obvious later, the infinitely large response function values, shown in Fig. 7, are also a direct consequence of the pressure perturbation going to zero. Furthermore, it is to be noted that since the square of the pressure perturbation will always be a positive quantity for all frequencies, the energy input to the waves will be positive to the left (where $(R_e)_r$ is positive) of the critical frequency and predominantly negative to the right (where $(R_e)_r$ is negative). That is, the burning propellant has a destabilizing effect on the acoustic waves for frequencies less than the critical frequency and a stabilizing effect at higher frequencies. Thus when designing a practically stable rocket motor, at least insofar as the contribution of the burning propellant is concerned, it must be ensured that the fundamental frequency of the motor corresponds to the stable, negative branch of the $(R_e)_r$ vs Ω curve.

The wave energy "gain" in the case of a rocket motor whose fundamental frequency coincides exactly with the above mentioned critical frequency would again depend upon the product $|p_1|^2(\mathcal{R}_e)_r$. Thus if $|p_1|^2$ goes to zero faster than $(\mathcal{R}_e)_r \to \infty$, as is the case here, the energy gain would be zero. That is, the waves would neither decay nor be amplified. However, if the contrary were true one would analytically expect a situation where the wave energy gain would be infinite. This latter case would necessarily imply that the normal velocity perturbation, v_1, be infinite (since the wave energy gain is proportional to $p_1 v_1$) and the present theory would break down. This latter circumstance corresponds physically to the rarely encountered case of "inherent" or "intrinsic" instability discussed in the literature (e.g., see Ref. 2).

ii) With the present model it is possible to find the exact frequency range over which the numerical results are valid. In Figure 7 the frequencies considered lie between $\Omega = 0.1$ and 4.5. The lower extreme of this range is just a convenient value that is chosen close to $\Omega = 0$, which corresponds to the steady state. The upper limit was established using the following argument. In order to find the response function for a given frequency, the steady-state solutions corresponding to a particular x-location were used. The procedure was then repeated for other values of frequency to study the frequency dependence. It should be noted that each Ω can be associated with the natural frequency of a combustion chamber whose length equals half the wavelength of the fundamental mode. As the value of Ω is increased, the corresponding chamber lengths decrease. Therefore, the results of the present analysis are relevant only for combustors that "contain" the x-station being considered. In other words,

the valid frequency range is limited by the condition

$$x \lesssim \ell \text{ (the combustor length)} \tag{5-1}$$

Using Equation (4-48) together with the definitions of the wavenumber, k, and the non-dimensional frequency Ω, the above restriction can be expressed as

$$\Omega \lesssim \left\{ \frac{\pi \alpha_s \bar{a}_e}{\bar{f}^2} \right\} \frac{1}{x} \tag{5-2}$$

Under the conditions considered for Figure 7

$$\bar{f} = 2.2186 \times 10^{-2} \text{ ft/sec.}$$

$$\bar{a}_e = 3089.66 \text{ ft/sec.}$$

$$x = 8.3395 \text{ ft.}$$

and $$\alpha_s = 2 \times 10^{-6} \frac{\text{ft}^2}{\text{sec}}$$

so that Eqn. (5-2) gives the upper limit frequency of $\Omega = 4.7293$. Hence the results of this unsteady analysis are only valid up to $\Omega = 4.7293$. This corresponds to a real frequency of 1163.91 cycles per second.

iii) There is a large difference in the values of $(R_e)_r$ and $(R_w)_r$, as evident from Fig. 7. As explained earlier, $(R_e)_r$ would be the appropriate quantity to consider in a stability analysis of the acoustic waves within the chamber. This is physically apparent since it is the boundary layer edge that acts as the "working boundary", transmitting the net "$p_1 v_1$" displacement work achieved as a result of the various gas phase processes coupled with the thermal response of the solid phase. It must be noted, however, that since no material leaves the boundary layer at its edge the response there is the result of a "piston-like" action. In

contrast, at the gas-solid interface the response is due to a "pumping" action with an unsteady mass flux entering the gas phase from the solid propellant. Therefore, while $(R_e)_r$ can be related to the energy gain or loss from the isentropic acoustic field outside the boundary layer, $(R_w)_r$ would be related to the energy of the "non-isentropic" perturbations within the boundary layer (and just above the burning surface). Physically, one can then expect the response function to vary across the boundary layer. The large difference between $(R_e)_r$ and $(R_w)_r$, as seen from Fig. 7, shows the importance of the boundary layer in modifying the response at the burning surface and is due to the gas phase combustion, viscous dissipation, compressibility and other effects discussed in Chapter IV. As will be shown later in this chapter, under certain propellant burning conditions it is possible to predict values of $(R_w)_r$ that correspond to a stable condition whereas the corresponding values of $(R_e)_r$ support instability - thereby showing the strong amplifying effect of the boundary layer. Thus, by using $(R_w)_r$ for simplicity in a stability analysis, instead of $(R_e)_r$, it is possible to introduce a significant error. Although, as discussed later, under typical rocket chamber conditions it is generally possible to predict unstable tendencies from the shape of the curve for $(R_w)_r$, it is important to know the magnitude of $(R_e)_r$ when designing a rocket motor.

iv) In past analyses, especially the "pressure-coupled" theories[1,2,36], it has been pointed out that the peaks in the response function vs frequency curves correspond to an "in-phase" driving of the pressure waves by the burning propellant. This type of tendency is also present in the results obtained in the present analysis. Figure 8 shows the phases of

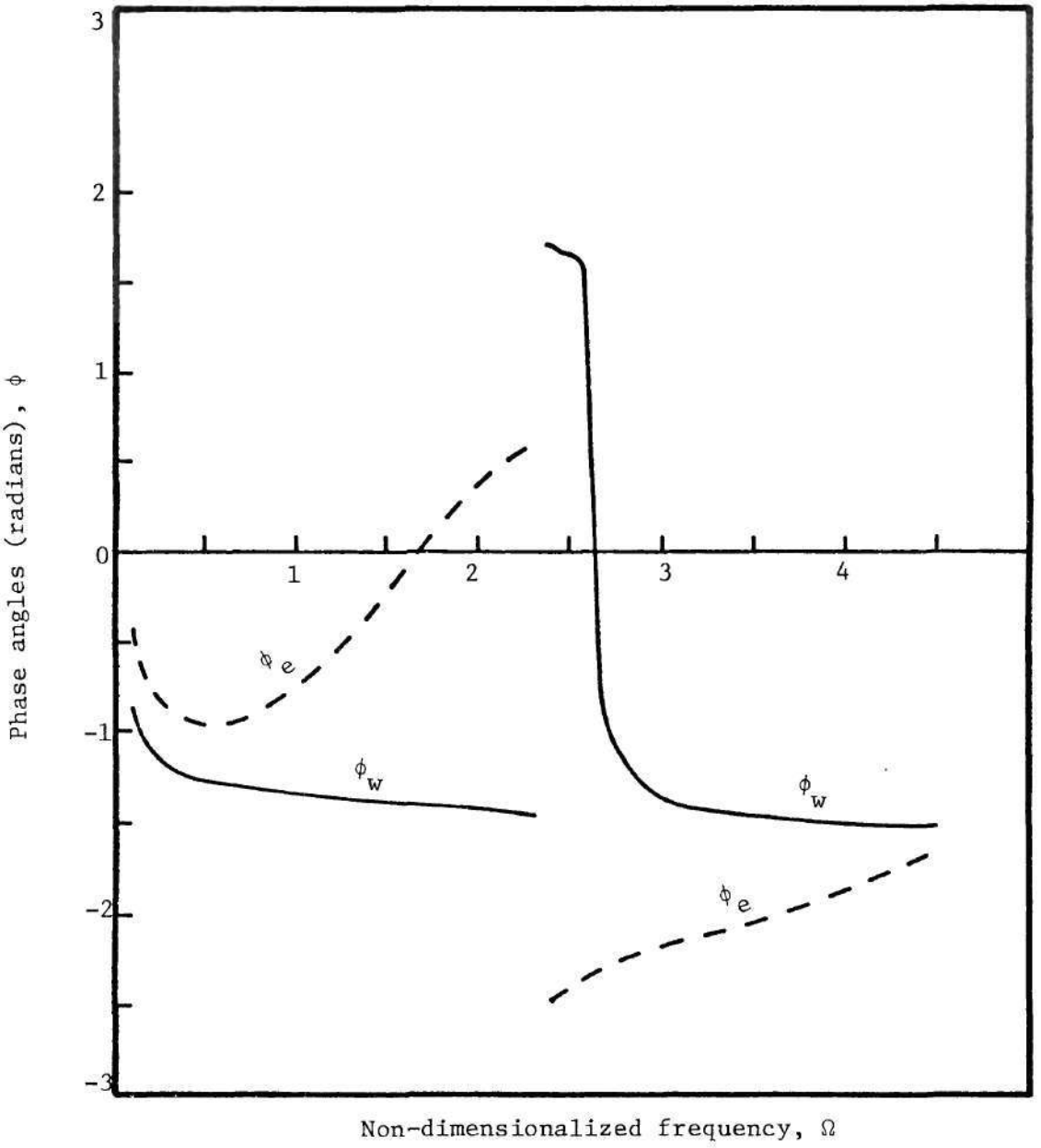

Figure 8. Variation of phase of the combustion response (relative to the pressure oscillation) with frequency, at the boundary layer edge and the gas-solid interface.

the normal mass flux perturbation, $\left[\frac{(\rho v)_1}{(\overline{\rho v})} \right]$, evaluated at the boundary layer edge and the gas-solid interface for different values of Ω. These phases were determined using the local pressure perturbation as reference. It is to be noted that the value of ϕ_e goes to zero at $\Omega \cong 1.7$ while ϕ_w goes to zero at $\Omega \cong 2.6$. Both of these frequencies are in the vicinity of the critical frequency (i.e., $\Omega \cong 2.3$) where the response functions become infinitely large. As discussed earlier, since the maximum energy "gain" by the waves - as reflected by the product $(\mathcal{R}_e)_r |p_1|^2$ - would be expected to occur for an Ω somewhat less than $\Omega = 2.3$, the trend shown by ϕ_e is in agreement with the idea of "in-phase" driving for $\phi_e = 0$. It should be pointed out that although the curves for ϕ_e and ϕ_w both pass apparently through zero again at $\Omega \cong 2.3$, this is only due to the fact that the pressure perturbation itself changes sign here, so that the phase reference is changed by π radians at the critical frequency. It must be remembered, however, that the longitudinal velocity oscillation "lags" the pressure oscillation by $\frac{\pi}{2}$ radians in the present case, and hence the phases of the normal mass flux perturbations relative to the velocity oscillation would vary accordingly.

v) Under the assumptions of the present analysis, as in most related studies considered to date, the gas phase is considered "quasi-steady" while the solid phase is unsteady. Physically this implies that the characteristic response times of the boundary layer processes (including combustion) are much shorter than the period of the imposed oscillation. On the other hand, the response time of the solid phase must be much greater than, or at least of the same order of magnitude as, the period

of the waves. Since the characteristic response time of the solid may be defined as the time it takes the thermal wave (which refers to the unsteady temperature fluctuations within the solid) to penetrate the solid thermal layer, the shape of the response function curves in Fig. 7 may be attributed to the behavior of both the unsteady thermal wave as well as the "quasi-steady" gas phase boundary layer. Figure 7 shows that the effect of the boundary layer is to further enhance the response of the unsteady solid causing an even greater destabilizing tendency to prevail. Other results presented later in this chapter consistently support this conclusion.

vi) Finally, it is relevant in the present study to consider also the variation of the real part of the normal mass flux perturbation at the boundary layer edge, $\left(\frac{\bar{m}_{e_1}}{\bar{m}_e}\right)_r$, with frequency. Figure 9 depicts this variation. From Eqn. (4-58) it is evident that the full effect of the imposed pressure and velocity oscillations, on the response of the burning propellant, is "contained" in the quantity, $\left(\frac{\bar{m}_{e_1}}{\bar{m}_e}\right)$. Also, as discussed later, it is the (cos kx) dependence of the pressure perturbation in the denominator that causes $(R_e)_r$ and $(R_w)_r$ to take on the infinite (or numerically very large) values shown in Fig. 7. For this reason, while the $(R_e)_r$ vs Ω plot of Fig. 7 is of importance from the stability viewpoint, the true undistorted physical behavior of the combustion response under the influence of both pressure and velocity oscillations is better represented by the $\left(\frac{\bar{m}_{e_1}}{\bar{m}_e}\right)_r$ vs Ω curve, shown in Fig. 9. This latter curve shows that the "pressure-and-velocity coupled" response of the solid pro-

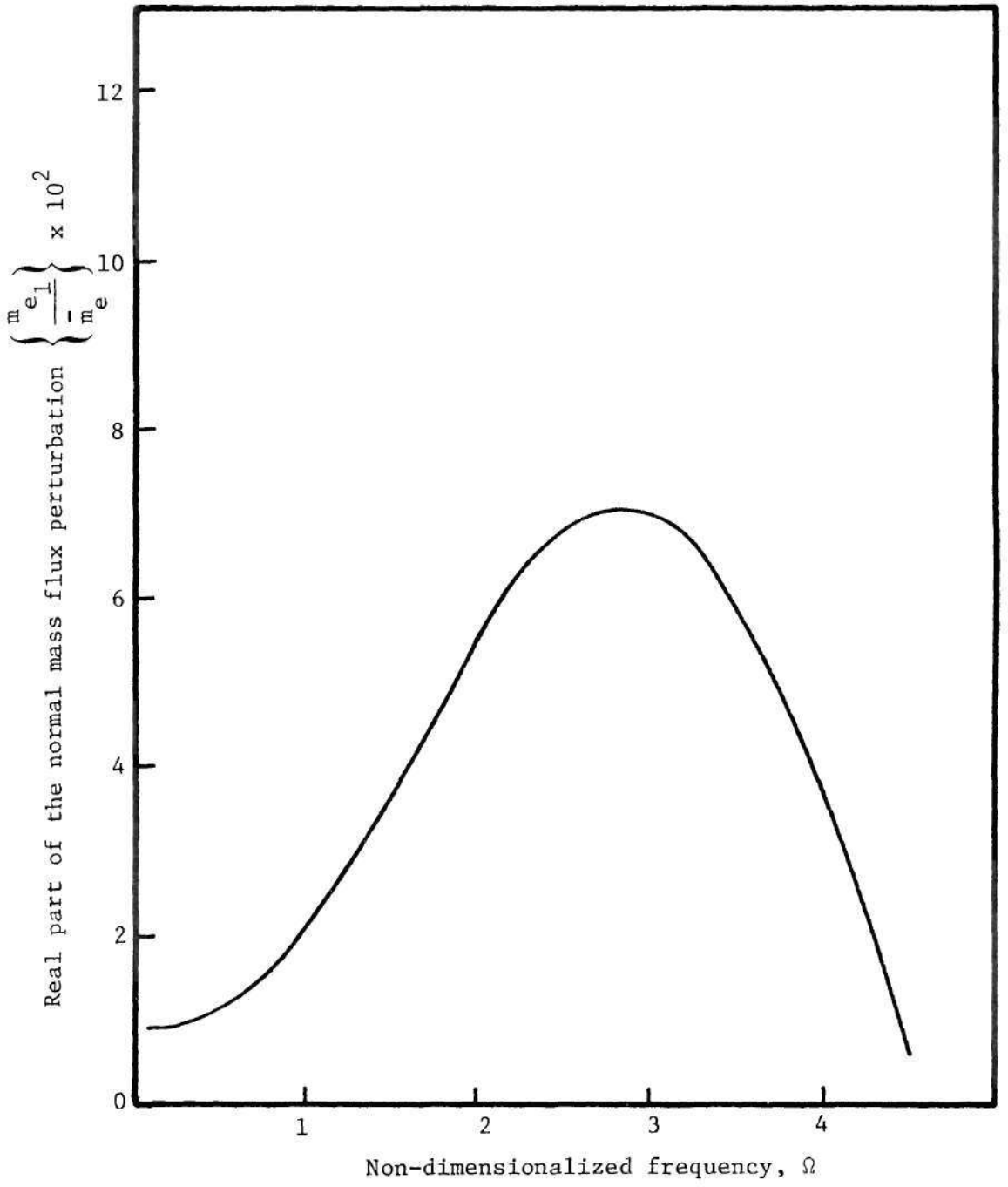

Figure 9. Variation of the real part of the normal mass flux perturbation with frequency at the boundary layer edge.

pellant increases with frequency up to $\Omega \cong 2.8$, where a peak occurs, and then decreases monotonically. Thus one can qualitatively expect a destabilizing trend for frequencies less than $\Omega \cong 2.8$. The peak itself suggests that at this frequency, the amount of displacement work being performed on the acoustic waves at the boundary layer edge is a maximum. However, owing to the out of phase nature of this energy transfer, the waves may not actually incur a maximum "gain" in energy at $\Omega \cong 2.8$.

For the sake of comparison, Fig. 9a shows the corresponding variation of the mass flux at the gas-solid interface with frequency. Note that $\left(\frac{m_{w_1}}{\bar{m}_w}\right)_r$ peaks at $\Omega \cong 1.2$. As pointed out earlier, $\left(\frac{m_{w_1}}{\bar{m}_w}\right)_r$ represents physically the normalized regression rate perturbation of the propellant; that is, the unsteady response at the burning surface. Thus, it is an indication of the amount of displacement work the burning surface itself can perform on the oscillations just above it. As explained in the discussion of the response function R, here also it is necessary to consider the quantity $|p_1|^2(R)_r$ or $|p_1|\left(\frac{m_1}{\bar{m}}\right)_r$ in order to draw any conclusions about stability. It is obvious (since $p_1 \sim \varepsilon \cos kx$) from Figs. 9 and 9a that peak "gain" in energy would be experienced by the waves just above the burning surface at a lower frequency than that at which the maximum displacement work is performed by the boundary layer edge on the isentropic waves in the external stream.

Having established the basic characteristics of the "pressure-and-velocity" coupled combustion response behavior for a typical solid rocket burning situation, the results of a parametric study will now be presented. This study was undertaken to gain an understanding of the

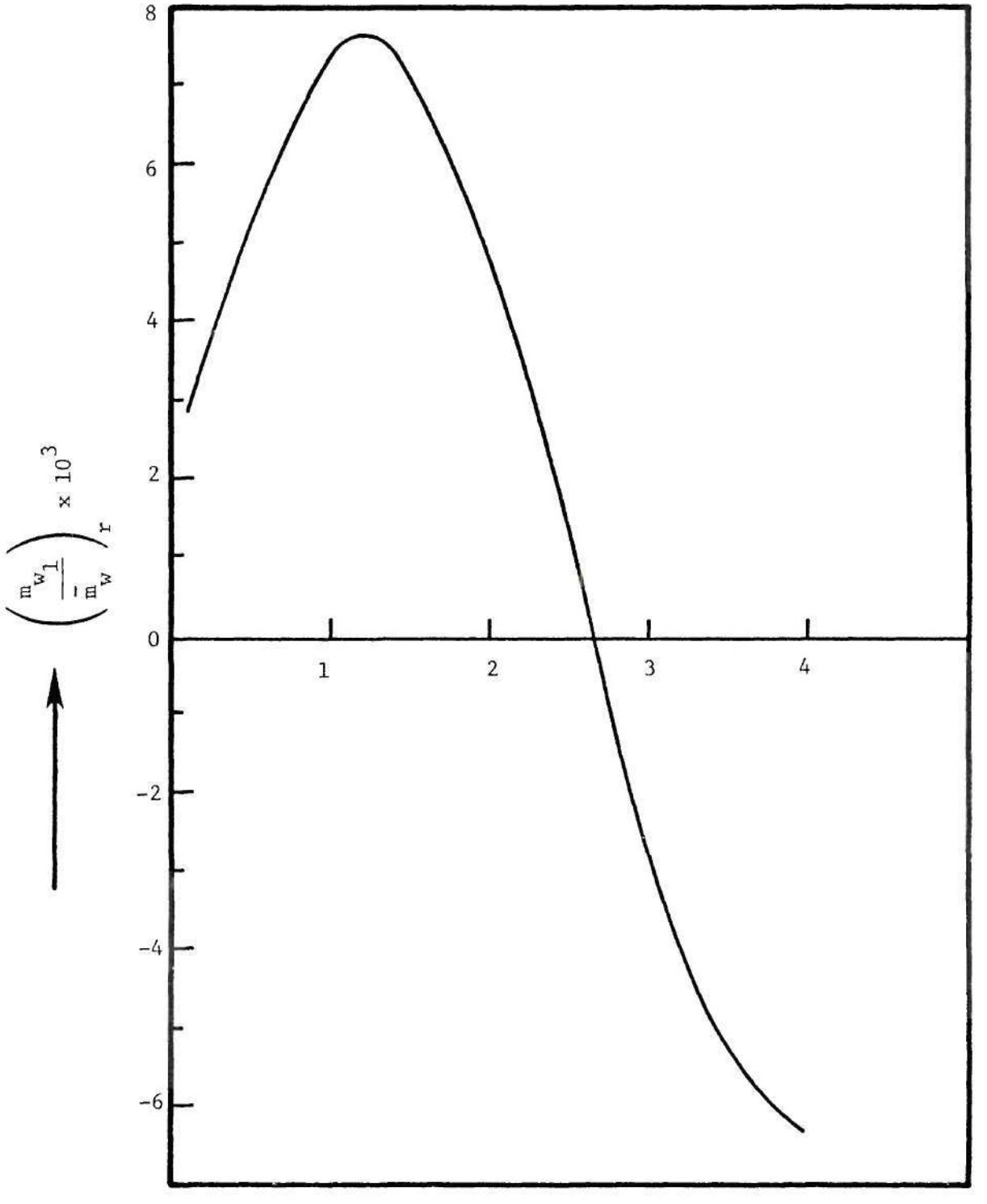

Figure 9a. Variation of the real part of the mass flux perturbation at the gas-solid interface with frequency.

importance of some of the parameters that affect the response functions R_e and R_w, discussed above. The parameters chosen characterise both the gas and solid phases. The gas phase parameters examined in this study were the Damkohler, Prandtl and Schmidt numbers; the activation energy of the gas phase reaction E, the steady pressure gradient parameter β, and the steady heat of reaction (related to $(h_2^{\circ}-h_1^{\circ})$). Most previous analyses of solid propellant combustion response did not study the influence of the above mentioned gas phase parameters. This was mainly because these parameters did not appear explicitly in the simplistic gas phase flame models that were considered. The solid phase parameters studied included those appearing in the expression for the pyrolysis law $\left(\text{i.e., } \dot{r} = A_s p^{n_s} \exp\left[-\frac{E_s}{R^{\circ}T_w}\right]\right)$; that is, the pressure exponent n_s and the activation energy E_s of the surface pyrolysis reaction. In addition to the above parameters, the dependence of the results upon the surface heat release (or absorption) parameter L and of changes in the steady regression rate $\bar{\dot{r}}$ were also studied. Finally, the variation of the response function with position (x) along the length of a solid propellant grain was also considered.

Among all the gas phase parameters considered it was found that the steady heat of reaction per unit mass did not affect the response functions noticeably. This is evident in Fig. 10 which shows the variation of the real parts of R_e and R_w with frequency. Even when the heat of formation of the product specie is reduced from h_2° = -3054.5 Btu/ℓbm to h_2° = -1174.5 Btu/ℓbm (keeping h_1° and all other parameters constant), the response function values remain virtually the same. The reason for

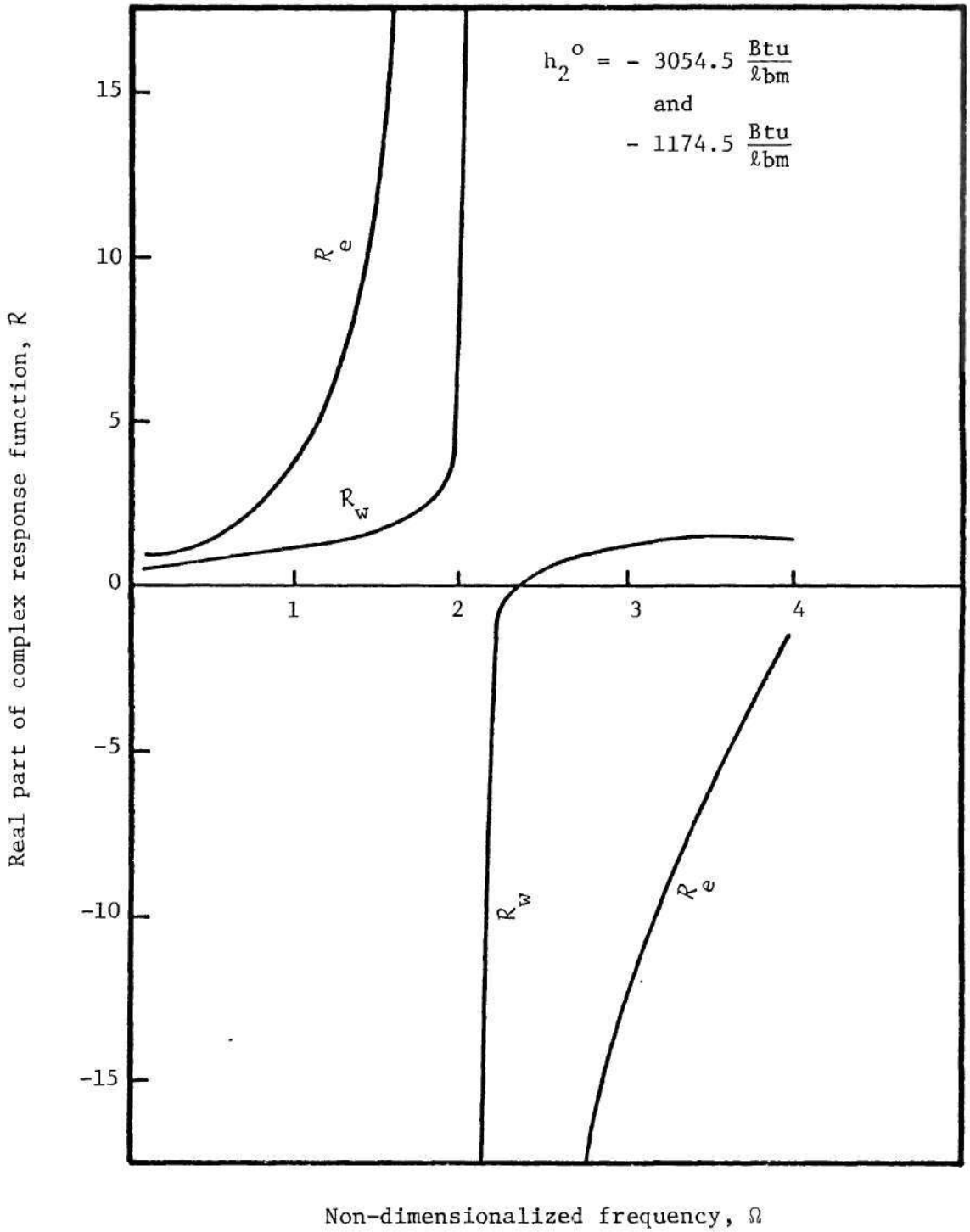

Figure 10. Effect of steady heat release in the gas phase on the real parts of the response functions at the gas-solid interface and the boundary layer edge.

this behavior is hard to pin-point owing to the complexity of the analysis.

In contrast to the negligible effect of the steady heat of reaction, as measured by the difference $\left(h_2^{\circ} - h_1^{\circ}\right)$ in the gas phase, the activation energy of the gas phase reaction, E, affected the response functions more noticeably. However, even the effect of this gas phase parameter was not too significant, besides being restricted only to frequencies corresponding to the "stable" negative branch of the curves. Figures 11 and 12 show this effect. It is also seen that for the higher value of $E = 81000 \frac{Btu}{\ell bm\text{-}mole}$, the height of the peak in the combustion response is slightly greater. The reason for the above effects is evident from Eqn. (4-30). The effect of increasing E is to increase the "sensitivity" of the gas phase reaction rate perturbation to the temperature perturbations within the boundary layer. This in itself may be expected to increase the response. However, there is also the competing effect due to the reaction rate perturbation being sensitive to the reactant mass fraction perturbation. The final result is established by a balance between these two competing effects.

The effect of all the other gas phase parameters, mentioned earlier, was found to be significant throughout the valid frequency range. The strong dependence upon the gas phase Damkohler number, D_1, is shown in Figs. 13 and 14. Increasing the Damkohler number shows an increasingly destabilizing trend. Again, Equation (4-30) suggests that the effect of increasing D_1 is to increase the sensitivity of the gas phase reaction rate perturbation to both the temperature as well as the reactant mass fraction perturbations within the boundary layer (since $\left(\frac{\omega_i}{\rho}\right)$ is increased).

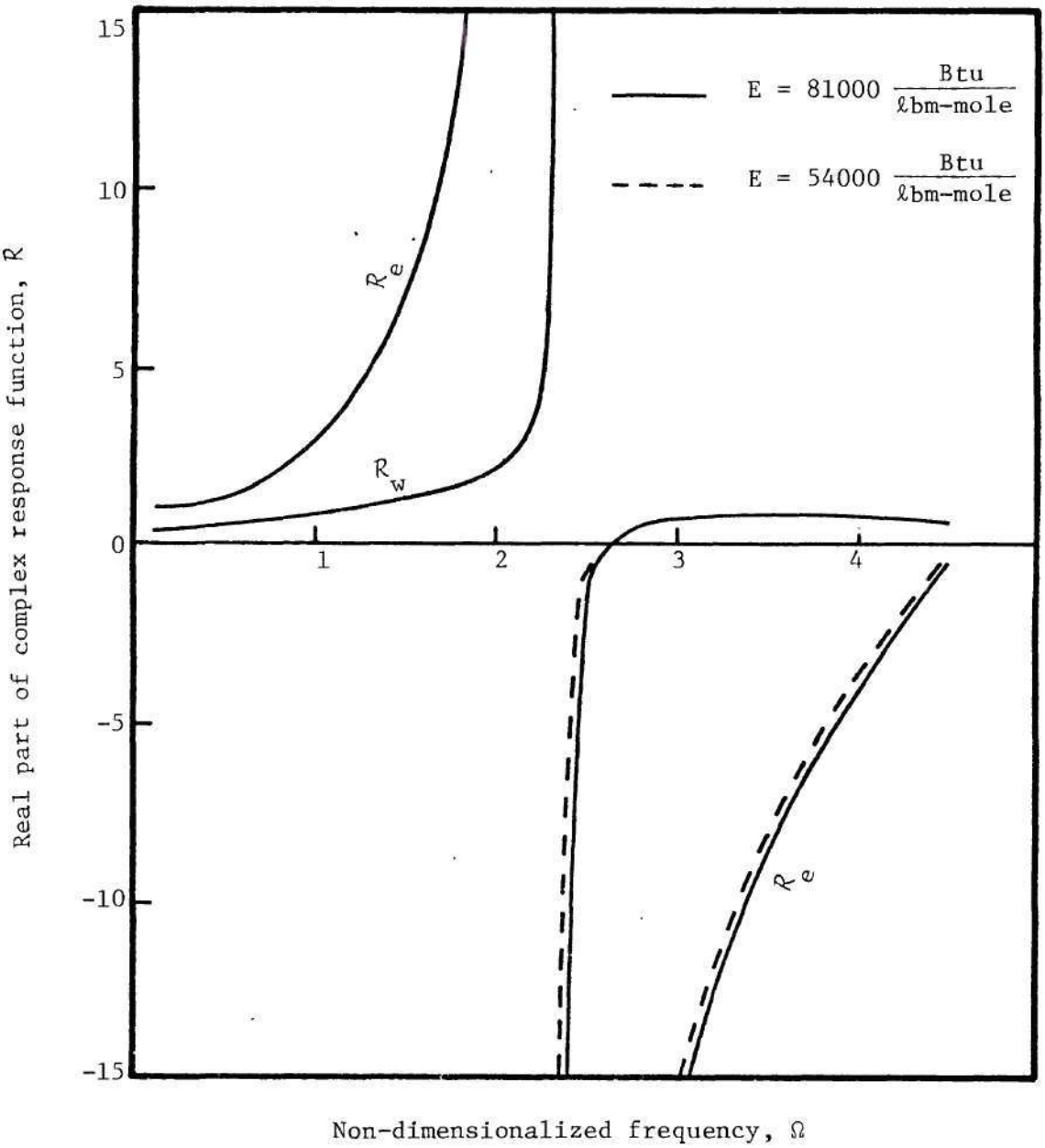

Figure 11. Effect of the activation energy of the gas phase reaction on the response function-frequency behavior at the boundary layer edge and gas-solid interface.

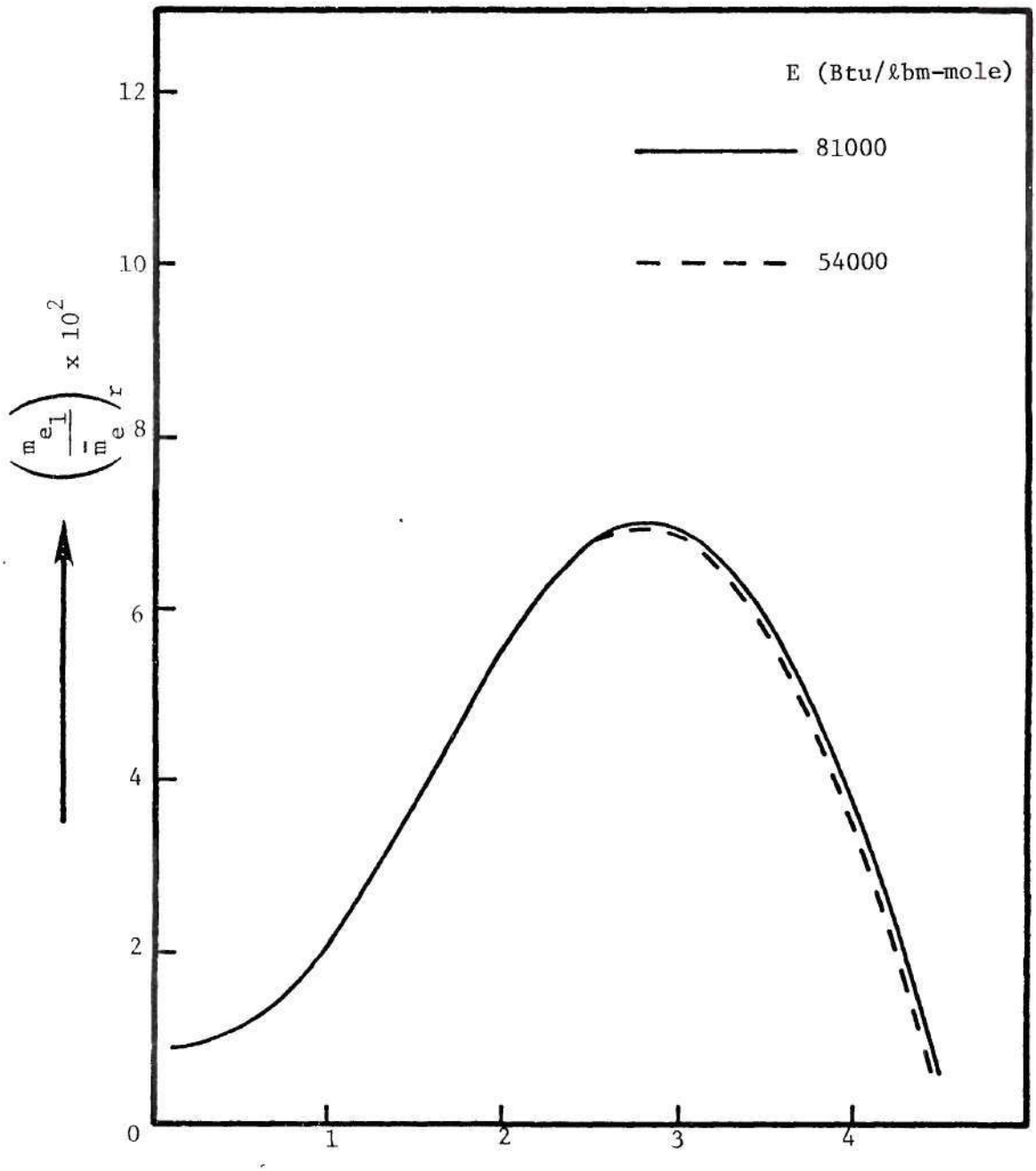

Figure 12. Effect of the activation energy of the gas phase reaction on the variation of the real part of the normal mass flux perturbation, at the boundary layer edge, with frequency.

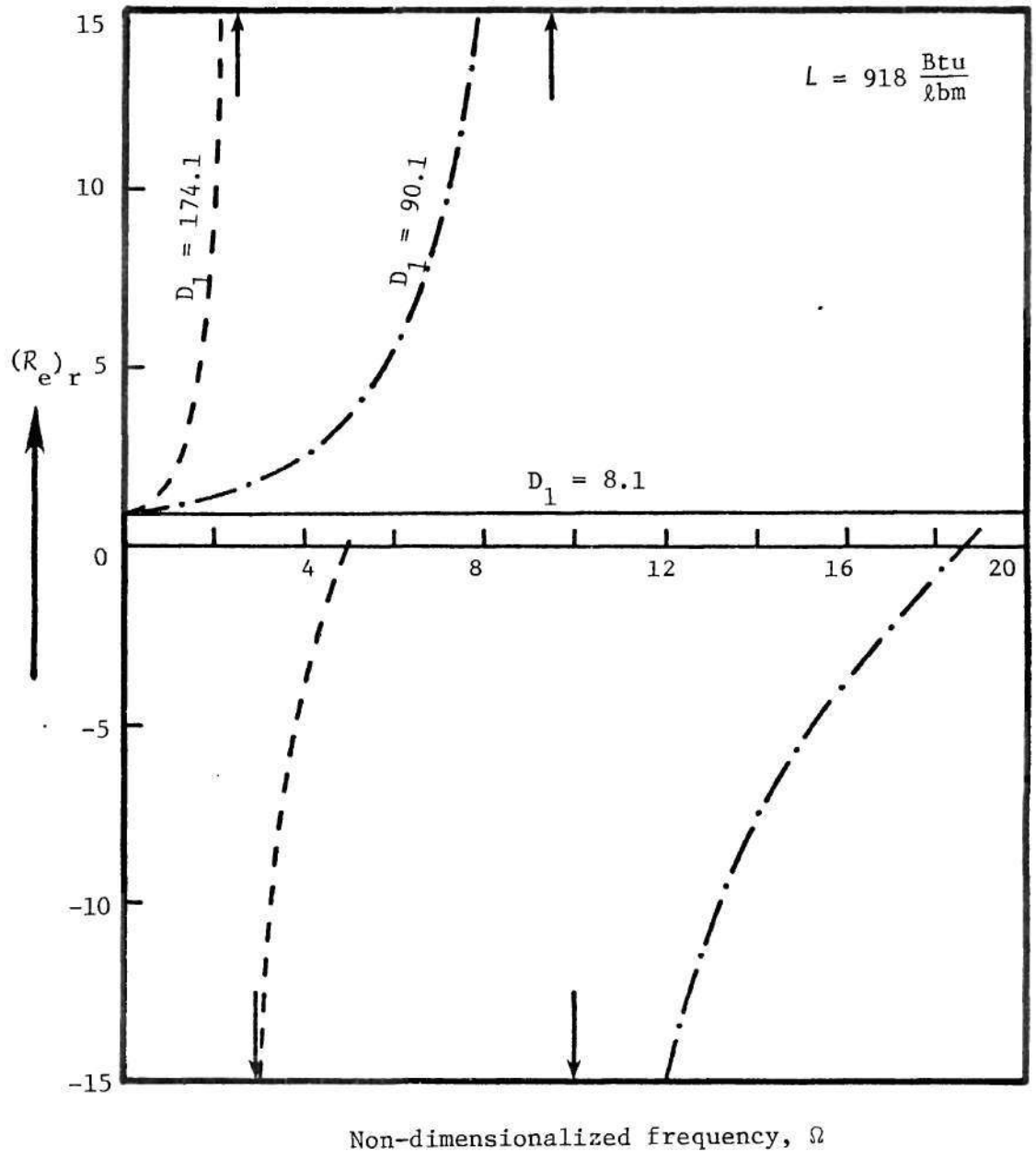

Figure 13. Effect of Damkohler number on the variation of the real part of the response function at the boundary layer edge, $(R_e)_r$, with frequency.

In the nearly frozen flow situation represented by $D_1 = 8.1$, a completely stable condition prevails, as expected, since there is an insignificant energy "gain" from the gas phase combustion. Furthermore, it should be noted that as the Damkohler number is increased, the peaks shift to lower frequencies. This effect is caused by the higher values of the steady regression rate ($\bar{\dot{r}}$) that result due to the increased heat transfer from the gas to the solid (as explained in Chapter III). Since the non-dimensional frequency Ω varies inversely as the square of the steady regression rate (see Eqn. (4-14)), Ω decreases as $\bar{\dot{r}}$ increases for a given dimensional frequency. Finally, it can be seen from Figs. 13 and 14 that the response function peaks become noticeably narrower as the Damkohler number is increased. In previous analyses (e.g., see Ref. 36) the width of the response function peaks has been related to the amount of net energy removal/addition from the waves - the greater the removal the wider the peaks**. Hence, in the present case, the peak is narrower when $D_1 = 174.1$, than in the case with $D_1 = 90.1$, since the waves would be expected to gain more energy, the higher the rate of combustion (i.e., less energy removal). The corresponding dependence of $(R_w)_r$ on frequency

---

** This argument has been based on an analogy drawn between the unsteady frequency response of a burning propellant and that of a mechanical system consisting of a mass, spring and dashpot. In the latter case, the frequency response peaks are known to become broader as the damping in the system is increased - that is, as energy is removed from the vibrating mass and the spring by the dashpot. It should also be pointed out that in the present case the change in width of the peaks cannot be explained as being only the effect of a changing steady regression rate (with different Damkohler numbers) on $\Omega \equiv \dfrac{\omega}{\bar{\dot{r}}^2/\alpha_s}$,

since the value of $\bar{\dot{r}}$ does not change significantly.

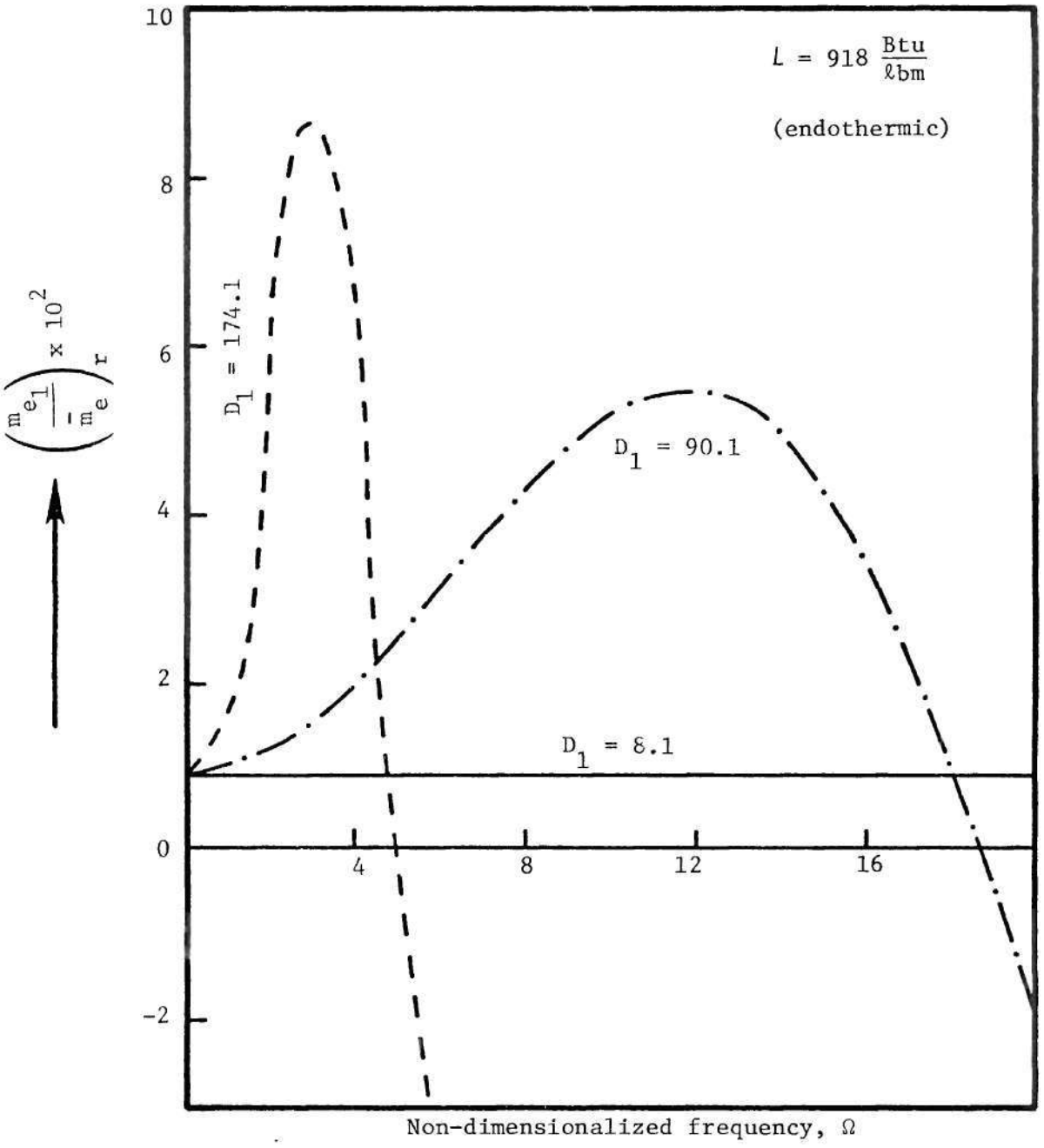

Figure 14. Effect of Damkohler number on the variation of the real part of the normal mass flux perturbation with frequency, at the boundary layer edge.

is shown in Fig. 15. This too shows an increasing tendency towards instability as D_1 increases. However, the effect of D_1 on $(\mathcal{R}_w)_r$ is not as pronounced. This is because in this case the surface heat absorption parameter L has a high endothermic value of 918 $\frac{Btu}{\ell bm}$. This large absorption of energy at the gas-solid interface reduces the amount of energy available for the oscillations just above the burning surface, and thus lowers $(\mathcal{R}_w)_r$ to values corresponding to a stable condition throughout the frequency range.

In contrast to the above mentioned situation where the surface reaction was highly endothermic, Figs. 16 and 17 show the effect of D_1 in the case when an exothermic heat release, corresponding to $L = -100$ $\frac{Btu}{\ell bm}$, is present at the gas-solid interface. The behavior of $(\mathcal{R}_e)_r$ remains basically the same as before. The combustion response curves in terms of $\left(\frac{\bar{m}_{e_1}}{\bar{m}_e}\right)_r$, as shown in Fig. 17, further support the above statements. The effect of L will be further discussed later in connection with the effects of solid phase parameters.

In connection with the effects of D_1 shown in Figs. 13 through 17, a useful consequence of the definition of the Damkohler number (as given by Eqn. (3-21)) is worth noting. Since D_1 is a non-dimensional grouping involving the parameters m, G, Z, T_o, α and x, varying D_1 is equivalent to varying one of these, keeping the others constant. This property of D_1 was exploited earlier in Chapter III to study the variation of the steady-state solutions with x. Here it may be used to study the effect of the mean flow, through the velocity gradient G, on the response function using the results of Figs. 13 through 17. In Figure 13 for the case $D_1 = 90.1$,

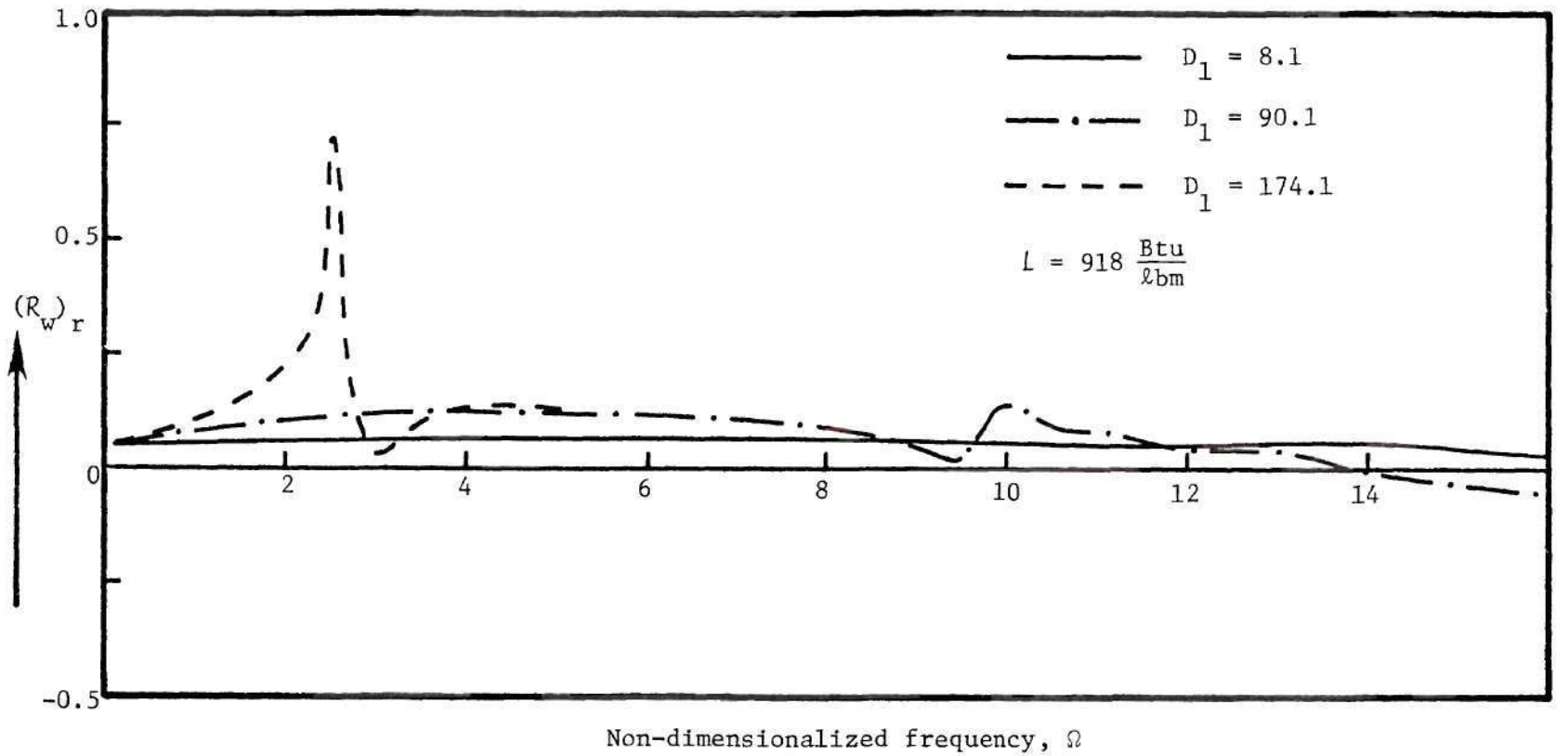

Figure 15. Effect of Damkohler number on the variation of the real part of the response function at the gas-solid interface, $(R_w)_r$, with frequency.

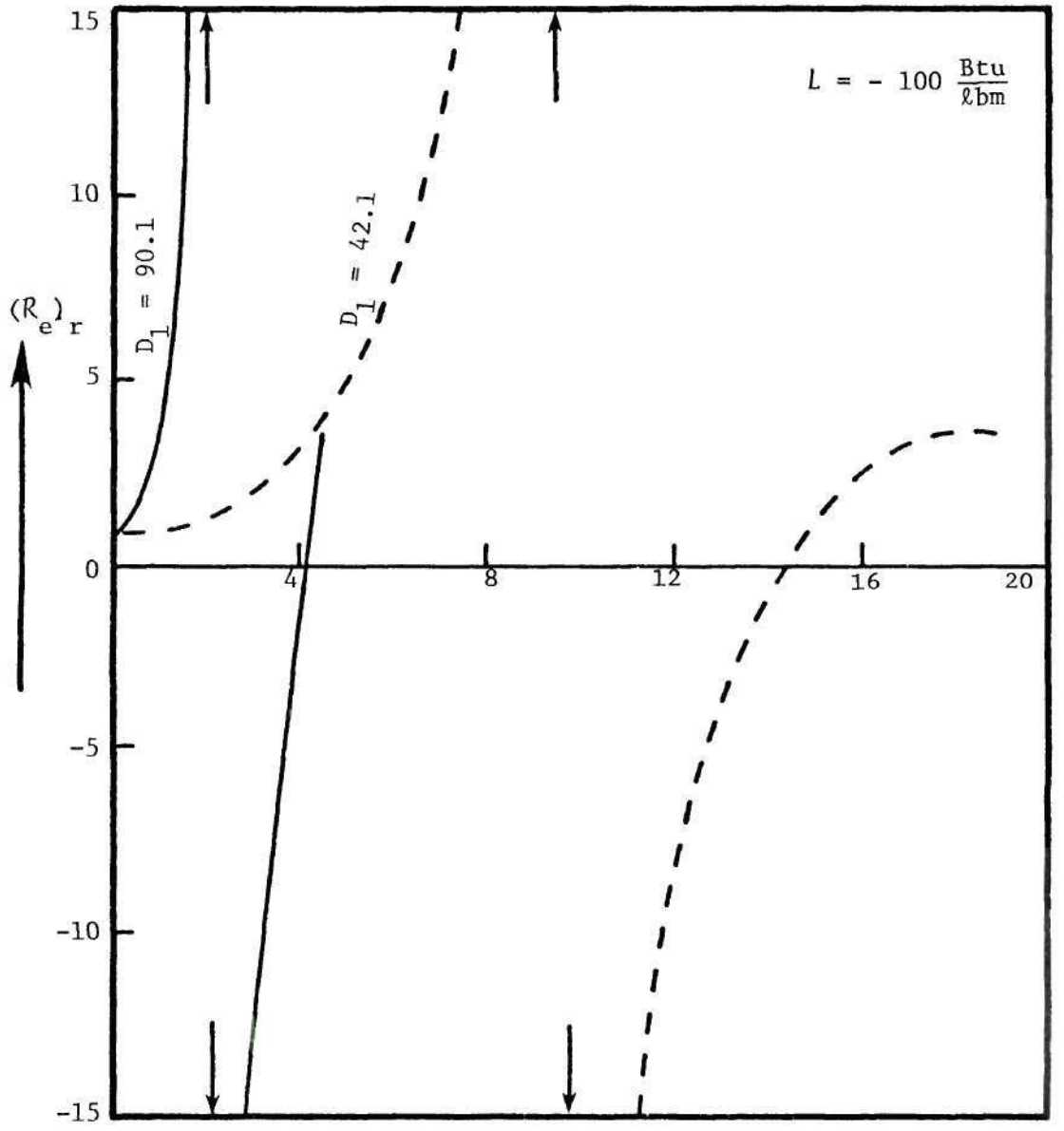

Figure 16. Effect of Damkohler number on the variation of the real part of the response function at the boundary layer edge, with frequency (for an exothermic heat release at the gas-solid interface).

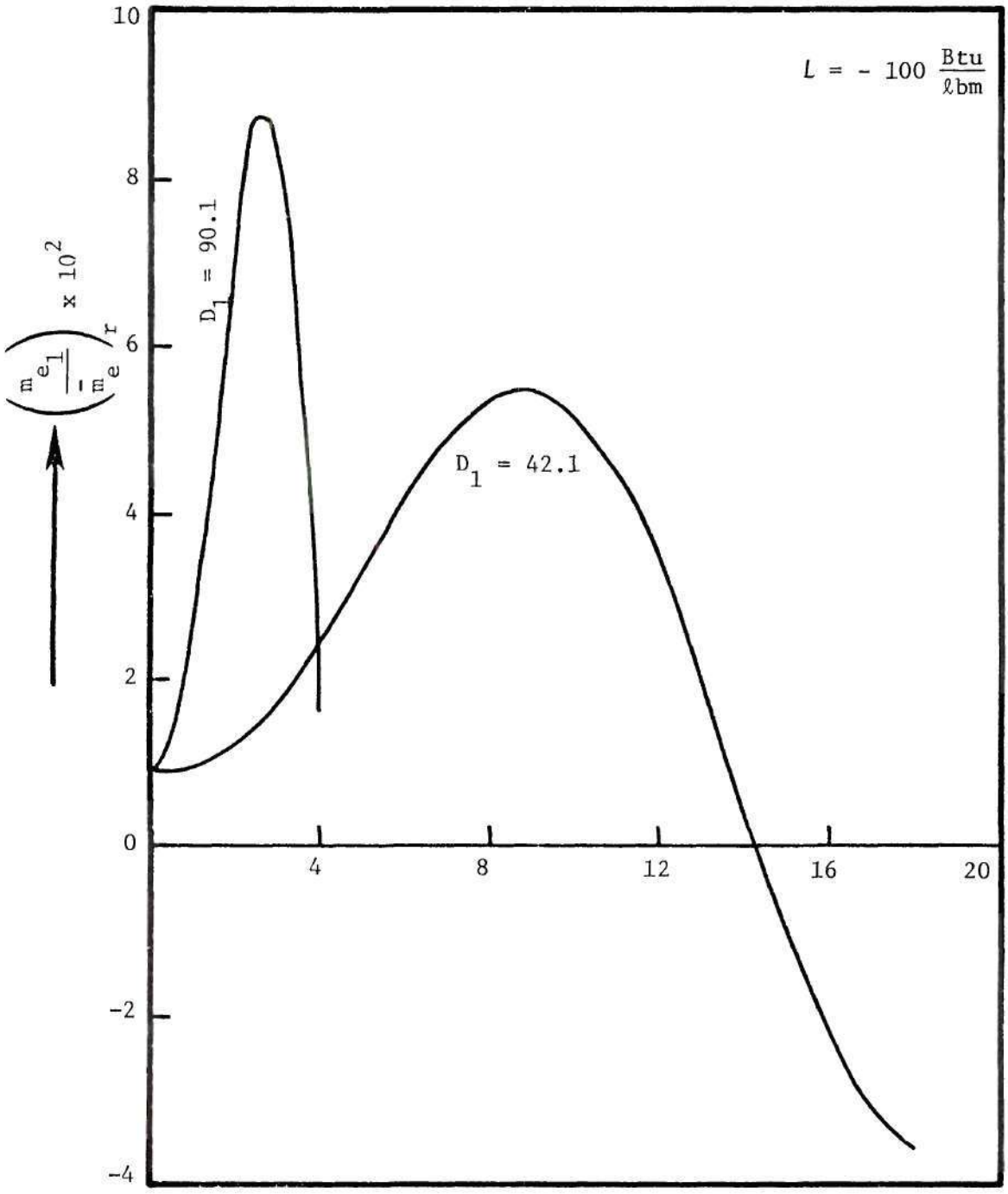

Figure 17. Effect of Damkohler number on the variation of the real part of the normal mass flux perturbation, at the boundary layer edge, with frequency.

the following parameters were used:

$$G = 200$$

$$Z = 1$$

$$T_o = 4680^\circ R$$

$$\alpha = 1$$

$$x = 8.3395 \text{ ft.}$$

$$m = 0.5$$

and the mean flow velocity was given by

$$\bar{u}_e = Gx^m = 603.2 \frac{ft}{sec}$$

For the case of $D_1 = 174.1$, using the above values of Z, T_o, α, x and m in Eqn. (3-21) yields a value for the velocity gradient of G = 103.5. This corresponds to a mean flow velocity of $\bar{u}_e = 298.9 \frac{ft}{sec}$. Hence, the effect of increasing D_1 from 90.1 to 174.1 in Figures 13,14 and 15 corresponds to decreasing the mean flow velocity in the external stream of the boundary layer from $603.2 \frac{ft}{sec}$ to $298.9 \frac{ft}{sec}$. Similarly in Figs. 16 and 17, for the case of an exothermic surface heat release, decreasing D_1 from 90.1 to 42.1 has the same effect as increasing the mean flow velocity, at a given x-location, from $\bar{u}_e = 603.2 \frac{ft}{sec}$ to $1236.07 \frac{ft}{sec}$. Physically, the above statements imply that if the steady chemical reaction rate (or the characteristic chemical time τ_c) were held constant at a given x-location, increasing Damkohler numbers would reflect decreasing mean flow velocities (or increasing flow times τ_f). Slower mean flows will, of course, reduce the steady erosion effect on the propellant's burning rate. However, there is also an opposing unsteady effect of the mean flow associated with the chemical reaction rate perturbation $\left(\frac{\omega_i}{\rho}\right)_1$.

As seen from Eqns. (4-30) to (4-32), decreasing $\bar{u}_e$ tends to increase the reaction rate perturbation in the gas phase by increasing the temperature perturbations. The net result of these effects leads to increasing values of $(R_w)_r$, $(R_e)_r$ and $\left(\frac{\bar{m}_{e_1}}{\bar{m}_e}\right)_r$ with decreasing mean flow speeds.

Next, the effect of the steady pressure gradient parameter m, or the related quantity $\beta \equiv \frac{2\xi}{\bar{u}_e}\frac{d\bar{u}_e}{d\xi}$, is considered. It is interesting to note that although the steady momentum equation (i.e., Eqn. (2-44)) does not contain the pressure gradient term, the first order momentum equation describing the behavior of the gas phase perturbations shows an explicit dependence on β (see Eqn. (4-25)). This is a result of the Lee's approximation which requires the quantity $\left[\frac{\bar{\rho}_e}{\bar{\rho}} - (\bar{f}')^2\right]$, multiplying the non-zero β, to tend to zero in the steady-state analysis. For the unsteady analysis, the complete "steady-state" momentum equation (including the effect of pressure gradient) is linearised. In this linearised momentum equation all first order terms multiplying β have to be retained. However, if β is zero, the complicated inhomogeneous term would drop out of Eqn. (4-25) and possibly a much simpler approach to the present problem can be adopted, after the method of Reference 37. In order to see the effect of the above mentioned pressure gradient term the response was found for the condition when $\beta = 0.6667$, and then the computations were repeated for the case $\beta = 0$. Figures 18 and 19 show these results. It is seen that $(R_w)_r$, $(R_e)_r$ and $\left(\frac{\bar{m}_{e_1}}{\bar{m}_e}\right)_r$ are all affected throughout the frequency range of interest. As seen from Eqn. (4-72), the effect of the steady pressure gradient, present through A*, lies in increasing the

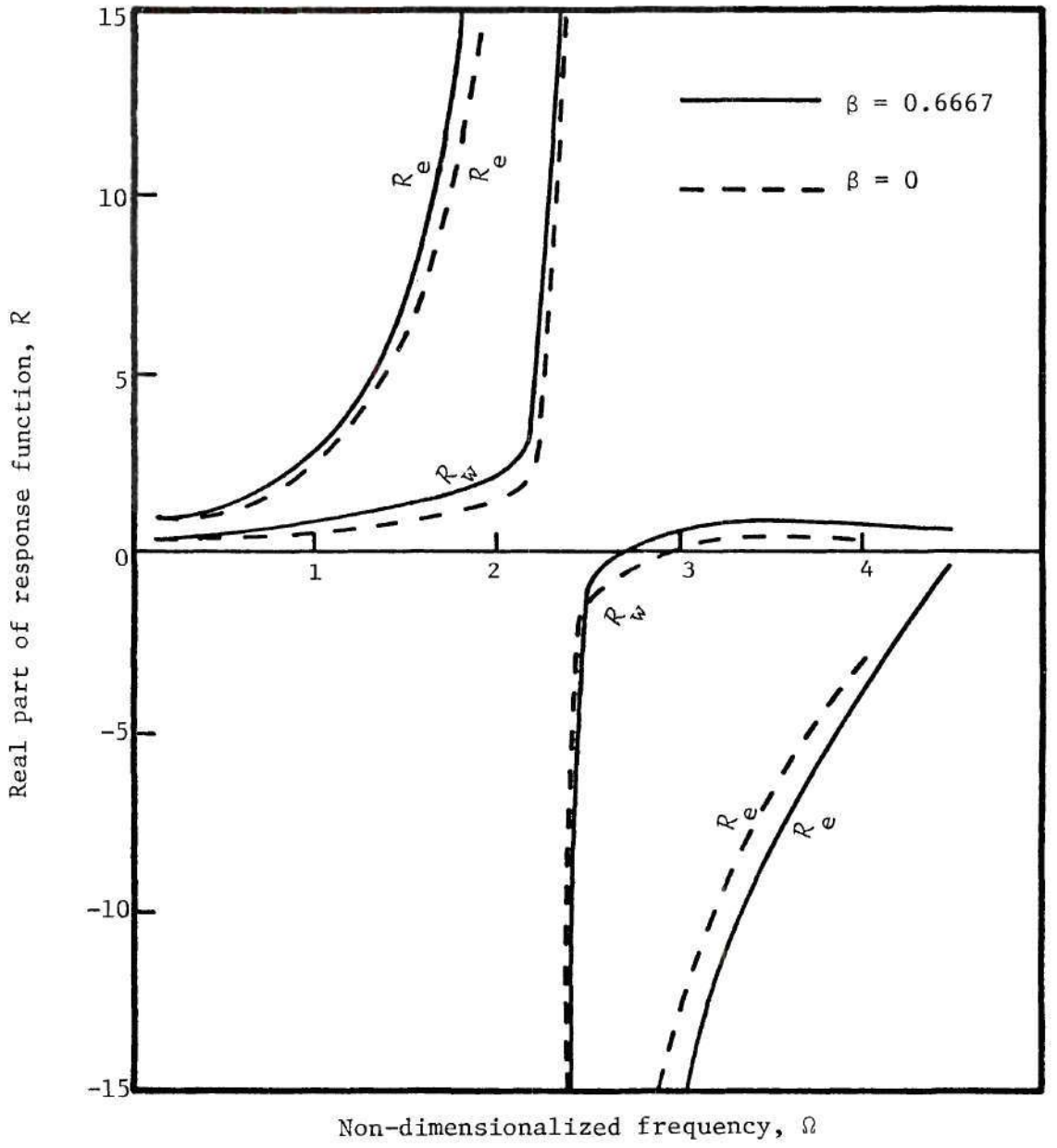

Figure 18. Effect of pressure gradient on the variation of the real part of the response function, at the interface and at the boundary layer edge, with frequency.

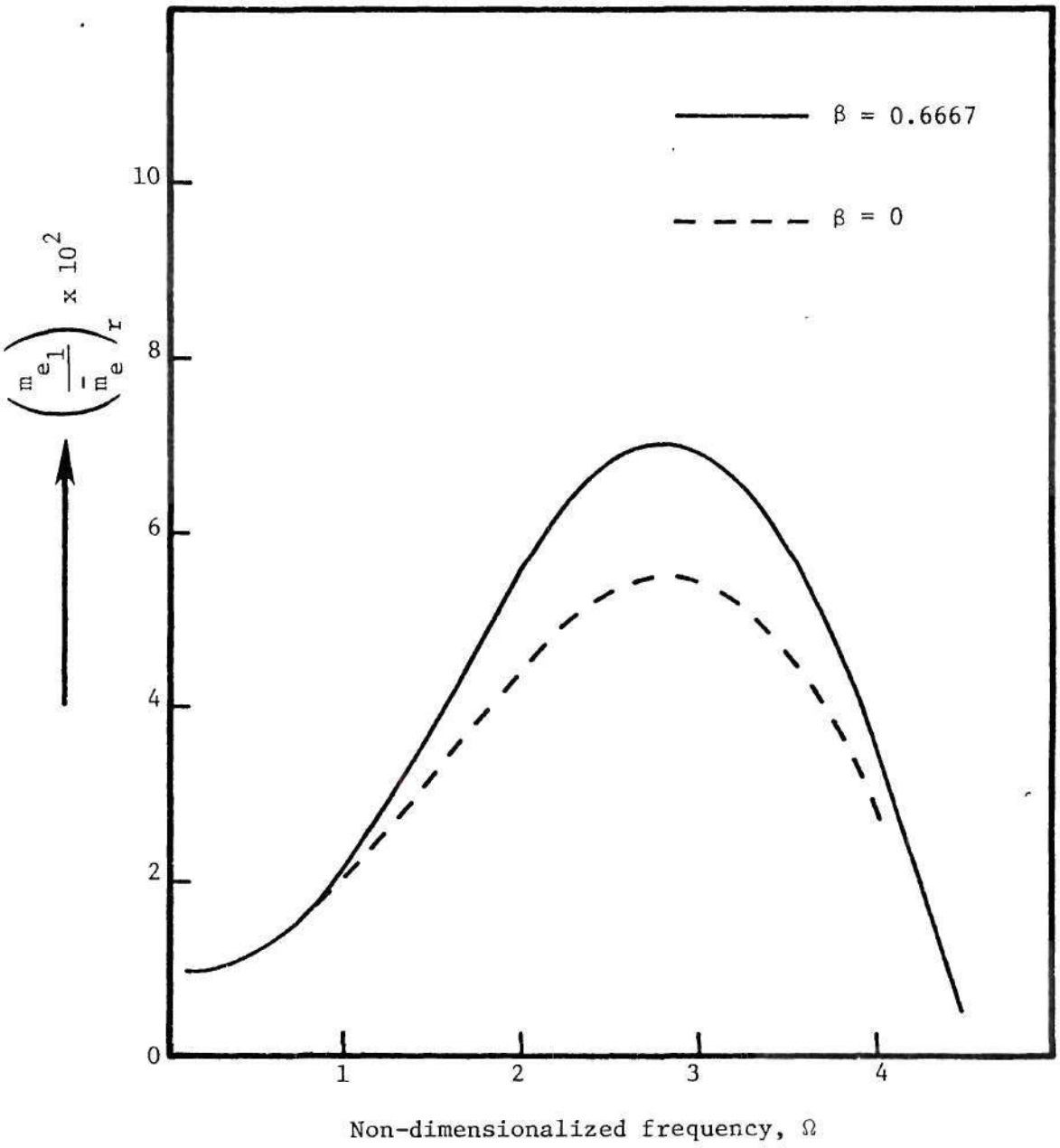

Figure 19. Effect of pressure gradient on the variation of the real part of the normal mass flux perturbation, at the boundary layer edge, with frequency.

sensitivity of the response at the boundary layer edge to both the compressibility effects within the boundary layer and to the velocity oscillations present in the external stream. These important effects cannot be ignored in the present analysis.

In the present analysis, another significant gas phase parameter is the Prandtl number, which also equals the Schmidt number. In earlier works, these numbers were taken to be unity because of the mathematical simplicity that resulted from using this assumption. However, Figure 20 shows that there is a significant difference in the values of both $(R_e)_r$ and $(R_w)_r$ when the more realistic case of Pr = Sc = 0.78 is considered. Reducing the value of Pr (or Sc) not only shifts the peaks to lower values of Ω but also increases the value of $(R_e)_r$ and $(R_w)_r$ corresponding to a given Ω. The former effect is due to an increase in the steady regression rate (as pointed out in Chapter III) while the latter is the result of the combined effects of changes in the heat flux perturbation and in the surface temperature perturbation, as evident from Eqn. (4-40). Reducing the Prandtl number increases the sensitivity of the burning rate perturbation to the heat flux perturbation from the gas to the solid at their interface. This manifests itself as a larger $(R_w)_r$. The boundary layer then further magnifies this response, as shown by the curve for $(R_e)_r$. The corresponding combustion response behavior, shown in Fig. 21 in terms of $\left(\frac{\bar{m}_{e_1}}{\bar{m}_e}\right)_r$, again conforms with the trends pointed out above in connection with $(R_e)_r$.

In contrast to the effect of the gas phase parameters discussed above, not all of which are significant in their influence, it was found

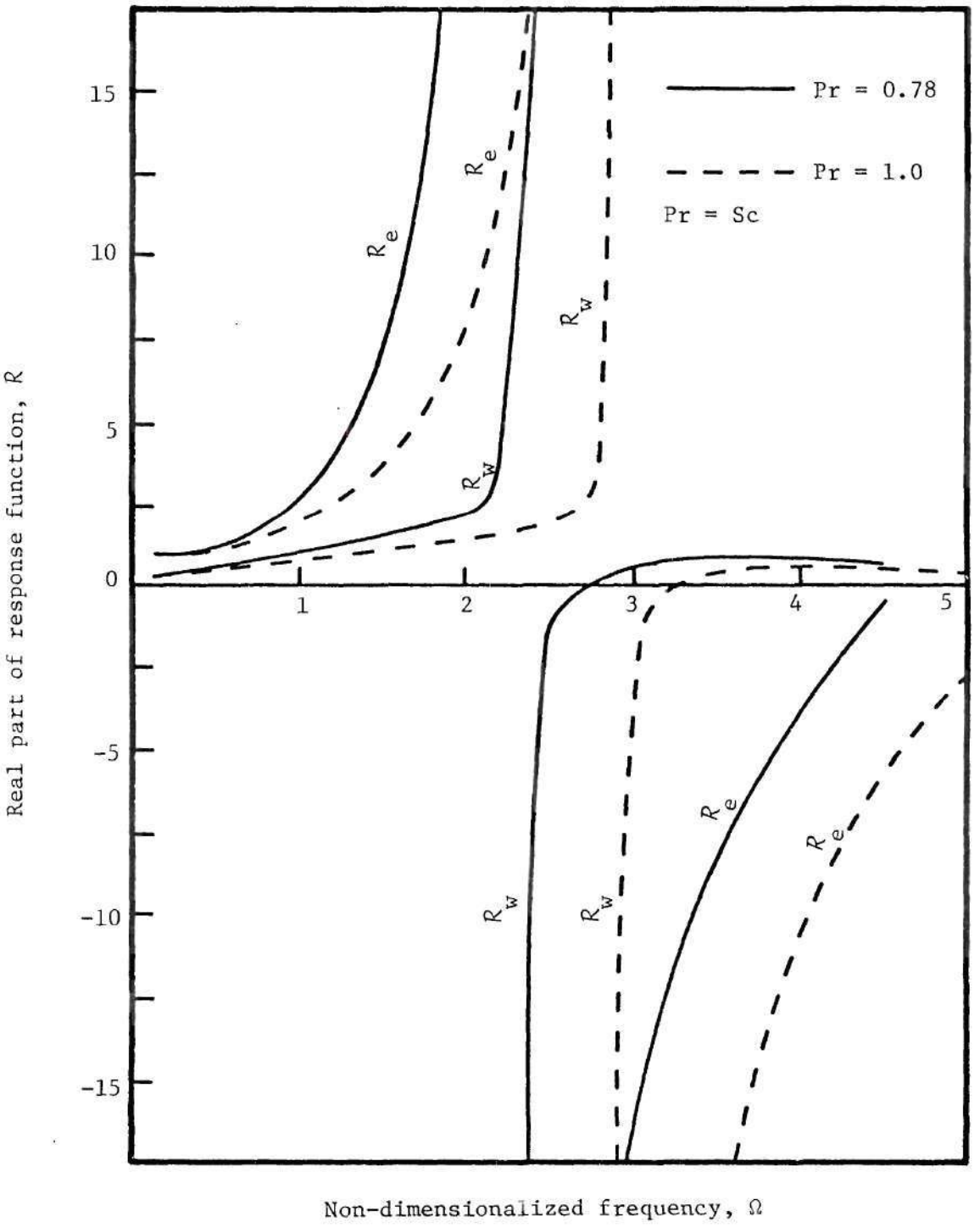

Figure 20. Effect of Prandtl and Schmidt numbers on the variation of the real parts of the response functions with frequency, at the gas-solid interface and the boundary layer edge.

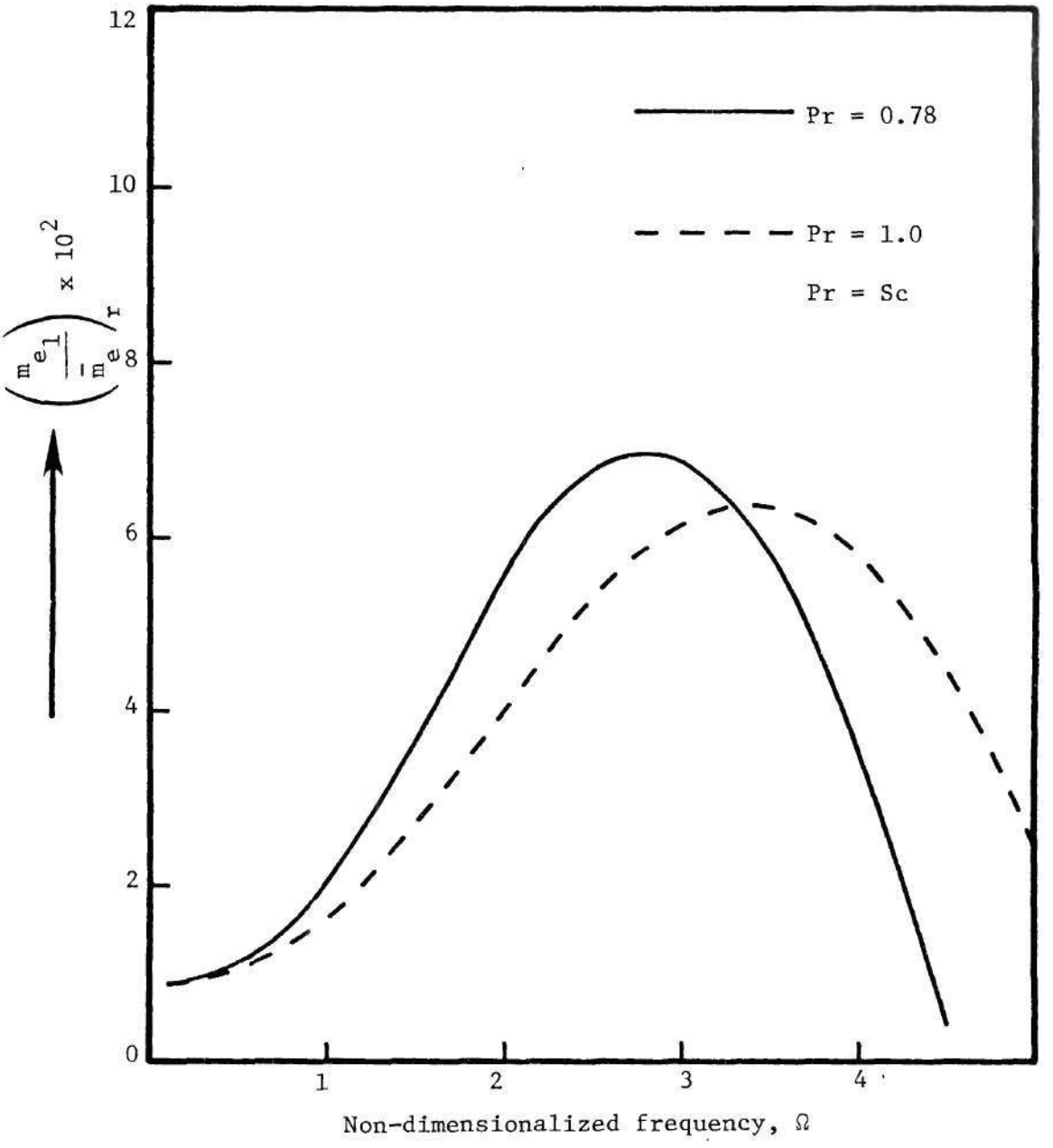

Figure 21. Effect of Prandtl and Schmidt numbers on the variation of the real part of the normal mass flux perturbation, at the boundary layer edge, with frequency.

that the propellant response was very sensitive to all of the considered solid phase parameters. Figures 22 and 23 show the effect of the interface heat release (or absorption) parameter L. As mentioned earlier, the effect of changing L from a large endothermic value to an exothermic one results in increasing the energy available to the waves, similar to the tendency noticed for increasing Damkohler numbers. This is also evident from Figs. 22 and 23 which show the behavior of $(R_e)_r$ and $\left(\frac{\dot{m}_{e_1}}{\dot{m}_e}\right)_r$ with frequency. The following features should be noticed:

a) As the pyrolysis reaction at the interface becomes more exothermic, the steady regression rate increases and this shows as a shift of the response peak to a lower frequency Ω.

b) The width of the peaks decreases as L becomes more exothermic.

c) Even when there is a large absorption of energy at the interface (as for $L = 918 \frac{\text{Btu}}{\ell\text{bm}}$), the strong amplifying influence of the boundary layer causes the response to peak - showing an unstable tendency. In the case of the exothermic release of energy at the interface the boundary layer further enhances the possibility of instability, as expected.

Figures 24 and 25 further illustrate the strong effect of L on the response function. Since L is an interface parameter, its influence shows mainly in the behavior of $(R_w)_r$. For the large endothermic value of $L = 918 \frac{\text{Btu}}{\ell\text{bm}}$, the $(R_w)_r$ vs Ω curve indicates a completely stable condition (see Figure 24). On the other hand, $(R_e)_r$ still shows a sharp positive "peak", emphasizing the strong destabilizing influence of the boundary layer. When a highly exothermic value of $L = -180 \frac{\text{Btu}}{\ell\text{bm}}$ is considered (as in Fig. 25) a "peak" appears in the $(R_w)_r$ curve also, as expected,

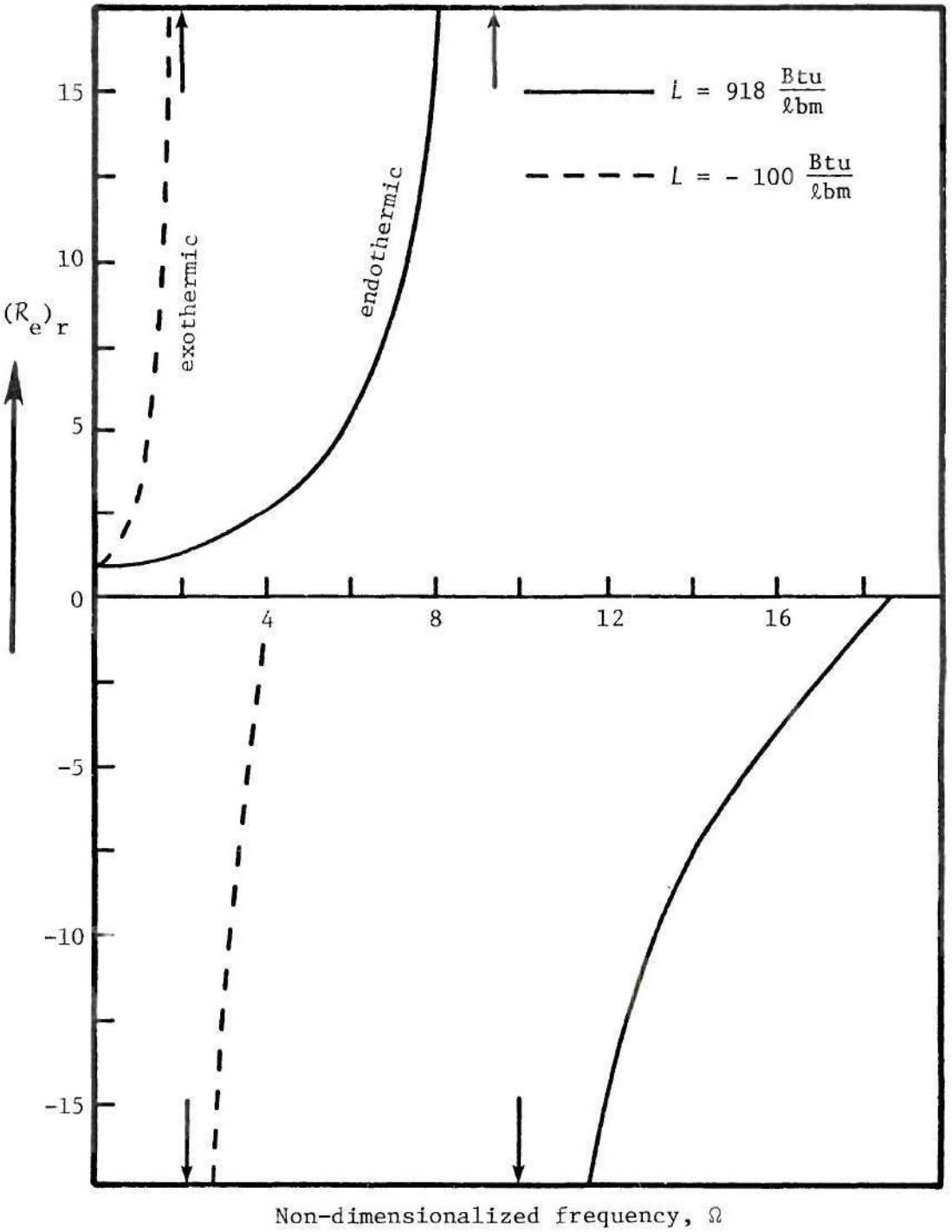

Figure 22. Effect of surface heat release (or absorption) parameter on the variation of the real part of the response function at the boundary layer edge.

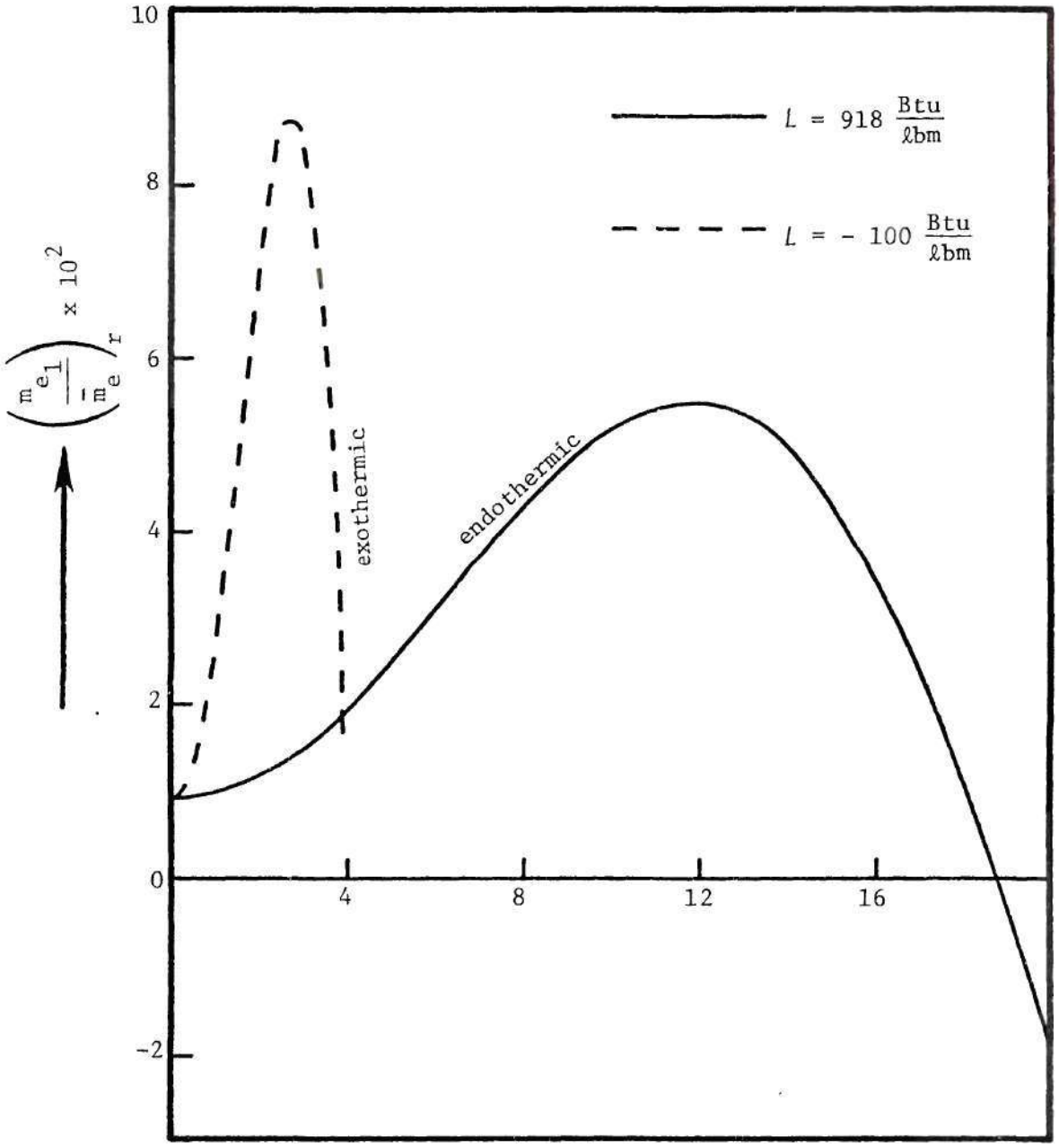

Figure 23. Effect of surface heat release (or absorption) parameter on the variation of the real part of the normal mass flux perturbation, at the boundary layer edge, with frequency.

since energy is being added to the oscillations immediately above the gas-solid interface. Again, the quantity $|p_1|^2(R_w)_r$ can be related to the energy "gain" or "loss" of the oscillations just above the burning surface. Physically the effect of an exothermic heat release at the interface would be to cause the surface temperature perturbation to increase (in contrast to the endothermic case) which in turn manifests itself as a higher regression rate perturbation, or $(R_w)_r$.

It is to be noted that most real solid rocket burning situations are characterised by highly exothermic surface reactions. Figures 24 and 25 reveal that in the absence of strong energy absorption at the gas-solid interface, as in the case of $L = 918 \frac{\text{Btu}}{\text{lbm}}$, the behavior of both $(R_w)_r$ and $(R_e)_r$ with frequency is similar. That is, under typical solid rocket burning conditions, the oscillations immediately above the burning surface as well as those outside the boundary layer will both either tend to be amplified or stabilized.

Another important parameter that affects the combustion response significantly is the activation energy of the pyrolysis reaction at the gas-solid interface, E_s. Again, the effect of E_s on $(R_w)_r$ is expected to be strong. Indeed, Fig. 26 shows this to be true. Three values of E_s covering a realistic range are considered. It is seen that as E_s increases from 18000 $\frac{\text{Btu}}{\text{lbm-mole}}$ to 54000 $\frac{\text{Btu}}{\text{lbm-mole}}$, the value of $(R_w)_r$ at a given Ω increases - showing a destabilizing trend. This trend is to be expected from Eqn. (4-39) from which it is seen that E_s is a measure of the sensitivity of the burning rate perturbations (and hence R_w) to the surface temperature perturbations. It should be noted that although the

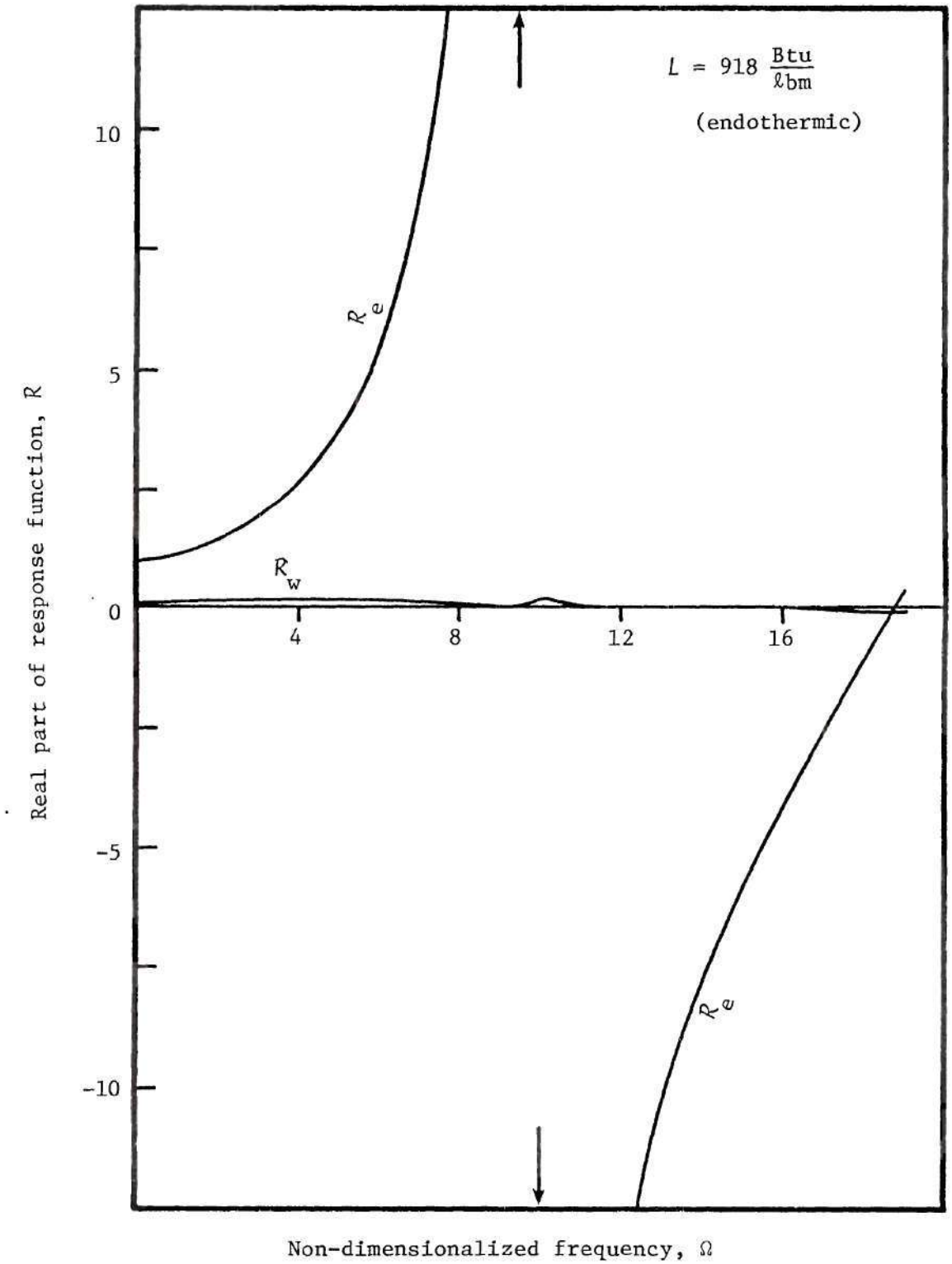

Figure 24. Comparison of the response function behavior with frequency, at the gas-solid interface and the boundary layer edge (for endothermic heat absorption at the interface).

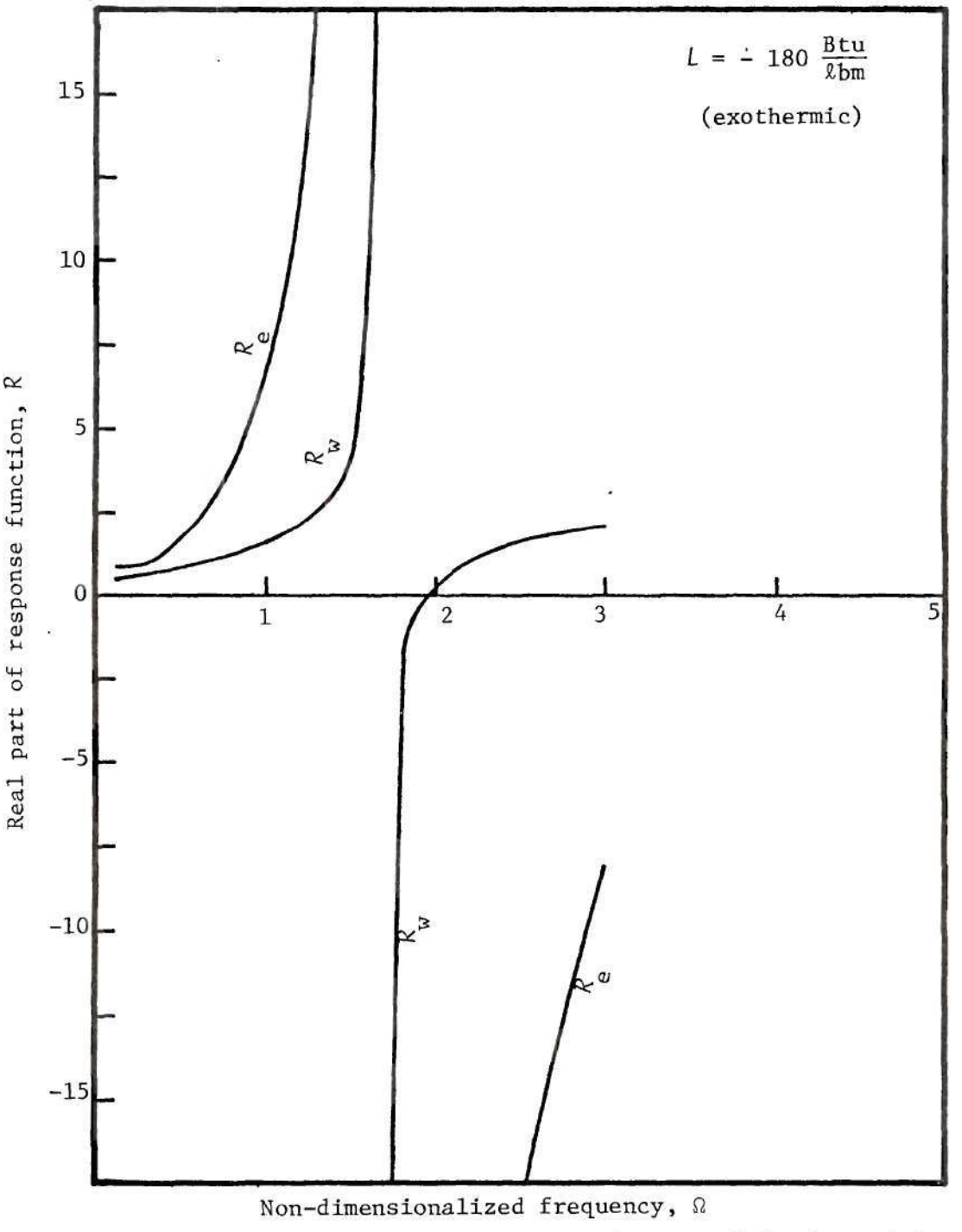

Figure 25. Comparison of the response function behavior, with frequency, at the gas-solid interface and the boundary layer edge (for a highly exothermic heat release at the interface).

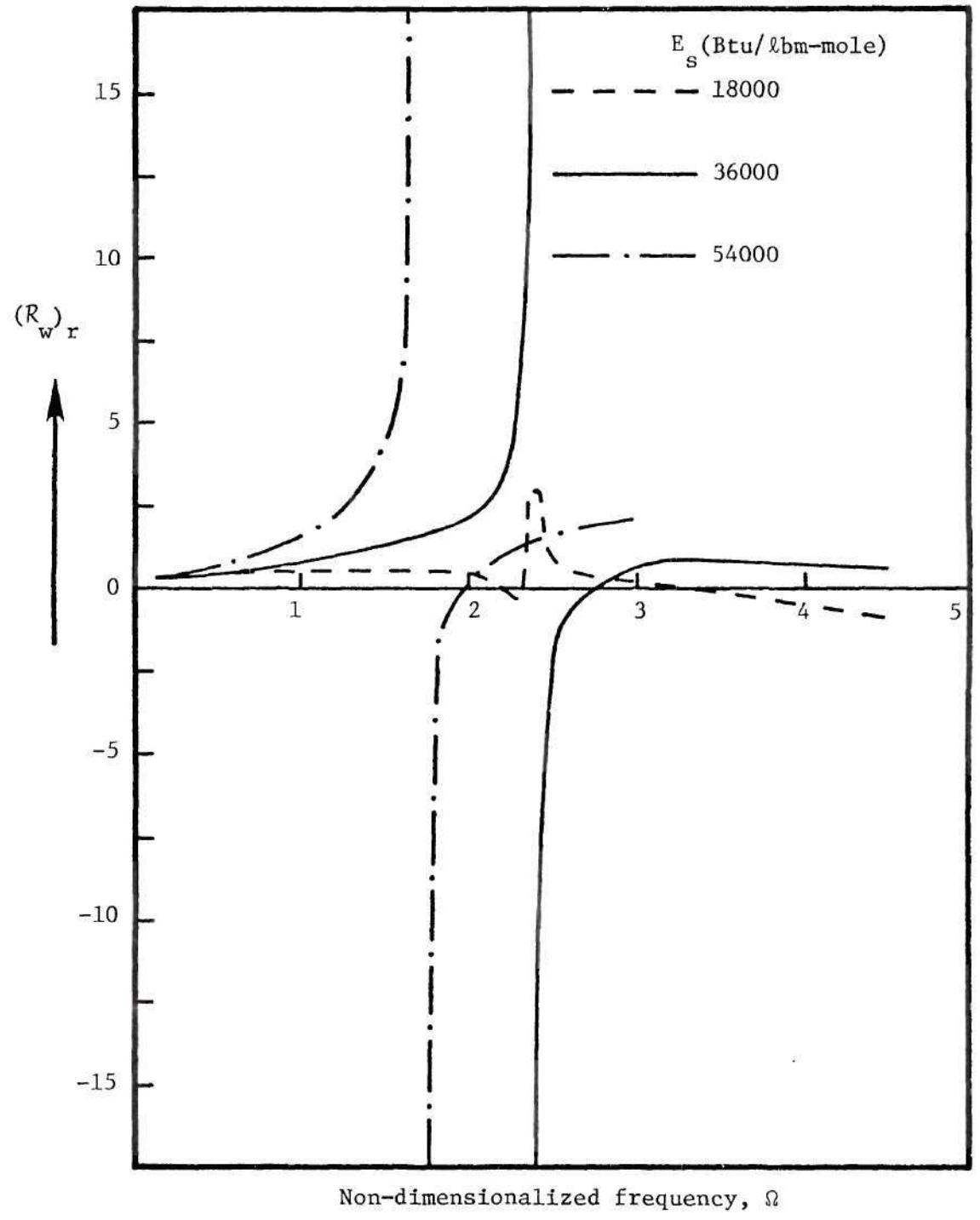

Figure 26. Effect of the activation energy for pyrolysis on the variation of the real part of the response function, at the gas-solid interface, with frequency.

direct effect of an increase in E_s, which is the energy required to activate the conversion of solid to gas by pyrolysis, is to reduce the steady regression rate, the regression rate perturbation is enhanced as dictated by Eqn. (4-39). Finally, it must be pointed out that the shift in the positions of the peaks in this case is not an effect of increasing E_s. It is a result of the different values of A_s (the pre-exponential constant in the pyrolysis law) that were used for the three cases considered. This was necessary to keep the steady regression rate within a realistic range. The corresponding curves of $(R_e)_r$ and $\left(\frac{m_{e_1}}{\bar{m}_e}\right)_r$ vs Ω are shown in Figs. 27 and 28, respectively. The basic trends discussed above apply to these curves also. The additional amplifying effect of the boundary layer is again evident.

To complete the study of solid phase parameters, the effect of the pressure exponent n_s on the combustion response was investigated. All the results presented so far were computed for the case of a pressure-independent pyrolysis law (i.e., $n_s = 0$). Now the more general case of a non-zero n_s is considered. Using a value of $n_s = 1.0$ (and with $A_s = 1.0$ to yield a realistic value for the regression rate) the response functions R_w and R_e were computed. Figure 29 shows the strong effect of a pressure dependent pyrolysis law at the gas-solid interface. For a given value of Ω, the response is reduced at the interface. The reason for this can be seen from the perturbed form of the pyrolysis law (see Eqn. (4-39)). The effect of a non-zero n_s is to render the burning rate perturbations sensitive to the pressure perturbations also, besides the sensitivity to temperature perturbations that already exists. However, the direct effect

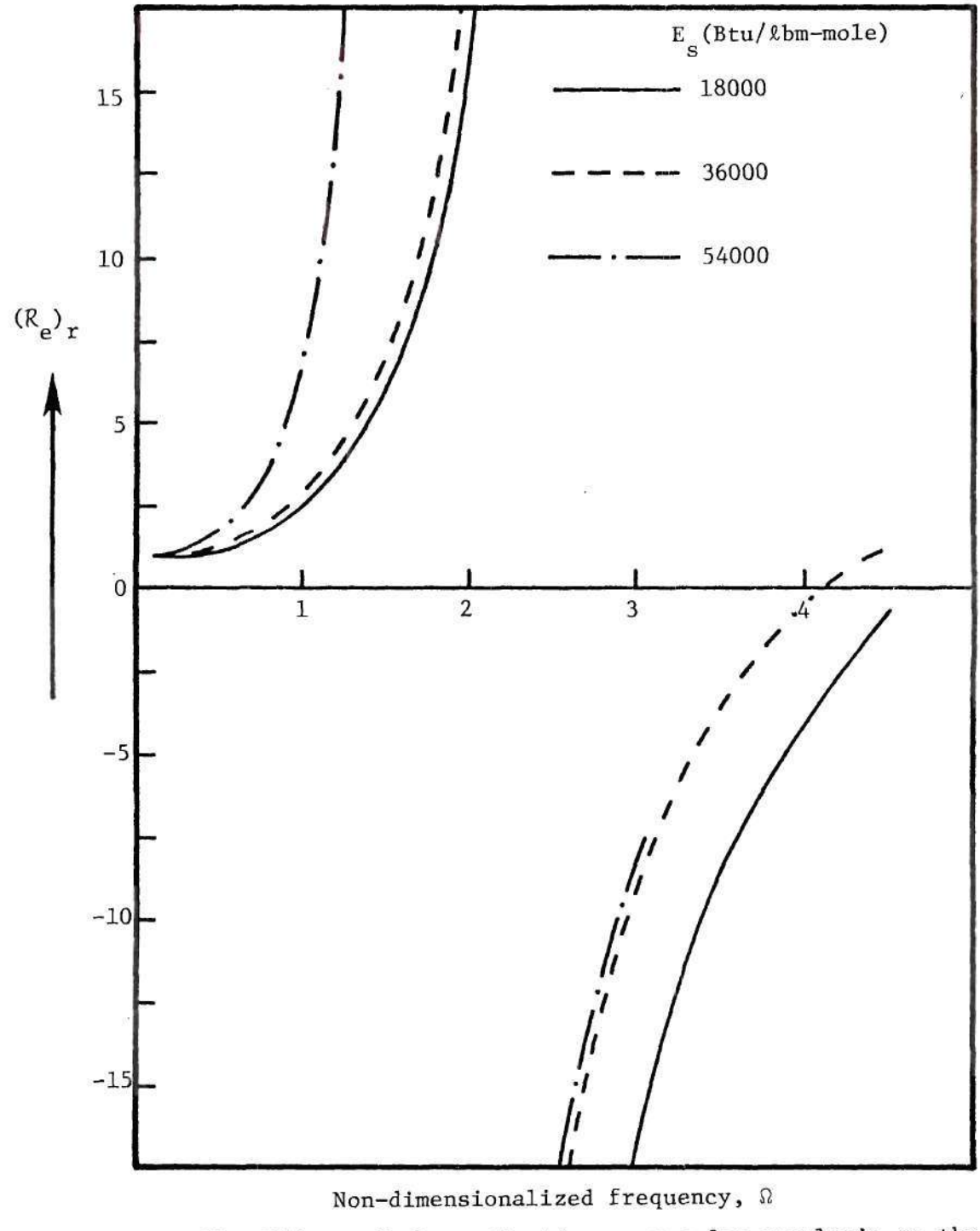

Figure 27. Effect of the activation energy for pyrolysis on the variation of the real part of the response function, at the boundary layer edge, with frequency.

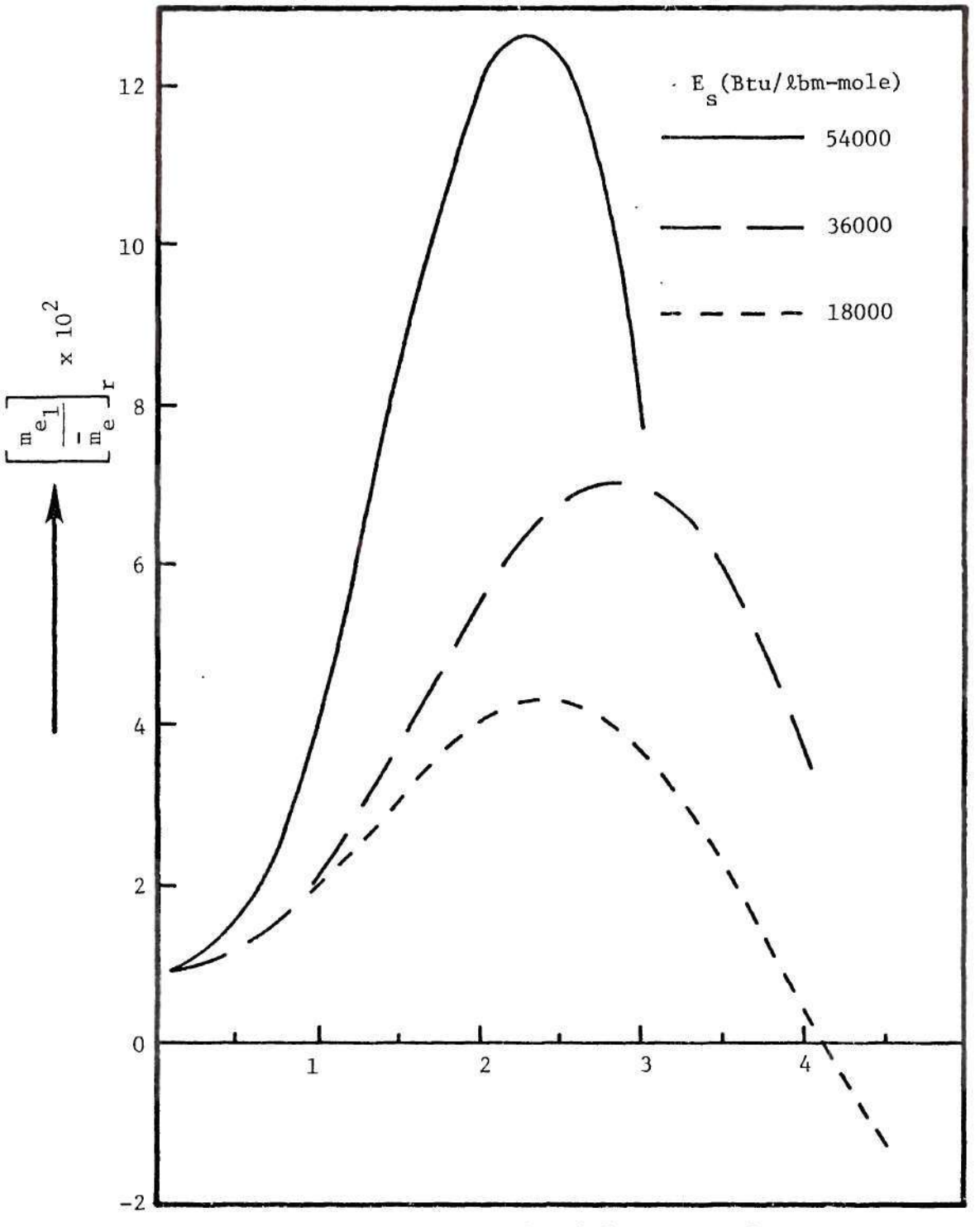

Figure 28. Effect of the activation energy for pyrolysis on the normal mass flux perturbation-frequency behavior at the boundary layer edge.

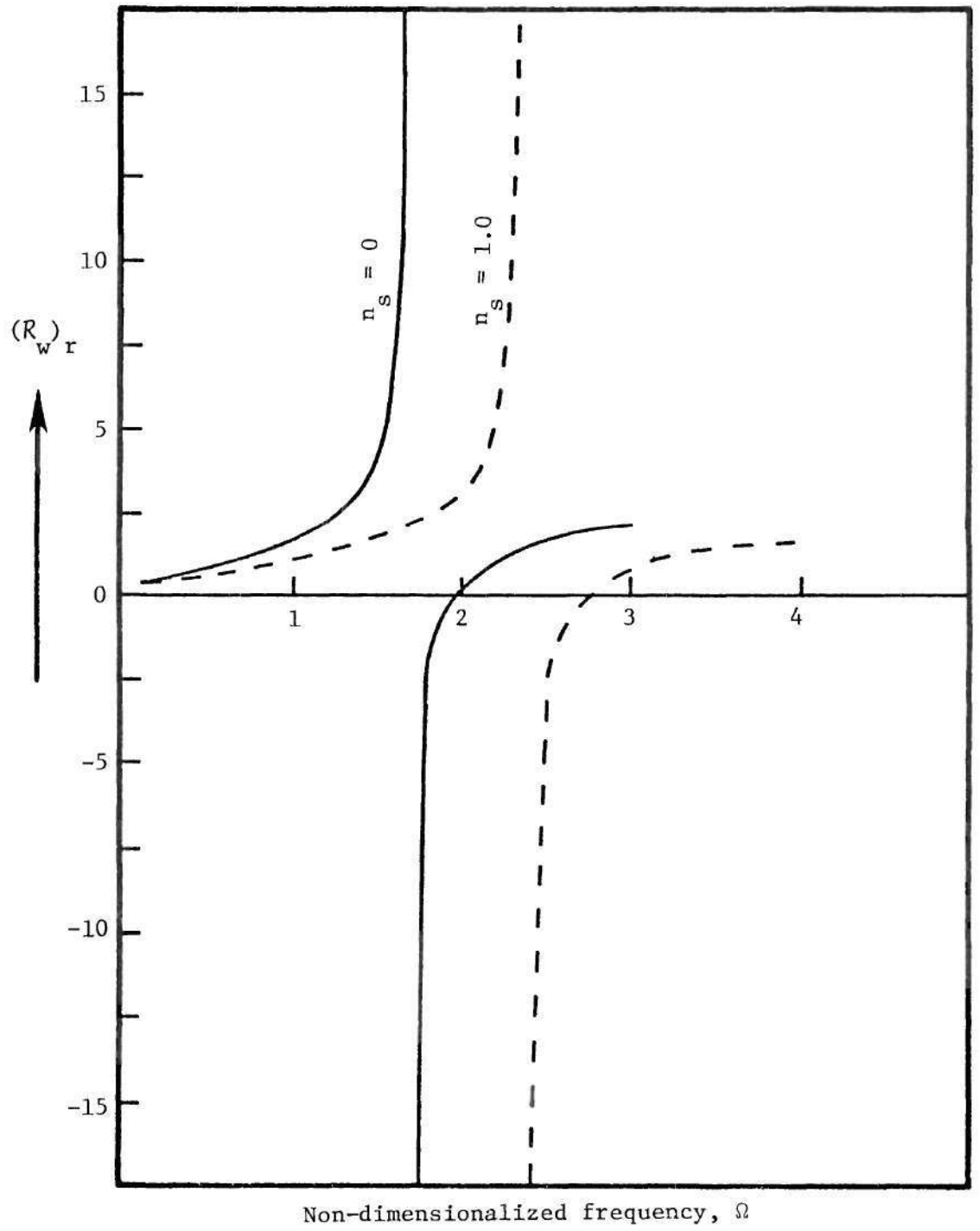

Figure 29. Effect of the pressure exponent in the pyrolysis law on the variation of the real part of the response function, at the gas-solid interface, with frequency.

of n_s tending to increase the response, by adding the influence of the pressure perturbations on the burning rate perturbations, seems to be more than compensated by the effect of the surface temperature perturbations. A similar trend was also reported by the author of Ref. 36, in connection with the response of a burning propellant to just pressure oscillations normal to its surface. Again, in Fig. 29, the shift in the frequency at which the peaks occur is a result of the different values of A_s used in the two cases considered, and is not due to n_s. The destabilizing trends at the gas-solid interface are further enhanced by the boundary layer, to influence the value of $(R_e)_r$ accordingly. This effect is shown in Fig. 30 and further substantiated by the $\left(\frac{\bar{m}_{e_1}}{\bar{m}_e}\right)_r$ vs Ω curves in Fig. 31.

The last part of the parametric study was concerned with studying how the response might vary with position along the length of the combustion chamber. Figure 32 shows the variation of the real part of R_e along a chamber that is 8.7 feet long. The computations were performed by obtaining all the steady-state profiles at different x-locations, covering the 8.7 ft. length, and then using the results at each location to yield the response function there at a given frequency. This frequency corresponded to a value of $\Omega = 4.5$** (or a real frequency of about 1114 c/s), which was also the fundamental frequency of the combustor.

** The real fundamental frequency corresponding to $\Omega \equiv \frac{\omega}{\bar{r}^2/\alpha_s} = 4.5$ will actually vary since $\bar{r}$ varies along the length of the combustion chamber. In fact, in this case this variation corresponds to chamber lengths between 8.7 to 8.75 feet - a variation of about 0.57%. This small variation has been assumed negligible here and the real natural frequency of the chamber is therefore considered constant.

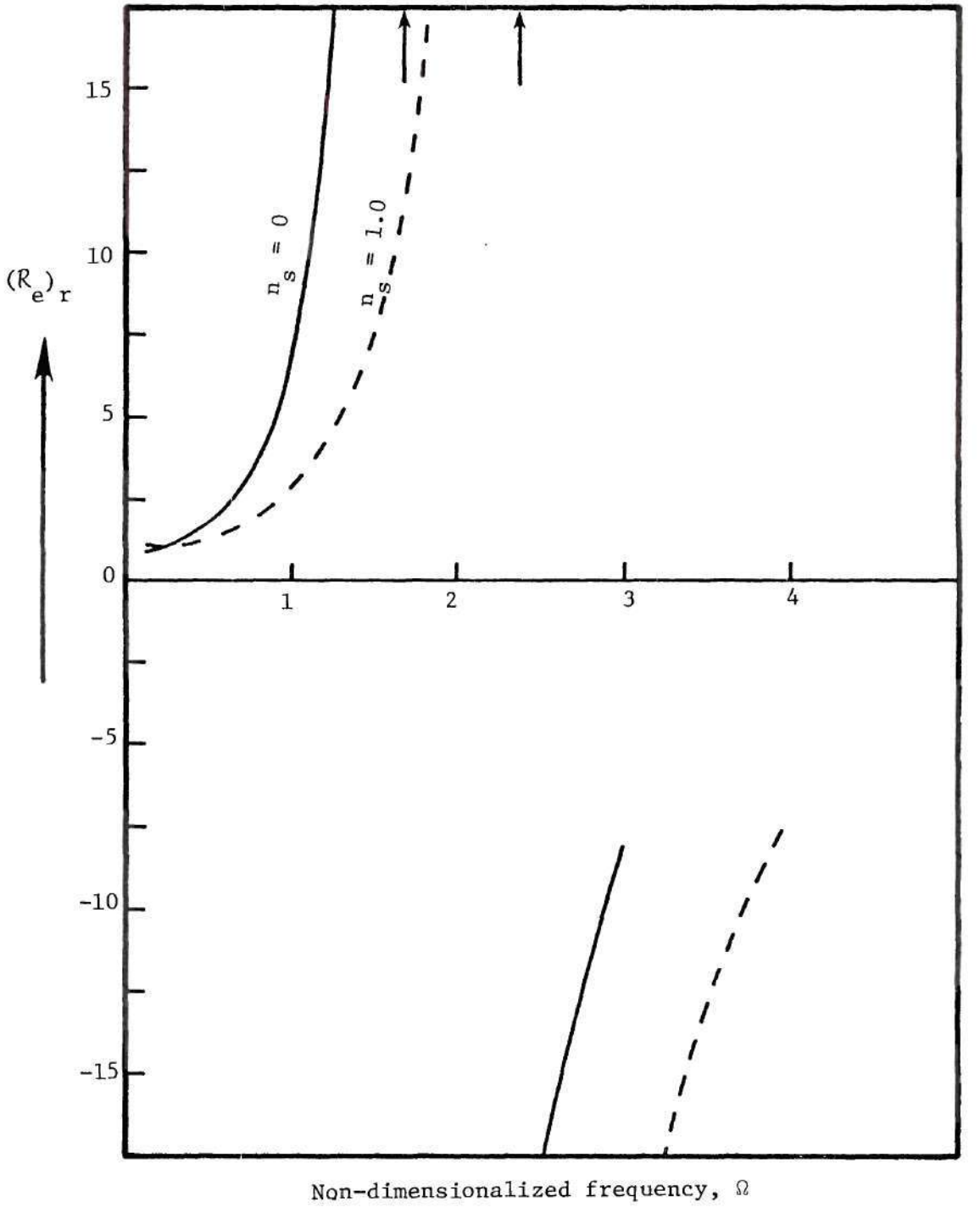

Figure 30. Effect of the pressure exponent in the pyrolysis law on the variation of the real part of the response function, at the boundary layer edge, with frequency.

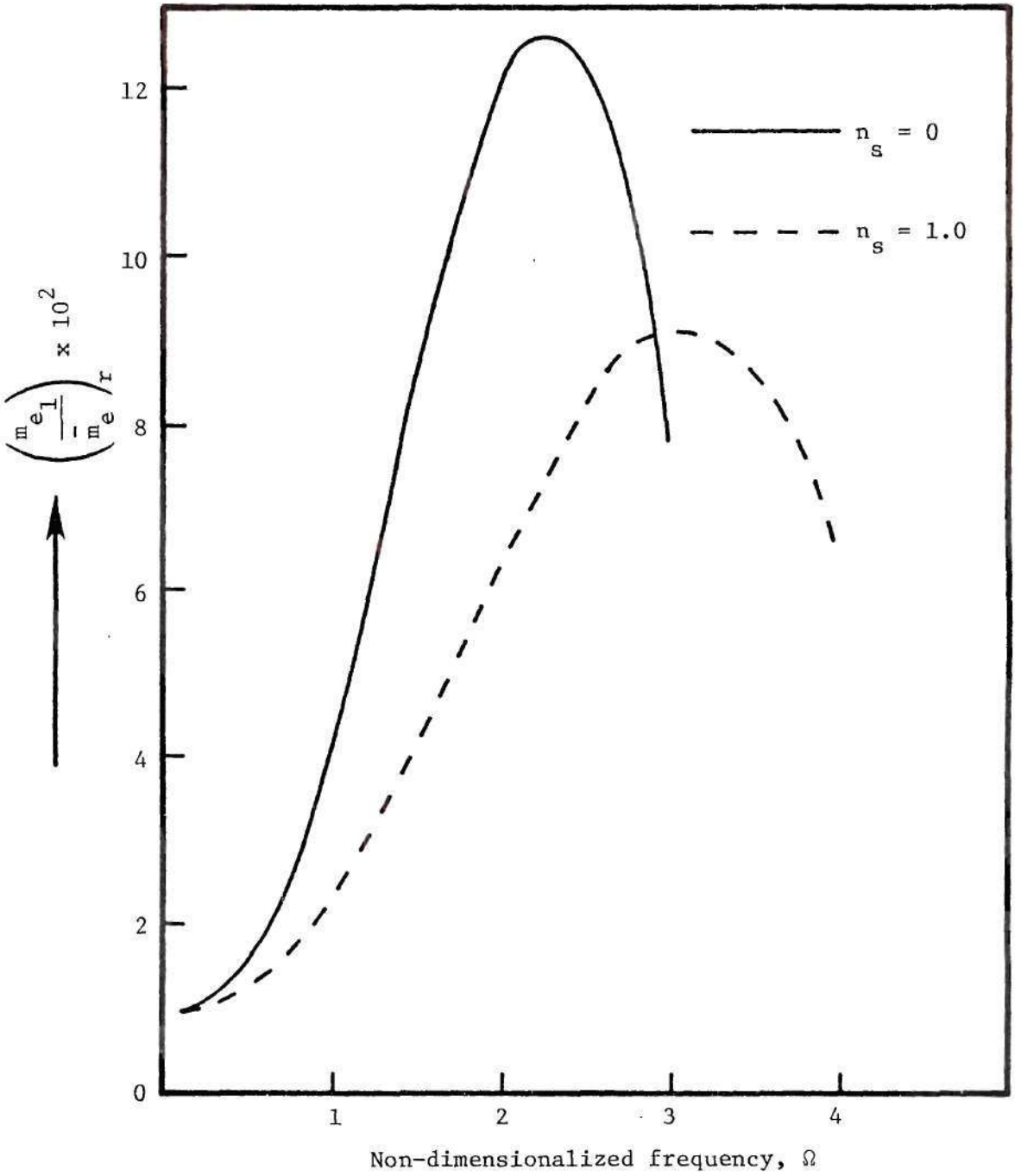

Figure 31. Effect of the pressure exponent in the pyrolysis law on the variation of the real part of the normal mass flux perturbation, at the boundary layer edge, with frequency.

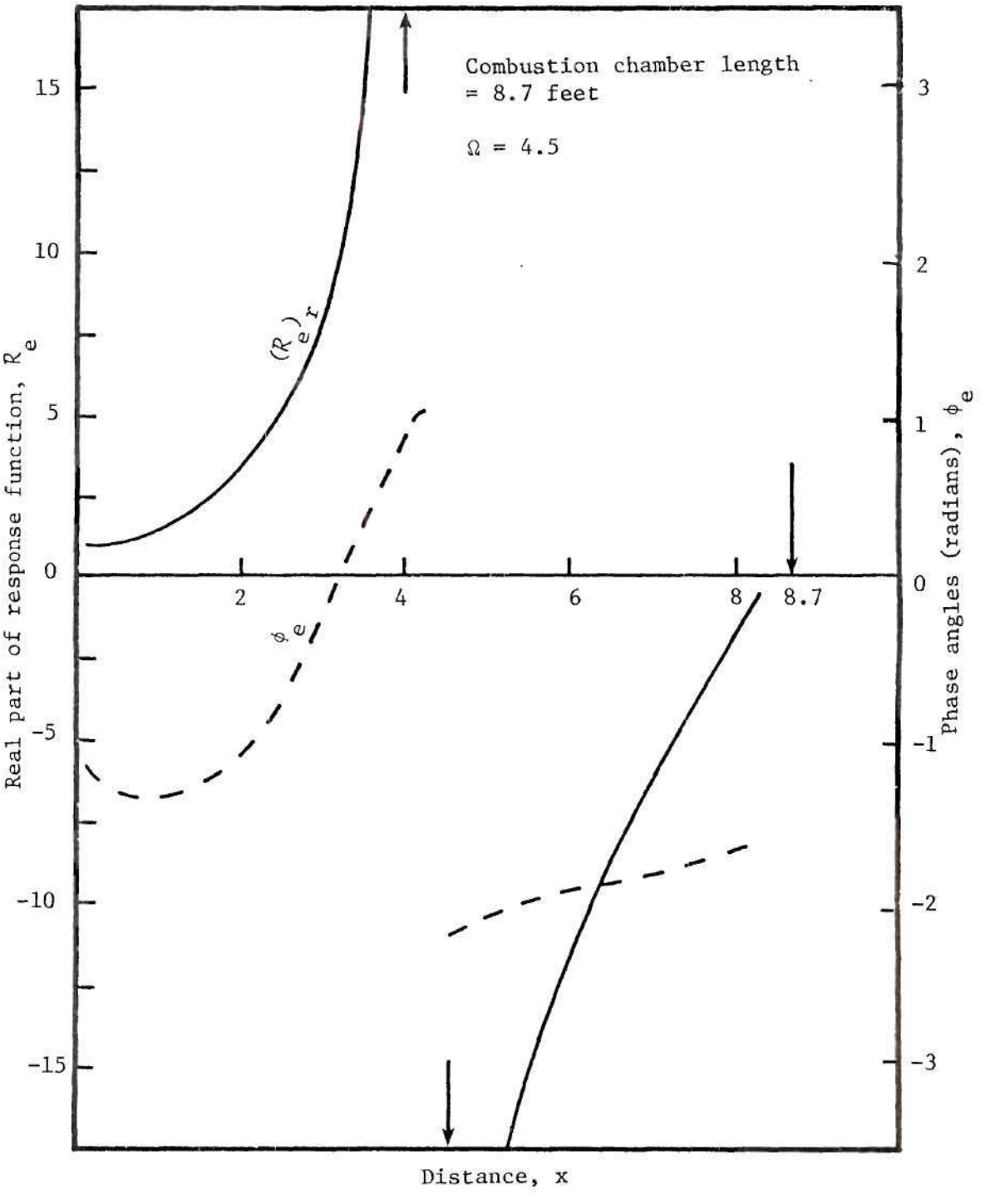

Figure 32. Variation of the real part of the response function, $(R_e)_r$, and phase (ϕ_e) with position (x) along the length of combustion chamber, operating at its natural frequency.

The values of other constants used in the computation are given under case "CU11" (Appendix E). From Fig. 32 it is interesting to note that the strongest possibility of combustion instability lies near the middle of the chamber where the displacement work done by the boundary layer edge on the acoustic oscillations in the chamber (i.e., $E \sim |p_1|^2 (R_e)_r$) is a maximum. The variation of the phase, ϕ_e, of the normal mass flux perturbation at the boundary layer edge relative to the pressure oscillation further indicates the occurrence of an "in-phase" driving near $x \cong 3.3$ ft. - confirming that the strongest instability can be expected in the close vicinity of this location. It is also seen from Fig. 32 that while a destabilizing tendency exists in the "left-half" portion of the chamber, a completely stable condition prevails in the "right-half" of the combustor. The above trends are also substantiated by the variation of $\left(\frac{m_{e_1}}{\bar{m}_e} \right)_r$ with x, shown in Fig. 33.

The reason for the above behavior is the strong combined influence of the longitudinal pressure and velocity oscillations, that exists in the chamber. Consider, for instance, the behavior of the standing pressure and velocity waves during one complete cycle. Figure 34 illustrates the sequence at quarter-cycle intervals, starting at the instant when a maximum compression occurs at the head end and a maximum rarefaction at the nozzle end (see Fig. 34(a)). The velocity oscillation at this instant is null everywhere (since velocity lags by $\frac{\pi}{2}$ radians), although a mean flow is present in the chamber. A quarter of a cycle later the pressure disturbance is null everywhere while a velocity oscillation, superposed on the mean flow and in the same direction, exists. The

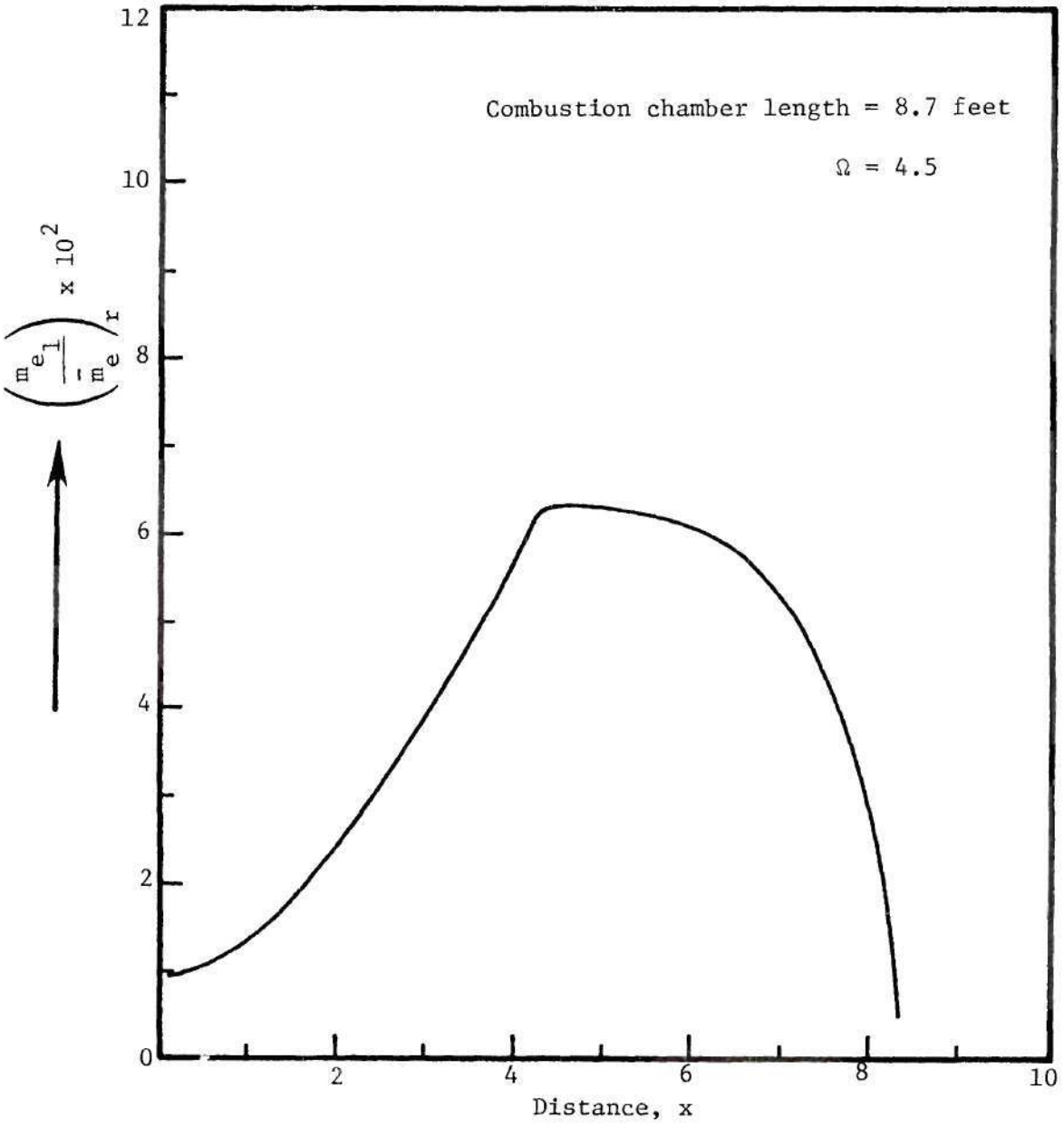

Figure 33. Variation of the real part of the normal mass flux perturbation, at the boundary layer edge, with position along the length of a combustion chamber, operating at its natural frequency.

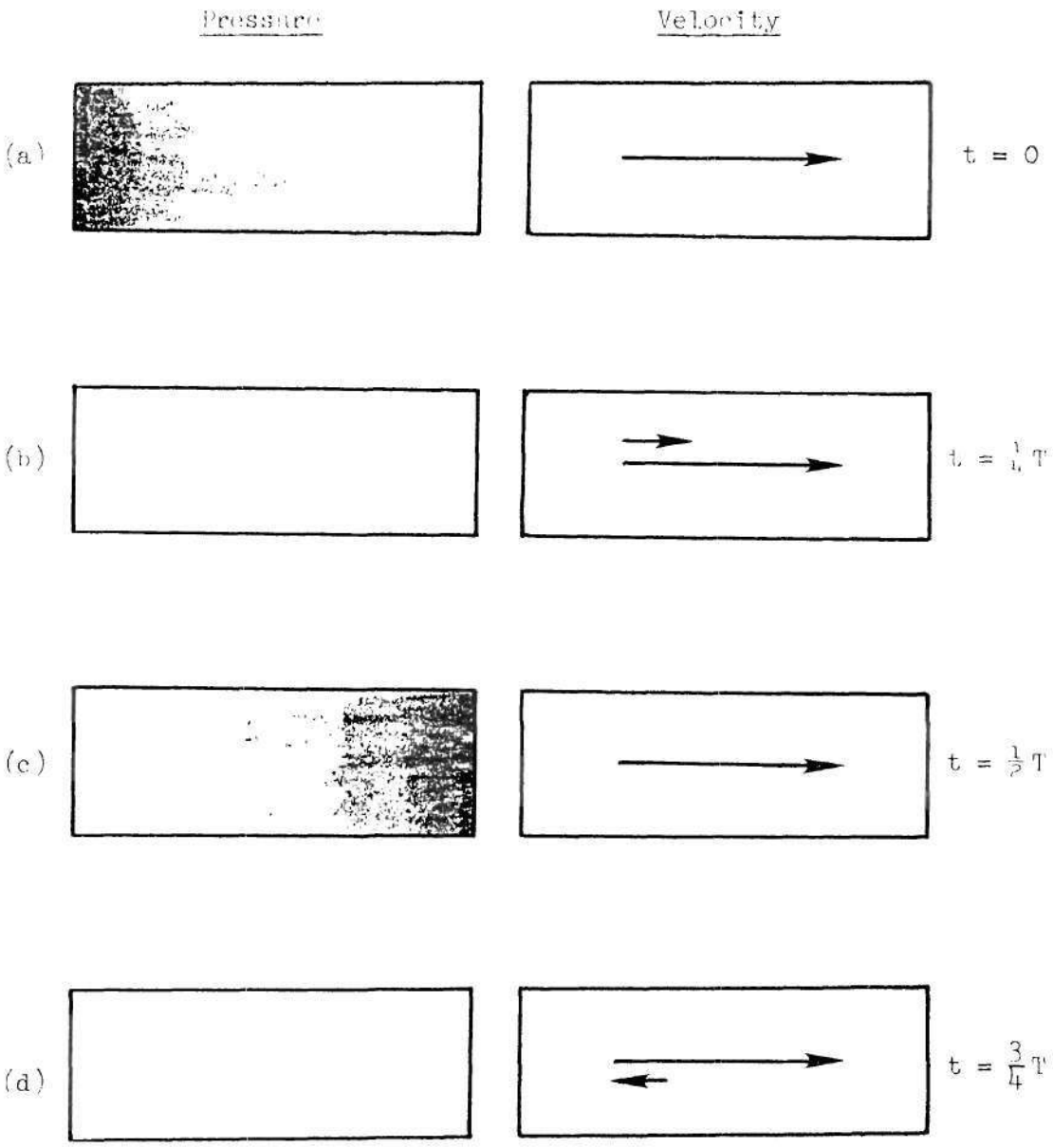

Figure 34. A schematic representation of longitudinal standing waves of pressure and velocity inside a combustor, at quarter cycle intervals. (The larger arrows denote the mean flow while the smaller ones refer to the velocity fluctuation).

amplitude of this oscillation is a maximum at the center and diminishes to zero at the ends of the chamber. Thus at this instant the axial velocity at the center is a maximum (see Fig. 34(b)). After exactly half a cycle has elapsed the pressure disturbance builds up to a maximum compression at the nozzle end and a maximum rarefaction at the head end. The amplitude of the velocity oscillation is again zero everywhere (see Fig. 34(c)). Finally, at the instant when three quarters of the time period has elapsed, the pressure oscillation is zero everywhere but the velocity oscillation is a minimum at the center of the chamber (i.e., opposing the mean flow) and goes to zero at the ends (Fig. 34(d)). Henceforth, the cycle repeats itself. From the above sequence of events it is clear that:

a) A pressure node and velocity antinode is present in the center of the chamber.

b) The pressure oscillations in the left and right halves of the chamber are out of "phase" (with respect to space) by π radians. On the other hand, the velocity oscillations in both halves have the same "phase".

Keeping this physical picture in mind, consider the analytical expression of the "pressure-and-velocity coupled" response function given in Equation (4-72). The complicated "complex" formula for R_e may be rewritten more simply as

$$R_e = \left\{ \left| \frac{m_{e_1}}{\bar{m}_e} \right| e^{i\phi_e} \right\} \Big/ \left| \left(\frac{p_1}{\bar{p}} \right) \right| \qquad (5\text{-}3)$$

Since $p_1 \sim \cos\left(\frac{\pi x}{\ell}\right)$, taking the real part of the above expression yields the following x-dependence.

$$(R_e)_r \sim \left\{ \left| \frac{m_{e_1}}{\bar{m}_e(x)} \right| \cos \phi_e(x) \right\} \Big/ \left| \cos\left(\frac{\pi x}{\ell}\right) \right| \qquad (5\text{-}4)$$

where $|m_{e_1}|$ is the amplitude of the normal mass flux perturbation at the boundary layer edge, $\bar{m}_e(x)$ is the steady normal mass flux at the edge and $\phi_e(x)$ is the phase of the normal mass flux perturbation relative to the local pressure perturbation. From the computed values of ϕ_e, shown in Fig. 32, it is obvious that cos ϕ_e is positive in the left half of the chamber where $|\phi_e| < \frac{\pi}{2}$ and negative in the right half where $|\phi_e| > \frac{\pi}{2}$. Also, as pointed out earlier, since the pressure oscillations are out of phase by π radians in the left and right halves of the chamber, cos $\left(\frac{\pi x}{\ell}\right)$ would be positive in the left half and negative in the right half. In view of the above, Eqn. (5-4) dictates that at the center of the chamber, $x = \frac{\ell}{2}$, the denominator goes to zero since there is a pressure node there. This causes the response function, $(R_e)_r$, to become infinite** or numerically very large in Fig. 32.

It is also to be noted from Eqn. (5-4) that while the real part of m_{e_1} should be sinusoidal in nature, $\left(\frac{m_{e_1}}{\bar{m}_e(x)}\right)_r$ may not be because $\bar{m}_e(x)$ possesses a certain x-variation of its own. This explains the non-sinusoidal trend exhibited in Fig. 33. Recall that, by contrast, the variation of this quantity with frequency had exhibited a sinusoidal behavior. This is simply because $\bar{m}_e$, at a given x, is not a function of Ω,

** By a similar argument it was possible to relate the infinite peaks in the response function vs frequency curves, discussed earlier, to the fact that at some critical value of Ω the denominator in Eqn. (5-4), which may be expressed alternatively as $\cos\left\{\frac{\bar{r}^2 x}{\bar{a}_e \alpha_s} \cdot \Omega\right\}$ using Eqn. (4-48), goes to zero.

so that the $\left(\frac{m_{e_1}}{\bar{m}_e}\right)_r$ vs Ω curves showed the undistorted sinusoidal behavior of $\left[m_{e_1}\right]_r$ with frequency.

Physically, the observed response behavior can be attributed to the combined effects of pressure and velocity coupling that are considered in the model. For instance, consider first the effect of just a standing pressure wave of the type described above - with a pressure node at the center of the chamber. Since the unsteady combustion response is directly related to the pressure perturbation, a maximum or a minimum response can be anticipated at the ends of the combustion chamber (where the extrema of pressure occur). The response at the center of the chamber will correspond to steady-state burning. These effects are the result of pure "pressure-coupling". On the other hand, if just a standing longitudinal velocity wave is considered to be superposed on the mean flow in the chamber, the unsteady, "velocity-coupled" combustion response would be a maximum at the center where the velocity antinode occurs. This is because the "erosion effect" on the propellant's burning rate is the highest when the parallel velocity oscillation is in the direction of the mean flow, since the velocity of the gas flow above the propellant surface is then a maximum. At the ends of the chamber, the response corresponds to the steady-state. In the present model, the response behavior shown in Fig. 32 is the result of a combination of the above limiting cases. The situation is even better represented in Fig. 33 which indicates the corresponding variation of just the normal mass flux perturbation at the boundary layer edge. Since the maximum or "peak" response occurs in the center of the chamber in the present case, one may conclude that the influence of

"velocity coupling" is stronger than that of "pressure coupling" in governing the variation of the unsteady response of the solid propellant with axial distance, x. That is, acoustic velocity oscillations parallel to the burning surface are more effective than the pressure oscillations in supporting axial-mode, intermediate frequency instability within the combustor.

Finally, in contrast to the behavior of $\left(\frac{\dot{m}_{e_1}}{\bar{\dot{m}}_e}\right)_r$ with distance x, it is interesting to study the corresponding variation of the mass flux perturbation at the gas-solid interface, $\left(\frac{\dot{m}_{w_1}}{\bar{\dot{m}}_w}\right)_r$, with position along the chamber length. This variation is depicted in Fig. 35. As noted earlier, since $\left(\frac{\dot{m}_{w_1}}{\bar{\dot{m}}_w}\right)_r$ represents the unsteady response of the burning surface to the oscillations immediately above it, one might expect that this quantity would reflect the amount of work done by the burning surface mainly on the pressure oscillations, since all tangential velocity oscillations go to zero at the surface itself (i.e., "no slip"). This tendency is apparent from Fig. 35 also which shows the response at the gas-solid interface peaking near the head end of the chamber due to the greater influence of "pressure coupling" effects there.

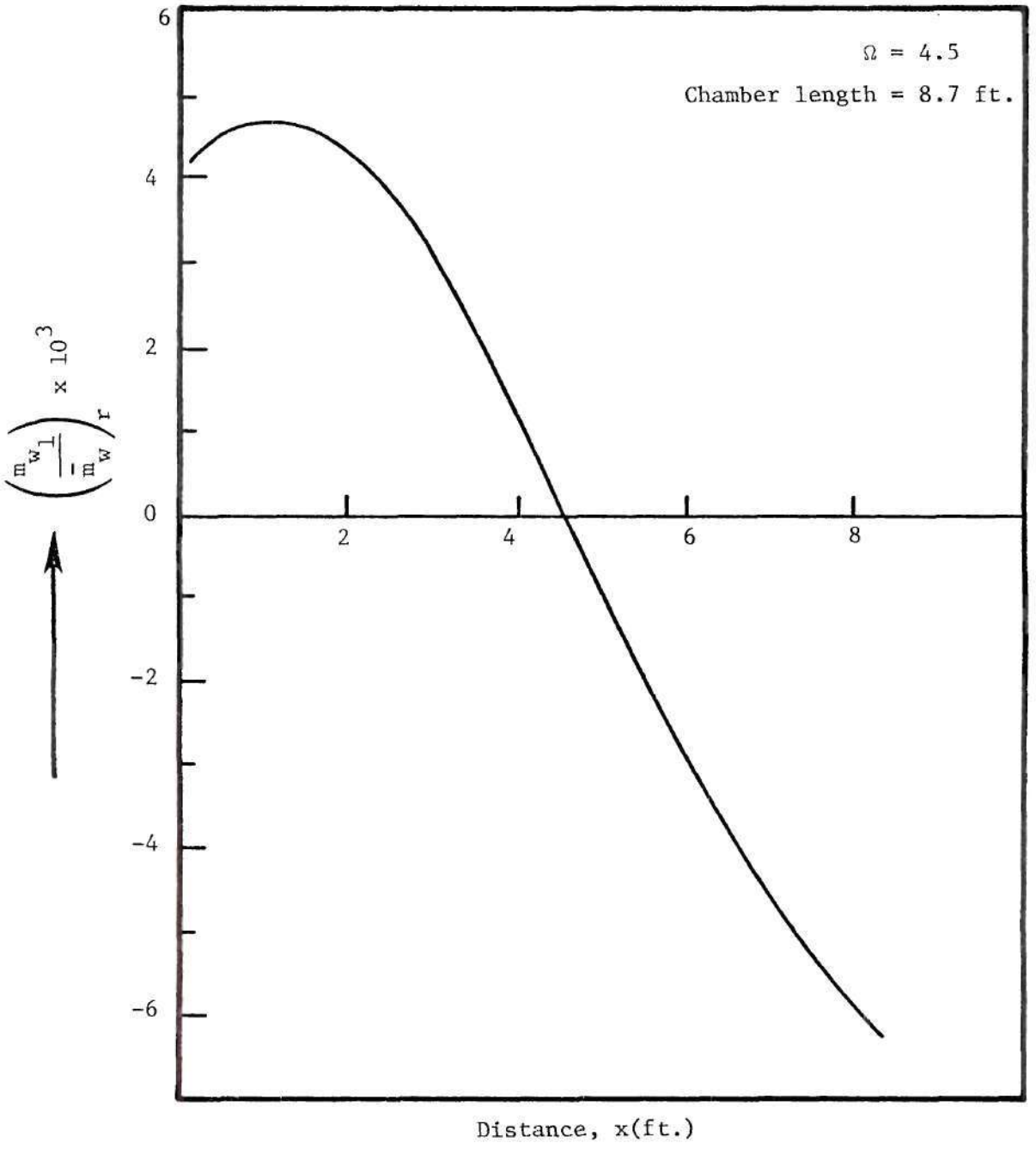

Figure 35. Variation of the real part of the mass flux perturbation at the gas-solid interface with position along the length of the chamber.

CHAPTER VI

CONCLUDING REMARKS

The unsteady, linearised combustion response of a burning solid propellant has been analysed using a two-dimensional description of the gas phase above the solid propellant surface. The model included the effects of laminar erosive burning in the steady state through an analysis of the chemically reacting boundary layer that forms over the surface. The method of parametric differentiation was utilised in the solution of the conservation equations governing the steady state boundary layer flow. Of the various parameters investigated for use in this numerical technique, it was found that the Damkohler number was the best - numerically efficient and devoid of mathematical difficulties. It was also easy to establish the starting solutions to the problem for Damkohler number equal to zero, the initial point in the integration. The steady state results indicated the strong influence of the Damkohler number upon the erosive burning behaviour.

Using the steady state solutions as input for the unsteady analysis, the "pressure-and-velocity coupled" response function of the burning propellant was computed. This response function was evaluated at the boundary layer edge as well as at the burning surface. It was seen that the appropriate response function to consider in combustor stability analyses would be the one at the boundary layer edge. This is because it is this boundary that separates the isentropic acoustic oscillations in the external stream from the "non-isentropic" effects within the boundary layer. Also, since the differences in the two response functions turned out to be significant, it can be concluded that

restricting attention to the burning surface alone may lead to misleading conclusions. However, the results show that for typical solid propellant burning situations, where there is an exothermic heat release at the burning surface, any instability exhibited by the response function at the gas-solid interface also shows up in the response function behaviour at the boundary layer edge. Furthermore, since the real part of the response function is larger at the boundary layer edge than at the gas-solid interface, it may be inferred that the net effect of the boundary layer is one of strong amplification.

A parametric study was conducted with the objective of determining the relative importance of various parameters that enter the analysis. Of the various parameters analysed it was found that the influence of those characterizing the gas phase varied from a negligible effect on the response functions with changes in the steady state heat release to a significant effect associated with the Damkohler, Prandlt and Schmidt numbers, and the steady state pressure gradient parameter. In contrast, all of the solid phase parameters considered - the pressure exponent, the activation energy of the surface pyrolysis, and the surface heat release (or absorption) parameter - had a strong effect on the behaviour of the response functions. In the present model the solid phase parameters dominated the behaviour of the response function at the gas-solid interface. The results showed that this response function invariably increased across the boundary layer when there was combustion present and the gas phase parameters had values typical of solid propellant burning conditions. At the edge of the boundary layer, the strong amplifying influence of this layer manifested itself through a

large positive peak in the frequency response curve. Even in cases where the response function at the gas-solid interface indicated a stable tendency (e.g., in the case when a highly endothermic reaction was present at the surface) the combustion and fluid mechanical processes within the boundary layer were sufficient to result in a "driving" condition at the boundary layer edge. Within the realistic range of variation of all the parameters considered, it was found that in the low to intermediate frequency range covered by the results, an unstable tendency prevailed at the lower frequencies. This tendency towards instability then increased with frequency up to a certain critical frequency after which a completely stable condition prevailed.

Finally, the variation of the response function with position along the length of a typical combustor, "oscillating" at its fundamental mode was studied. The results showed a strong tendency towards instability in the central portion of the combustion chamber. Based on physical arguments related to the development of the standing waves in pressure and velocity within the chamber, it was seen that in the present model the center was the location of the extrema in the unsteady velocity parallel to the burning surface. Thus the "erosion effect" could be expected to be a maximum or a minimum at the center of the chamber. Connecting this behaviour with the effect of the pressure wave, it was concluded that the "velocity coupling" influence was more dominant than that of "pressure coupling". That is, the acoustic velocity oscillations parallel to the burning surface are more important than the associated pressure oscillations when considering the possibility of axial-mode, intermediate frequency instability in the combustor.

Based on the conclusions of the present analysis the following suggestions for future research emerge:

a) The steady state theory of erosive burning needs to be extended to include the effects of turbulence, heterogeneities in propellant composition, and more realistic chemical kinetics. This will help in the more accurate prediction of "real-world" trends. In such an analysis, solution to the full chemically reacting boundary layer equations must be sought numerically. The method of parametric differentiation could again be used for the solution of this complex problem since it has been successfully applied in the solution of partial differential equations[29, 38]. In extending the analysis one should keep in mind that the large surface blowing rates that occur in real solid rocket combustors may preclude any boundary layer formation and one may be forced to consider the solution of the full Navier Stokes equations for a reactive flow - a monumental problem.

b) The unsteady analysis should be extended to include the more general case of large amplitude oscillations in pressure and velocity (i.e., a non-linear analysis). Such a generalization is required in view of the fact that "velocity coupling" effects on the response function of the propellant can be entirely different in the presence of large amplitudes as predicted qualitatively by several authors (e.g., see Refs. 4 and 5). The mathematical difficulties of a full non-linear analysis must also be overcome. Furthermore, there is a need for a completely unsteady gas phase analysis so that a wide range of frequencies may be considered and the problem of high frequency instability can then be investigated.

Finally, there seems to be a distinct need for experiments to measure the combustion response parameters under conditions where the effect of parallel, longitudinal, standing oscillations in pressure and velocity superposed on the mean flow over a side-burning propellant grain can be studied. To date, most experiments have concentrated on obtaining such information from tests performed with T-burner apparatus using propellant samples placed perpendicular to the direction of the acoustic waves[39]. While such experiments have yielded useful insight into the important effects of velocity and/or pressure coupled response, the question of the true response of a solid propellant in the more realistic case with combined pressure and velocity effects, simultaneously prevailing, remains without any experimental verification.

APPENDIX A

AN ALGORITHM FOR THE SOLUTION OF A LINEAR BOUNDARY VALUE PROBLEM

In this section a non-iterative numerical scheme is presented for the solution of a linear boundary value problem involving ordinary differential equations. Such problems were encountered in the solution of the steady-state chemically reacting boundary layer equations in "locally similar" form (Chapter II) as well as in the unsteady combustion response analysis (see Chapter IV).

Consider a two-point, linear, boundary-value problem defined by the set of n ordinary differential equations:

$$\frac{d}{dt}[y] = [A(t)][y] + [f(t)] \tag{A-1}$$

subject to the initial conditions:

$$y_i(t_o) = C_i \quad , \; i = 1,2....\gamma \tag{A-1a}$$

and terminal conditions:

$$y_{i_m}(t_f) = C_{i_m} \quad , \; m = 1,2....n-\gamma \tag{A-1b}$$

The solution procedure consists of splitting the above problem into two initial value problems - one consisting of a homogeneous differential equation and the other of an inhomogeneous one. The final solution is then constructed as the sum of the homogeneous and particular solutions. The following steps are involved:

Step 1

Integrate the homogeneous equations

$$\frac{d}{dt}[u^{(j)}] = [A(t)][u^{(j)}(t)], \; j = 1,2....n-\gamma$$

$(n-\gamma)$ times subject to the initial conditions

$$u_i^{(m)}(t_o) = \begin{cases} 1 & , i = \gamma + m \\ 0 & , i \neq \gamma + m \end{cases}$$

where $m = 1, 2, \ldots . n-\gamma$.

Store the profiles $u_i^{(m)}(t)$, $i = 1, 2 \ldots . n$, for $t_o < t < t_f$.

Step 2

Integrate the particular equation

$$\frac{d}{dt}[v] = [A(t)][v] + [f(t)]$$

once with the initial conditions:

$$v_i(t_o) = y_i(t_o) = C_i \quad , i = 1, 2 \ldots . \gamma$$

$$v_i(t_o) = 0 \quad , i = \gamma+1 \ldots . n$$

Again store the profiles $v_i(t)$, $i = 1,2 \ldots . n$, for $t_o < t < t_f$.

The general solution to Equation (A-1) and corresponding boundary conditions can be written as a linear combination of the homogeneous and particular solutions:

$$y_i(t) = \sum_{j=1}^{n} b_j \, u_i^{(j)}(t) + v_i(t) \quad , i = 1,2 \ldots . n \quad \text{and } t_o < t < t_f. \qquad \text{(A-2)}$$

Since there are γ initial conditions specified in the original problem (i.e., Equation (A-1a)), substituting these into Equation (A-2) yields:

$$y_i(t_o) = b_i + v_i(t_o) \quad , i = 1,2 \ldots . \gamma$$

But $v_i(t_o)$ are chosen to be the originally specified initial conditions of the problem so that

$$b_i = 0 \quad , i = 1,2 \ldots . \gamma$$

Hence, the first γ equations in Equation (A-2) state that the first γ initial conditions on v_i are same as those in the original problem. Then, if the rest of the initial conditions on v_i are taken to be zero it can be shown from Equation (A-2) that

$$y_{\gamma+i}(t_o) = b_{\gamma+i} \quad , \; i = 1,2....n-\gamma$$

That is, the above $b_{\gamma+i}$ represent the missing initial conditions of the original problem and may be determined by solving the remaining algebraic equations of the system in Equation (A-2) at the terminal point $t = t_f$.

Step 3

Solve the system of $n-\gamma$ linear algebraic equations:

$$y_{i_m}(t_f) = \sum_{j=1}^{n-\gamma} \beta_j \, u_{i_m}^{(j)}(t_f) + v_{i_m}(t_f) \quad , \; m = 1,2...n-\gamma$$

for the unknowns $\beta_j = b_{\gamma+j}$, $j = 1,2...n-\gamma$ to determine the missing initial conditions.

Step 4

Construct the general solution using

$$y_i(t) = \sum_{j=1}^{n-\gamma} \beta_j \, u_i^{(j)}(t) + v_i(t) \quad , \; i = 1,2....n$$

It is to be noted that the above procedure requires the homogeneous differential equations to be integrated only $(n-\gamma)$ times. Furthermore, it must be realised that if some of the initial conditions in a problem do not appear explicitly in the form of Equation (A-1a), but rather as linear algebraic equations, the procedure remains unchanged except that these implicit conditions are solved with the system in Step 3.

APPENDIX B

VALUES OF CONSTANTS USED FOR STEADY-STATE RESULTS

The values of constants used in obtaining the results presented in Chapters III and V are shown below for the two cases that were considered as base. Note that the different steady state results used in the unsteady analysis were obtained by altering a few of the constant values indicated under Case 2, as indicated in Appendix E.

Constant	Case 1	Case 2	Units
m	1	0.5	
T_o	2200	4680	^oR
p_o	44000	63400	$\ell b_f/ft^2$
T_u	540.6	530.6	^oR
C_s	0.31	0.32	Btu/ℓbm-^oR
C_p	0.3	0.3	Btu/ℓbm-^oR
L	1052	-180	Btu/ℓbm
$\rho_e\mu_e$	5×10^{-6}	5×10^{-4}	FPS
α	1	1	
n^*	1	1	
ρ_s	121	121	$\ell bm/ft^3$
A_s	6.7×10^4	300	ft/sec
n_s	0	0	
E_s	54000	36000	Btu/ℓbm-mole
Sc(=Pr)	0.7 and 1.0	0.78	
E	27800	81000	Btu/ℓbm-mole
y_{1e}	0.05	0.01	
y_{2e}	0.95	0.99	
h_1^o	-174.5	-174-5	Btu/ℓbm
h_2^o	-1350.0	-3054.5	Btu/ℓbm

Constant	Case 1	Case 2	Units
W_1	58	58	
W_2	29	29	
v_1'	1	1	
v_2'	0	0	
v_1''	0	0	
v_2''	2	2	

APPENDIX C

DERIVATION OF THE LINEARISED GAS PHASE EQUATIONS

To begin with the "first-order" (linearised) differential equations describing the conservation of momentum, energy and species will be derived. These are Equations (4-25) through (4-27) of the unsteady analysis presented in Chapter IV.

Starting with the physical boundary layer equations of continuity, momentum, energy and species (i.e., Eqns. (2-4) to (2-9)) and the definition of the stream function ψ given by

$$\rho u = \psi_y$$

$$\rho v = -\psi_x$$

one proceeds to transform these equations into (ξ,η) space (using the redefined co-ordinates of Eqn. (4-20)). Using the transformations

$$\frac{\partial}{\partial x} \equiv \bar{\rho}_e \bar{\mu}_e \bar{u}_e \left[\frac{\partial}{\partial \xi} + \frac{\partial \eta}{\partial \xi} \frac{\partial}{\partial \eta} \right]$$

$$\frac{\partial}{\partial y} \equiv \frac{\bar{u}_e \rho}{(2\xi)^{1/2}} \frac{\partial}{\partial \eta}$$

the "convective" and "diffusion" operators of Equations (2-5) and (2-6) may be written as:

$$L_1[\ \ ] = \frac{\rho \bar{u}_e^{\,2} - \bar{\rho}_e \bar{\mu}_e}{(2\xi)^{1/2}} \left[\psi_\eta \frac{\partial}{\partial \xi} - \psi_\xi \frac{\partial}{\partial \eta} \right] \qquad \text{(C-1)}$$

$$L_2[\ \ ] = \frac{\rho \bar{u}_e^{\,2}}{2\xi} \frac{\partial}{\partial \eta} \left(\rho\ Q \frac{\partial}{\partial \eta} \right) \qquad \text{(C-2)}$$

Next, introducing the expansions of Equations (4-21) through (4-24) into

the physical boundary layer equations together with the above transformations one obtains for the various terms in the momentum equation, the following expressions:

$$L_1[u] = \rho \bar{u}_e^2 \bar{\rho}_e \bar{\mu}_e \left[\left\{ \bar{f}'^2 + 2\bar{f}'f_1' \right\} \left(\frac{\partial \bar{u}_e}{\partial \xi} - \frac{\bar{u}_e}{2\xi} \right) \right\} \bar{f}\bar{f}'' + \bar{f}''f_1 + \bar{f}f_1'' \left\} \right] \qquad (C\text{-}3)$$

$$\rho_e u_e \frac{\partial u_e}{\partial x} = \rho \bar{u}_e^2 \bar{\rho}_e \bar{\mu}_e \left[\left\{ \frac{\bar{\rho}_e}{\bar{\rho}} \right\} \frac{d\bar{u}_e}{d\xi} + \left\{ \frac{\bar{\rho}_e}{\bar{\rho}} \right\} \frac{d\bar{u}_e}{d\xi} \left\{ \frac{\rho_{e_1}}{\bar{\rho}_e} + \frac{2u_{e_1}}{\bar{u}_e} \right\} + \right.$$

$$\left. + \left\{ \frac{\bar{\rho}_e}{\bar{\rho}} \right\} \bar{u}_e \frac{\partial}{\partial \xi} \left(\frac{u_{e_1}}{\bar{u}_e} \right) - \left\{ \frac{\bar{\rho}_e}{\bar{\rho}} \right\} \left(\frac{\rho_1}{\bar{\rho}} \right) \frac{d\bar{u}_e}{d\xi} \right] \qquad (C\text{-}4)$$

$$L_2[u; Q \equiv \mu] = \frac{\rho \bar{u}_e^2}{2\xi} \frac{\partial}{\partial \eta} \left[(\rho\mu) \frac{\partial u}{\partial \eta} \right]$$

Since it is assumed that

$$\frac{\rho\mu}{\rho_e \mu_e} = 1$$

it follows that

$$\rho\mu = \rho_e \mu_e = \bar{\rho}_e \bar{\mu}_e \left\{ 1 + \frac{(\rho_e \mu_e)_1}{\overline{\rho_e \mu_e}} \right\} \qquad (C\text{-}5)$$

Taking $\mu_e \sim T$ and using the perfect gas law it can be shown that

$$\frac{(\rho_e \mu_e)_1}{\overline{\rho_e \mu_e}} = \frac{p_1}{\bar{p}} \qquad (C\text{-}6)$$

Using these results in the "diffusion" operator one obtains

$$L_2[u; Q \equiv \mu] = \rho \bar{u}_e^2 \bar{\rho}_e \bar{\mu}_e \left[\bar{f}''' + \bar{f}''' \left(\frac{p_1}{\bar{p}} \right) + f_1''' \right] \left\{ \frac{\bar{u}_e}{2\xi} \right\} \qquad (C\text{-}7)$$

Substituting Equations (C-3), (C-4) and (C-7) into the momentum equation (Eqn. (2-7)) and separating the first order terms from the zeroth order quantities one obtains the perturbed momentum equation, Equation (4-25), after the assumptions expressed by Eqns. (2-38) and (2-39) have been used.

The perturbed (linearised) forms of the energy and species equations are derived along similar lines as the momentum equation above. The transformed expressions for the various terms in these equations are:

$$L_1[h_t] = \rho\bar{u}_e{}^2\bar{\rho}_e\bar{\mu}_e \left[-\left\{ \bar{f}\bar{\theta}' + \bar{\theta}'f_1 + \bar{f}\theta_1' \right\} \frac{\bar{h}_{t_e}}{2\xi} \right] \tag{C-8}$$

$$L_2[h_t; Q \equiv \frac{\mu}{Pr}] = \rho\bar{u}_e{}^2\bar{\rho}_e\bar{\mu}_e \left[\bar{\theta}'' + \theta_1'' + \bar{\theta}''\left(\frac{p_1}{\bar{p}}\right) \right] \frac{1}{Pr} \left\{ \frac{\bar{h}_{t_e}}{2\xi} \right\} \tag{C-9}$$

$$L_2\left[\frac{u^2}{2}; Q \equiv \mu\left(1 - \frac{1}{Pr}\right) \right] = \rho\bar{u}_e{}^2\bar{\rho}_e\bar{\mu}_e \left[\bar{f}'\bar{f}'' + \bar{f}'f_1'' + \bar{f}''f_1' + \bar{f}'\bar{f}''\left(\frac{p_1}{\bar{p}}\right) \right] *$$

$$* \left\{ \frac{\bar{u}_e^2}{2\xi} \right\} \left[1 - \frac{1}{Pr} \right] \tag{C-10}$$

$$L_1[y_i] = \rho\bar{u}_e{}^2\bar{\rho}_e\bar{\mu}_e \left[\frac{-\bar{f}\bar{y}_i' + \bar{f}y_{i_1}' + \bar{y}_i'f_1}{2\xi} \right] \tag{C-11}$$

$$L_2[y_i; Q \equiv \frac{\mu}{Sc}] = \rho\bar{u}_e{}^2\bar{\rho}_e\bar{\mu}_e \left[\bar{y}_i'' + y_{i_1}'' + \bar{y}_i''\left(\frac{p_1}{\bar{p}}\right) \frac{1}{2\xi \cdot Sc} \right] \tag{C-12}$$

Again, substituting Equations (C-8) through (C-10) into the boundary layer energy equation, using the assumptions given by Equations (2-40) to (2-42) and separating orders of magnitude one obtains the required perturbed energy equation (i.e., Eqn. (4-26)). The perturbed species equation, Equation (4-27), is also obtained similarly except that Equations (C-11) and (C-12) are substituted into the boundary layer species equation and use is made of the assumption of constant composition in the external

stream (see Eqn. (2-43)).

Next, the rate law as given by Equation (4-28) is linearised to yield an expression for the term $(\frac{\omega_i}{\rho})_1$, related to the chemical rate perturbation, in the "first order" species equation, in terms of the pertinent variables of the present analysis. To obtain this, Equations (4-28) and (4-29) are combined to express the unsteady rate law in the form:

$$\frac{\omega_i}{\rho} = - Z B_i T_e^{\alpha} \rho_e^{n^*-1} \left[\frac{F}{C_p T_e}\right]^{1-n^*+\alpha} \left[\frac{\Sigma y_i/W_i}{\Sigma y_{i_e}/W_i}\right]^{1-n^*} \cdots$$

$$\cdots \exp\left[-\frac{EC_p}{R^o F}\right] \prod_j y_j^{a_j} \qquad \text{(C-13)}$$

where

$$F \equiv \theta \bar{h}_{t_e} - \Sigma y_i h_i^o - \frac{\bar{u}_e^2 f,2}{2 g_c J_c} + C_p T_u \qquad \text{(C-14)}$$

Specialising Equation (C-13) to the case of a first order reaction (with $n^* = 1$) being considered in the present analysis, Equation (C-13) yields:

$$\frac{\omega_i}{\rho} = \left[-\frac{ZB_i}{(C_p)^{\alpha}}\right] F^{\alpha} \exp\left[-\frac{EC_p}{R^o F}\right] \prod_j y_j^{a_j} \qquad \text{(C-15)}$$

Consider the following linearisations:

$$F^{\alpha} = \bar{F}^{\alpha}\left[1 + \frac{F_1}{\bar{F}}\right]^{\alpha} = \bar{F}^{\alpha}\left[1 + \alpha \frac{F_1}{\bar{F}}\right]$$

$$\exp\left[-\frac{EC_p}{R^o F}\right] = \exp\left[-\frac{EC_p}{R^o \bar{F}}\left\{1 - \frac{F_1}{\bar{F}}\right\}\right]$$

$$= \exp\left[-\frac{EC_p}{R^o \bar{F}}\right] \exp\left[\frac{EC_p}{R^o \bar{F}}\left\{\frac{F_1}{\bar{F}}\right\}\right]$$

$$= \left[1 + \frac{EC_p}{R^o \bar{F}} \left\{ \frac{F_1}{\bar{F}} \right\} \right] \exp \left[- \frac{EC_p}{R^o \bar{F}} \right]$$

$$\prod_j y_j^{a_j} = y_1 = \bar{y}_1 + y_{1_1}$$

Substituting these expansions back into Equation (C-15) and separating the different orders of magnitude obtain:

$$\left(\frac{\omega_i}{\rho} \right)_1 = \left(\frac{\overline{\omega_i}}{\rho} \right) \left\{ \frac{F_1}{\bar{F}} \left[\alpha + \frac{EC_p}{R^o \bar{F}} \right] + \frac{y_{1_1}}{\bar{y}_1} \right\}$$

This is the required expression and was used in Chapter IV as Equation (4-30). F_1 and $\bar{F}$ are defined by Equations (4-31) and (4-32).

Finally, the linearised boundary conditions of Equations (4-37) through (4-43) may be obtained by transforming the physical conditions at the gas-solid interface and the boundary layer edge into (ξ,η) space and using the expansions of Equations (4-21) through (4-24).

Momentum boundary conditions

i) The no-slip condition at the gas-solid interface (y = 0) requires u = 0. Using Equation (4-22) this may be expressed, to first order, as

$$f_1'(0) = 0$$

ii) At the boundary layer edge ($y \to \infty$) since the velocity from within the boundary layer equals that of the unsteady external stream:

$$u = u_e = \bar{u}_e + u_{e_1}$$

Again, using Equation (4-22) for u in the left hand side of the above equation, one gets to first order, that

$$f_1'(\infty) = \frac{u_{e_1}}{\bar{u}_e}$$

iii) The condition of overall mass balance at the gas-solid interface requires

$$(\rho v)_w = \rho_s \dot{r}$$

Making use of the transformed expression for $(\rho v)_w$ derived earlier in Equation (4-73), and the Arrhenius pyrolysis law

$$\dot{r} = A_s p^{n_s} \exp\left[- \frac{E_s}{R^o T_w} \right]$$

one gets

$$- \frac{\bar{\rho}_e \bar{\mu}_e \bar{u}_e}{(2\xi)^{1/2}} \left[\bar{f}(0) + f_1(0) \right] = \rho_s A_s p^{n_s} \exp\left[- \frac{E_s}{R^o T_w} \right]$$

Linearising the right hand side, noting that $T_w \equiv \frac{F_w}{C_p}$ (see Eqn. (4-29)), and separating the different orders of magnitude one obtains to first order the required perturbed form of the pyrolysis law

$$\frac{f_1(0)}{\bar{f}(0)} = n_s \left(\frac{p_1}{\bar{p}} \right) + \frac{E_s C_p}{R^o \bar{F}_w} \left(\frac{F_{1w}}{\bar{F}_w} \right)$$

Energy boundary conditions

iv) The energy balance condition at the gas-solid interface is derived using the continuity of wall temperature condition i.e.

$$\left\{ T_w \right\}_{0^+} = \left\{ T_w \right\}_{0^-}$$

When perturbed this yields the condition

$$\left\{ T_{w_1} \right\}_{0^+} = \left\{ T_{w_1} \right\}_{0^-}$$

for the continuity of wall temperature fluctuations. In terms of the gas and solid phase dependent variables being used in the present analysis, this latter condition may be expressed as:

$$H_{1w} \bar{T}_e = \frac{F_{1w}}{C_p} \tag{C-16}$$

Substituting for H_{1w} and F_{1w} from Equations (4-17) and (4-31) respectively, one gets

$$\frac{\frac{\lambda}{\lambda_s} \left. \frac{\partial H_1}{\partial \zeta} \right|_{\zeta = 0^+} - \left[\frac{C_p}{C_s} L + \frac{is}{\Omega} \right] R_1}{\Lambda} + \frac{iR_1 s}{\Omega} = \left[\frac{\theta_1(0)\bar{h}_{t_e} - \Sigma\, y_{i_1}(0) h_i^o}{C_p \bar{T}_e} \right] \tag{C-17}$$

Using the definition $H_1 \equiv \frac{T_1}{\bar{T}_e}$, the heat flux from the gas side may be expressed in terms of other gas phase variables to yield:

$$\frac{\lambda}{\lambda_s} \left. \frac{\partial H_1}{\partial \zeta} \right|_{\zeta = 0^+} = \frac{\lambda}{\lambda_s} \frac{\alpha_s}{\bar{r}\, \bar{T}_e} \left[\left. \frac{\partial \left(\frac{F_1}{C_p} \right)}{\partial y} \right|_{y = 0^+} \right] \tag{C-18}$$

Employing the transformation of $\frac{\partial}{\partial y}$ to $\frac{\partial}{\partial \eta}$ given in the beginning of this appendix and grouping terms to introduce the Prandlt number $Pr \equiv \frac{\mu C_p}{\lambda}$, Equation (C-18) may be re-expressed as

$$\frac{\lambda}{\lambda_s} \left. \frac{\partial H_1}{\partial \zeta} \right|_{\zeta = 0^+} = - \frac{1}{Pr} \frac{1}{C_s \bar{T}_e} \frac{1}{\bar{f}(0)} \left[\theta_1'(0)\bar{h}_{t_e} - \Sigma\, y_{i_1}'(0) h_i^o \right] \tag{C-19}$$

where use has also been made of Equation (4-75). Putting Equation (C-19) into (C-17) and rearranging terms one obtains the required energy

balance condition given in Equation (4-40).

v) At the boundary layer edge the continuity of total enthalpy requires

$$h_t = h_{t_e}$$

Using the expansion for h_t from Equation (4-23) and the definition given in Equation (2-17), the above equation yields

$$\bar{h}_{t_e}[\bar{\theta}(\infty) + \theta_1(\infty)] = C_p(T_e - T_u) + \Sigma\, y_{i_e} h_i^o + \frac{u_e^2}{2g_c J_c}$$

Perturbing the right hand side terms and separating orders of magnitude one obtains to first order

$$\theta_1(\infty) \equiv \frac{h_{t_{e_1}}}{\bar{h}_{t_e}} = \frac{C_p \bar{T}_e \left(\frac{T_{e_1}}{\bar{T}_e}\right) + \frac{\bar{u}_e^2}{g_c J_c}\left(\frac{u_{e_1}}{\bar{u}_e}\right)}{\bar{h}_{t_e}}$$

Species boundary conditions

vi) The species balance condition at the gas-solid interface may be written as:

$$\rho D \left.\frac{\partial y_i}{\partial y}\right|_{y=0} = (\rho v)_w [y_i(0) - (y_{i_w})_-]$$

Using the transformed expression for $(\rho v)_w$ derived earlier (see Eqn. (4-73)) and the transformation from $\frac{\partial}{\partial y}$ to $\frac{\partial}{\partial \eta}$, one obtains

$$\frac{(\rho\mu)}{Sc}\, y_i'(0) = -\frac{\bar{\rho}_e \bar{\mu}_e \bar{u}_e}{(2\xi)^{1/2}}\left[(\bar{f}(0) + f_1(0))(y_i(0) - (y_{i_w})_-\right]$$

Substituting Equations (C-5) and (C-6) for $\rho\mu$ and separating orders of magnitude the perturbed form of the species balance condition given in Equation (4-42) is obtained, to first order.

vii) At the boundary layer edge, continuity of species mass requires

$$y_i = y_{i_e}$$

Since the external stream oscillations are chemically frozen by assumption, perturbing the above equation yields to first order:

$$y_{i_1}(\infty) = 0$$

This completes the derivation of the linearised gas phase equations governing the behavior of perturbations in the quasi-steady boundary layer.

APPENDIX D

EVALUATION OF THE RESPONSE FUNCTIONS

The response functions at the boundary layer edge and at the gas-solid interface, as expressed by Eqns. (4-72) and (4-76) respectively, are evaluated numerically. In order to do this the system of "complex" differential equations and boundary conditions formulated in Chapter IV - governing the behavior of perturbations in the gas and solid phases - has to be first solved. This linear boundary value problem consisting of seven first order "complex" differential equations is split into its real and imaginary parts to yield a "real" linear boundary value problem of fourteenth order. A computer program is formulated to handle the solution of this latter problem, using a non-iterative technique developed earlier for the solution of similar problems (see Appendix A). This "unsteady program" uses the steady state solutions, computed earlier using another program and stored, as input. Thus the "unsteady program" begins by providing the solutions for the profiles of all steady-state quantities as well as their perturbations, across the boundary layer, at a given x-location. The thickness of the boundary layer specified to the unsteady program is the same as the one used for the steady program (i.e., $\eta = 8$). From the obtained solutions it is possible to reconstruct the "complex" solution for every perturbation profile by simply adding the real and imaginary parts, at every η across the boundary layer. This information would have been sufficient to find the response functions R_e and R_w if the quantities I_{ξ_1} and $\bar{I}_{\xi}$ were not involved in the expression for R_e. These quantities involve axial gradients of the steady-state

density as well as its perturbation, as seen from Eqns. (4-65) and (4-67). In order to estimate these gradients, therefore, it is necessary to compute all the profiles at several x-locations close to the desired one. However, owing to the slowly varying nature of the solutions with x, in this analysis, it was sufficient to just consider two more x-locations - one on either side of the desired one - and compute these axial derivatives using a parabolic interpolation scheme given in Ref. 34 as "DGT3". The integration of all the definite integrals involved in the response function formula (i.e., $\bar{I}$, I_1) is achieved using Simpson's rule. Of course, the profiles of $\bar{\rho}$ and ρ_1, that are needed, are easily constructed from the steady and perturbed forms of the equation of state for a perfect gas once the temperature and mass fraction profiles have been established.

APPENDIX E

A CLASSIFICATION OF COMPUTER RUNS

In this appendix the values of constants used to obtain the results of the unsteady response analysis, that were presented in Chapter V, are given. As pointed out earlier, for every unsteady case there was a corresponding steady-state case. For the unsteady computer program, the following constants were used in all the runs:

$$\gamma = 1.2$$

$$\varepsilon = 0.01$$

$$\alpha_s = 2\text{x}10^{-6}\ \frac{ft^2}{sec}$$

The constant values used in the steady-state program were based on those given under Case 2 (Appendix B). The changes in these base values are shown below corresponding to the particular runs in which they were made. "CS-" refers to the steady-state cases and "CU-" to the unsteady cases.

Steady State Cases	Parameters that changed their values from Case 2, Appendix B	Unsteady Cases	Damkohler Numbers characterising the case
CS1	$A_s = 6.7*10^5\ \frac{ft}{sec}$	CU1	8.1
	$E_s = 54000\ \frac{Btu}{\ell bm\text{-}mole}$	CU2	90.1
	$L = 918\ \frac{Btu}{\ell bm}$	CU3	174.1
CS2	Same as CS1 except $L = -100\ \frac{Btu}{\ell bm}$	CU4	90.1
		CU5	42.1

Steady State Cases	Parameters that changed their values from Case 2, Appendix B	Unsteady Cases	Damkohler Numbers characterising the case
CS3	Same as CS2 except $h_2^o = -1174.5 \frac{Btu}{\ell bm}$	CU6	90.1
CS4	Same as CS1 except $L = -180 \frac{Btu}{\ell bm}$	CU7	90.1
CS5	Same as CS4 except $n_s = 1.0$ $A_s = 1.0$	CU8	90.1
CS6	Same as Case 2 of Appendix B	CU10	90.1
CS7	Same as CS6 except $E = 54000 \frac{Btu}{\ell bm\text{-}mole}$	CU11 CU15 CU16	90.1 90.1
CS8	Same as CS6 except $E_s = 18000 \frac{Btu}{\ell bm\text{-}mole}$ $A_s = 2.5 \frac{ft}{sec}$	CU12	90.1
CS9	Same as CS7 except Pr = Sc = 1.0	CU13	90.1

REFERENCES

1. Price, E. W. and Culick, F.E.C., "Combustion of Solid Rocket Propellants," AIAA Professional Study Series.

2. Culick, F.E.C., "Review of Calculations for Unsteady Burning of a Solid Propellant," AIAA Journal, Vol. 6, No. 12, 1968, pp. 2241-2255.

3. Hart, R. W., Bird, J. F. and McClure, F. T., "The Influence of Erosive Burning on Acoustic Instability in Solid Propellant Rocket Motors," Progress in Astronautics and Rocketry, Vol. 1, 1960, pp. 423-449.

4. Culick, F.E.C., "Stability of Longitudinal Oscillations with Pressure and Velocity Coupling in a Solid Propellant Rocket," Combustion Science and Technology, Vol. 2, 1970, pp. 179-201.

5. Dehority, G. L. and Price, E. W., "Axial Mode, Intermediate Frequency Combustion Instability in Solid Propellant Rockets," Naval Weapons Center (China Lake) Report No. NWC TP 5654, 1974.

6. Lengellé, G., "A Model Describing the Velocity Response of Composite Propellants," AIAA Paper No. 73-1224, 1973.

7. Summerfield, M., et.al., "Burning Mechanism of Ammonium Perchlorate Propellants," Progress in Astronautics and Rocketry, Vol. 1, 1958, pp. 141-182.

8. Williams, F. A., "Combustion Theory," Addison-Wesley Publishing Co., Inc., 1965.

9. Williams, F. A., Barrère, M. and Huang, N. C., "Fundamental Aspects of Solid Propellant Rockets," AGARDograph No. 116, Technivision Services, 1969.

10. Tsuji, H., "An Aerothermochemical Analysis of Erosive Burning of Solid Propellant," Ninth Symposium (International) on Combustion, 1962, pp. 384-393.

11. Rosenhead, L., "Laminar Boundary Layers," Oxford University Press, Oxford, England, 1963.

12. Hayes, W. D. and Probstein, R. F., "Hypersonic Flow Theory," Academic Press, New York, 1959.

13. Lees, L., "Convective Heat Transfer with Mass Addition and Chemical Reactions," Third AGARD Colloquium, Combustion and Propulsion, 1958, pp. 451-498.

14. Chung, P. M., "Chemically Reacting Non-Equilibrium Boundary Layers," Advances in Heat Transfer, Vol. 2, 1965, pp. 110-268.

15. Gallo, W. F., et.al., "Nonsimilar Nature of the Laminar Boundary Layer," AIAA Journal, Vol. 8, No. 1, 1970, pp. 75-81.

16. Marvin, J. G. and Sinclair, R. A., "Convective Heating in Regions of Large Favorable Pressure Gradient," AIAA Journal, Vol. 5, No. 11, 1967, pp. 1940-1948.

17. Dorrance, W. H., "Viscous Hypersonic Flow," McGraw Hill Publishing Co., New York, 1962.

18. Dorodnitsyn, A., "Laminar Boundary Layer in a Compressible Fluid," Dokl. Akad. Nauk SSSR, Vol. 34, No. 8, 1942, pp. 213-219.

19. Kelly, H. J., "Gradient Theory of Optimal Flight Paths," ARS Journal, Vol. 30, 1960, p. 947.

20. Bryson, A. E. and Denham, W. F., "A Steepest Ascent Method for Solving Optimum Programming Problems," Journal of Applied Mechanics, Vol. 29, 1962, p. 247.

21. Bellman, R. and Kalaba, R., "On the Fundamental Equations of Invariant Imbedding," Proceedings of the National Academy of Sciences U.S., Vol. 47, 1961, p. 336.

22. Blottner, F. G., "Finite Difference Methods of Solution of the Boundary Layer Equations," AIAA Journal, Vol. 8, 1970, pp. 193-

23. Tong, H., et.al., "Non-equilibrium Chemistry Boundary Layer Integral Matrix Procedure," Aerotherm Final Report No. 73-67, Acurex Corp., 1973.

24. Lee, E. S., "Quasi-Linearisation and Invariant Imbedding," Academic Press, 1968.

25. Liu, T. and Davy, W. C., "Non-Equilibrium Boundary Layer at a Stagnation Point for a Hydrogen-Helium Stream Over Ablating Graphite," Ames Research Center, NASA.

26. Krier, H. and Kerzner, H., "Finite-Thickness Diffusion Flames Over a Pyrolysing Fuel Plate," AIAA Journal, Vol. 12, No. 8, Technical Notes 1974, p. 1157.

27. Kiriya, V. S., "The Motion of a Body in a Resisting Medium," Transactions of Tbilisi State Univ., Vol. 44, 1951, p. 1.

28. Davidenko, D. F., "On the Approximate Solution of Systems of Nonlinear Equations," Ukrai. Mate. Zhur., No. 5, 1958, p. 196.

29. Rubbert, P. E. and Landahl, M. T., "Solution of Non-linear Flow Problems Through Parametric Differentiation," Phy. of Fluids, Vol. 10, 1967, No. 4, p. 831.

30. Falkner, V. M. and Skan, S. W., "Some Approximate Solutions of the Boundary Layer Equations," Phil. Mag., Vol. 12, 1931, p. 865.

31. Narayana, C. L. and Ramamoorthy, P., "Compressible Boundary Layer Equations Solved by the Method of Parametric Differentiation," AIAA Journal, Tech. Notes, Vol. 10, No. 8, p. 1085.

32. Hamming, R. W., "Numerical Methods for Scientists and Engineers," Second Ed., McGraw Hill, 1973.

33. Conte, S. D. and Carl de Boor, "Elementary Numerical Analysis," McGraw Hill, New York, 1972.

34. IBM Application Program, System/360 Scientific Subroutine Package, Version III, Programmer's Manual, Program No. 360A-CM-03X.

35. Williams, F. A., "Response of a Burning Solid to Small Amplitude Pressure Oscillations," Journal of Applied Physics, Vol. 33, p. 3153.

36. Culick, F.E.C., "Calculation of the Admittance Function for a Burning Surface," Astronautica Acta, Vol. 13, 1967, pp. 221-237.

37. Strahle, W. C., "New Considerations on Causes for Combustion Instability in Liquid Propellant Rockets," Combustion Science and Technology, Vol. 2, 1970, pp. 29-40.

38. Ives, D. C., "An Approximate Solution of the Boundary Layer Equations Using the Method of Parametric Differentiation," MIT Fluid Dynamics Research Laboratory Report T67-1, AFOSR 67-1512, 1967.

39. Stepp, E. E., "Effect of Pressure and Velocity Coupling on Low-Frequency Instability," AIAA Journal, Vol. 5, No. 5, 1967, pp. 945-948.

VITA

Rajeev Srivastava was born on August 6, 1948. He attended St. Columba's High School in New Delhi, India.

Mr. Srivastava then studied in the Indian Institute of Technology and in 1970 received the Bachelor of Technology degree in Mechanical Engineering. Later in 1971, Mr. Srivastava graduated from the Rensselaer Polytechnic Institute of Troy, New York, with a Master of Science degree in Aeronautical Engineering. He entered the Georgia Institute of Technology in September, 1971.

Mr. Srivastava is presently employed at the Department of Engineering and Applied Science, Yale University, New Haven, Connecticut as a research staff member. He joined Yale in February, 1976.